Sandia National Laboratories
Waste Isolation Pilot Plant (WIPP)
Test Plan TP 00-07

Experimental Study of WIPP Engineered Barrier MgO at Sandia National Laboratories Carlsbad Facility

Task 1.3.5.4.3.1

Rev. 2

Effective Date: 10/02/02

Prepared by:

Anna Snider (6822)
Yongliang Xiong (6821)

Sandia National Laboratories
Carlsbad, NM

WIPP:1.3.5.3.3.3:TD:QA:DPRP1:NF:Test plan for MgO, TP 00-07, Rev. 2

APPROVAL PAGE

Author:	*Original signed by F. Hansen for* Anna Snider (6822)	*10-02-02* Date
Author:	*Original signed by Yongliang Xiong* Yongliang Xiong (6821)	*Oct. 2, 2002* Date
Technical Reviewer:	*Original signed by Donald Wall* Donald Wall (6822)	*10/02/02* Date
Management Reviewer:	*Original signed by F.Hansen* Frank Hansen (6822)	*10/02/02* Date
QA Reviewer:	*Original signed by M.J. Mitchell* Marty Mitchell (6820)	*2 Oct 02* Date

TABLE OF CONTENTS

1.0 DEFINITION OF ABBREVIATIONS AND ACRONYMS

ASTM	American Society for Testing and Materials
BET	Brunauer, Emmett, and Teller
CCA	Compliance Certification Application
CBFO	US DOE Carlsbad Field Office
CO_2	Carbon dioxide
DAS	Data acquisition system
DOE	Department of Energy
EBSD	Electron backscatter diffraction
EDS	Energy dispersive system
GC-MS	Gas chromatography mass spectrometer
GWB	Generic Weep Brine (synthetic Salado Formation brine)
HA	Humic acids
ICP-OES	Inductively-coupled plasma optical emission spectrometer
ISA	Isosaccharinic acid
LANL	Los Alamos National Laboratory
LOI	Loss on ignition
MgO	Magnesium Oxide
M&TE	Measuring and test equipment
NIST	National Institute of Standards and Technology
NBS	National Bureau of Standards
NP	Nuclear Waste Management Program Procedure
NWMP	Nuclear Waste Management Program
RWP	Radiological work permit
SEM	Scanning electron microscope
SNL	Sandia National Laboratories
SP	NWMP Activity/Project Specific Procedure
STTP	Actinide Source Term Test Program
TDIC	Total dissolved inorganic carbon

TOP	Technical operating procedure
TP	Test Plan
TRU	Transuranic
WID	Westinghouse Waste Isolation Division
WIPP	Waste Isolation Pilot Plant
XRD	X-ray diffraction

2.0 REVISION HISTORY

This is the second revision of this Test Plan (TP). The current revision is in response to a Corrective Action Request (CAR) # W-02-05. The previous TP did not cover hydration experiments on the engineered barrier magnesium oxide (abbreviated as MgO thereafter) nor solution chemistry of carbonation processes of the engineered barrier. More experimental details are also needed in order for a qualified technical person to sufficiently reproduce any experiment described hereafter. Descriptions of experiments concerning possible isosaccharinic acid (ISA) production, and the affect of MgO on humic acid solubilites have been removed. A separate TP will be written describing ISA experiments and subsequent analysis. The influence of MgO on the solubilities of humic acids will be described under TP 02-02, "Generation of Colloids from the WIPP Backfill".

3.0 PURPOSE AND SCOPE

MgO is being used in the Waste Isolation Pilot Plant (WIPP) to mitigate the effect of microbial CO_2 generation on actinide mobility in a post-closure repository environment (Bynum *et al.*, 1998; Papenguth *et al.*, 1998). MgO will sequester CO_2 and buffer brine pH at a moderately basic level, thus minimizing solubilities of actinides in WIPP brines. In the past, a series of experiments have been conducted at Sandia National Laboratories (SNL) to verify the efficacy of MgO as a chemical control agent in the WIPP (See Test Plans TP 97-01 and TP 98-05). The experimental conditions in the current revision bracket those expected in the WIPP. Therefore, the results from these experiments directly support re-certification and the Performance Assessment (PA).

With the development of a laboratory facility at the SNL Carlsbad Program Group, MgO experiments were transferred to Carlsbad and new experiments have been initiated. This Test Plan provides guidance only for the studies of MgO to be conducted at SNL-Carlsbad Laboratory. The following tasks are planned:

- *Characterization of the MgO being emplaced in the WIPP.* The purpose of this study is to analyze Premier Chemical's MgO (or any subsequent supplier) to determine what impurities might be present and in what quantities, and to describe the granular texture. Analysis is done using the JEOL 5900LV scanning electron microscope (SEM), the Brucker X-ray Diffractometer (XRD), and chemically by a gravimetric silica method (Kolthoff and Sandel, 1961). The results will influence the quantity of MgO that will be emplaced in the WIPP in order to sequester all the CO_2 produced from possible microbial activity, and would provide important information such as the content of CaO, which might influence the reaction path calculations.

- *Further study on the hydration of Premier Chemicals MgO.* The hydration of MgO must occur before the engineered barrier can react with CO_2, which may be formed from possible microbial degradation of organic materials in the waste package. Hydration may also be the rate-limiting step to carbonate formation. These experiments are being conducted to evaluate several factors affecting MgO hydration rate under both inundated and humid conditions.

The results will help determine hydration rates and pathways, and whether the reaction solid products passivate the reactivity of MgO.

- *Further study of the kinetics of magnesium carbonate formation and conversion to magnesite under WIPP-relevant conditions.* The reaction of MgO with CO_2 can produce a series of magnesium carbonate minerals with magnesite ($MgCO_3$) as the most stable phase (Königsberger *et al.*, 1999). Different magnesium carbonate and hydroxycarbonate minerals can have different buffering capabilities for controlling CO_2 fugacity and brine pH. In the WIPP Compliance Certification Application (CCA), it is assumed that metastable magnesium carbonate minerals will be ultimately converted to magnesite. The first objective of this task is to obtain the rates of carbonation of the engineered barrier to metastable magnesium carbonate(s). The second objective is to estimate the kinetics of the conversion of the metastable magnesium carbonate to magnesite to provide additional data to support the CCA assumption. This task will also support the US Department of Energy (DOE) Carlsbad Field Office's (CBFO's) effort to simplify the existing MgO engineered barrier system.

- *Experimental determination of iron concentrations in GWB and ERDA-6 in contact with the engineered barrier owing to metal corrosion.* The influence of corrosion of metals on the chemical environment in the WIPP has been well envisioned before by Brush (1990). Should low-carbon steel, that is used as the waste packaging material for the WIPP, corrode in brines then iron would dissolve. This may influence the brine chemistry and the solid mineral assemblage of the WIPP. Siderite ($FeCO_3$) has lower solubility than that of magnesium carbonate(s) expected in the final assemblage of the WIPP after the closure. Therefore, the formation of siderite may also consume some of carbon dioxide generated by microbial activity and might influence the important physicochemical parameters such as pH and f_{CO_2}. The iron concentrations under buffered conditions relevant to the WIPP will support the future EQ3/EQ6 calculations and therefore the actinide solubility calculations.

4.0 EXPERIMENTAL PROCESS DESCRIPTION

4.1 Overall Strategy and Process

4.1.1 Experimental Design

Task 1. Characterization of the MgO being emplaced in the WIPP.

Premier Chemicals is the vendor currently supplying MgO to the WIPP. This material is produced by calcining magnesite ore in a rotary kiln, mined at Gabbs, NV , and consists of angular grains of material ≤ 3/8 inch in diameter (much of the material is fine powder.) The ore bodies were hosted in Upper Triassic dolomites, which were deformed and intruded by felsic dikes and stocks. The geological origin of such ore bodies can provide additional information for the interpretation of impurities in the engineered barrier material. The material has a minimum of 90 wt.% of MgO (as stated on the Material Safety Data Sheet issued before 2000), and is relatively impure, containing up to 10 percent Mg-Ca silicates. The chemical makeup of a typical sample of Premier MgO, as listed in the Material Safety Data Sheet issued before 2000, is

as follows: 2.8 wt.% of SiO_2, 1.3 wt.% of Fe_2O_3, 0.8 wt.% of Al_2O_3, 3.9 wt.% of CaO, and 91.0 wt.% of MgO (90 % minimum). Note that the impurity oxides listed here do not exist as free oxides in the MgO (with the exception of a fraction of the CaO and SiO_2) but are combined mineralogically as calcium-magnesium silicates, aluminates, and ferrites. As of October 2000, Premier Chemicals has adjusted the chemical composition to a minimum of 95 wt.% of MgO+CaO.

The purpose of this task was to analyze Premier Chemical's MgO to determine what impurities might be present and in what quantities, and to describe the granular texture of Premier Chemical's MgO. Physical analyses were done using the JEOL 5900LV scanning electron microscope (SEM), and the Brucker X-ray Diffraction unit (XRD). Chemical analyses were done using a gravimetric determination of silica method (Kolthoff & Sandell, 1961).

All samples are analyzed by using the SEM and the XRD. The SEM is utilized to identify major and minor mineral phases, and to document the grain textures, the physical distribution of the minerals, and the intergranular porosity.

The gravimetric determination of silica method by Kolthoff & Sandell (1961) is adopted to determine the amount of SiO_2 present in the current batch of Premier Chemical's MgO being emplaced in the WIPP. Before analysis, MgO is crushed to a size of < 200 mesh (75 μm). MgO is then mixed with sodium carbonate and ignited. Samples are first leached with HCl, and then placed on hotplates to evaporate overnight. Remaining solids are filtered, re-ignited, and weighed. Liquid is retained from the filtering for analysis by the Perkin Elmer inductively coupled plasma optical emission spectrometer (ICP-OES), for identification of any aluminates that might be present. From the silica results, the weight percentage of Mg_2SiO_4 or $CaMgSiO_4$ is determined.

ICP-OES (Perkin Elmer DV 3300) is used to determine the concentration of Al, Mg, Ca, and Si in liquid left from the gravimetric determination of silica. The results are used to determine whether all silicates were filtered out in the above method and if any lime and aluminates constitute certain percentages of Premier MgO.

Task 2. Further study on the hydration of Premier Chemicals MgO

Hydration experiments were developed to determine hydration rates and pathways, and whether the reaction solid products inhibit the reactivity by passivation of MgO under both inundated and humid conditions. These experiments will be run at fixed and variable brine/MgO ratios. Many samples will be agitated daily to eliminate the effect of mass transport, whereas others will be non-agitated to better represent WIPP relevant conditions.

Inundated Experiments

In the first set of experiments, five grams of Premier MgO is placed in 125 ml polypropylene bottles. Each bottle contains 100 ml of one of four solutions—deionized (DI) water, 4.0 M NaCl, and synthetic Salado (GWB) and Castile (ERDA-6) brines. The first two simple solutions are included in an effort to develop an understanding of the effect of the ionic strength on the hydration process. The bottles are sealed and no special effort is made to exclude

CO_2 from these experiments (and all other hydration experiments). CO_2 diffusion into the system will be insignificant relative to the hydration rate. Samples are aged in ovens at 25-90° C, and are agitated frequently. Sample agitation is performed to eliminate the formation of a cemented cake of hydration products, removing the possibility that cake formation will inhibit hydration by limiting brine access to the bulk MgO. However, hydration products may still inhibit further hydration by coating individual particles, or by plugging the internal porosity in the MgO grains. The effects of cake formation on hydration are being examined in a separate set of experiments described in detail below. Periodically, samples are removed from the ovens, cooled, and the pH measured. The solid fraction is then vacuum filtered out by using Whatman #40 filters, and rinsed with DI water to remove any remaining brine. Then the filtered solids are dried, ground, and characterized by XRD and SEM. The loss on ignition (LOI) at 500° C (brucite dehydrates at ~350°C) is used to calculate the amount of hydrated material in each sample.

To date two hydration products, magnesium hydroxide (brucite) and magnesium chloride hydroxide hydrate, have been recognized. Magnesium chloride hydroxide hydrate is present only in the GWB and continues to be formed instead of brucite until the Mg^{2+} concentration falls below ~0.7 M. Therefore, the second set of experiments is designed to test whether relative proportions of brucite to magnesium chloride hydroxide hydrate will vary as a function of the volume of brine present. This set of experiments evaluates the effect of variable brine volumes present in GWB/MgO systems. Five grams of MgO are placed in 125 and 250 ml polypropylene bottles containing GWB volumes ranging from 60–250 ml, and aged for 28 days at 70°C. It is possible that in the future lower brine to MgO ratios may need to be investigated.

In addition, the third set of experiments is being conducted to assess the effect of brine to MgO volume ratios on the hydration rates in a manner similar to the inundated hydration experiments described above, except 2.5 times as much GWB is used in this set of experiments. The aim of this set of experiments is to compare the resulting hydration rate curves with those of the above mentioned inundated experiments. The comparison will define the effect of the brine to MgO ratios on the hydration rates. Samples are placed in the 70°C oven and are sampled at the same interval as the first inundated samples at 70°C.

Cemented Cake Experiments

The effects of possible formation of a cemented cake of hydration products on hydration rates are being examined. In this set of experiments, five (15 g)-, ten (30 g)-, and 15 (45 g)-mm-thick layers of Premier MgO are placed in 125 ml polypropylene containers with 100 ml GWB or ERDA-6, and are placed in ovens at 25°–90° C. The samples are not agitated. Sampling is being carried out over weeks to months. Samples are taken from the oven, cooled, and pH is measured. Samples in their entirety are filtered, dried, and crushed, then analyzed by LOI and XRD. The SEM is used to perform cross-sectional analysis on select samples before they are crushed.

Humid Experiments

The humid hydration experimental runs involves uncrushed Premier MgO as starting material and are being conducted at temperatures of 25°C, 40°C, 60°C, and 80°C and relative

humidities of 35%, 50%, 75%, and 95%. These humidities bracket the expected WIPP value of 70%. Premier Chemicals MgO is contained in 6-well polycarbonate trays, with three grams of MgO in each well. Four trays are stacked in sealed polypropylene containers. Each container contains a saturated salt solution providing the desired relative humidity (Table 1). Relative humidity will vary a few percent with temperature, exception being NaBr $\cdot 2H_2O$. Currently, the humidity change with temperature is being investigated.

Table 1. Saturated Salt Solutions and the Relative Humidity Values they Produce.

Salt Solutions	RH Value, %*
K_2SO_4	96
NaCl	75
NaBr	53
$MgCl_2$	33

* RH values vary a few % with temperature

The trays in each container are elevated above the salt solution on plastic blocks. Holes have been drilled in the bottom and top of each tray; and the upper lip of each well is notched. The holes and notches allow for circulation through each sample well. This set of experiments consists of 384 samples (four temperatures, four relative humidities, four trays, six wells per tray).

Samples will be periodically collected over a period of months to years depending on reaction rates. Each sample is dried and analyzed by LOI and XRD. The fraction of brucite will be determined by weight loss at 500°C. This technique assumes that brucite is the only reaction product of hydration of MgO. A few samples will be analyzed by XRD to verify that carbonate formation is not significant under humid conditions.

Task 3. Further study of the kinetics of Mg carbonate formation and conversion

Reaction of MgO with CO_2 can produce a series of magnesium carbonate minerals with magnesite as the most stable phase (Königsberger et al., 1999). Different magnesium carbonates impose different values of CO_2 fugacity and brine pH. The objectives of current experiments in this task are to gain a more mechanistic understanding of MgO carbonation processes and determine which magnesium carbonate phase will eventually control the f_{CO_2}. These experiments will help determine: (1) how solution chemistry affects magnesium carbonate formation; which in turn will control brine f_{CO_2} and possibly pH; (2) the carbonation rates of Premier Chemicals MgO and brucite under various conditions. MgO is expected to first hydrate as brucite, and is expressed by Eq. (1),

$$MgO_{(s)} + H_2O \text{ (aq. or gas)} = Mg(OH)_{2(s)} \qquad (1)$$

and hydration rates can be obtained from hydration experiments described in detail above, the experiments planned here will focus on the formation of magnesium carbonate minerals from

the reaction of brucite with CO_2 to determine the carbonation rates. Using hydromagnesite as an example, the carbonation of brucite can be expressed as the following reaction,

$$5Mg(OH)_{2\,(s)} + 4CO_2\ (aq.\ or\ gas) = Mg_5(CO_3)_4(OH)_2 \cdot 4H_2O_{\,(s)} \qquad (2)$$

However, in order to investigate the overall carbonation rates from MgO to magnesium carbonate(s), additional experiments will be conducted using MgO as a starting material, which may correspond to the combination of reactions (1) and (2). As suggested by reaction (2), the carbonation can take place in both aqueous (inundated) and gaseous (humid) media. Hence, experiments will be designed to investigate the carbonation rates in both scenarios, which will be described in detail below.

Brucite will be purchased or synthesized using Premier MgO backfill. (Brucite crystals will be crushed into fine-grained powder, and the specific surface area of brucite powders will be determined using the B.E.T. (Brunauer, Emmett, and Teller) autocontrol physical adsorbent instrument (ASAP2000) (Wang et al., 1999).

Experiments Using MgO as Starting Material

The first set of carbonation rate experiments are run at two different partial pressures of CO_2, under atmospheric conditions ($3\text{-}4x10^{-4}$ atm) and 5% CO_2 ($5x10^{-2}$ atm). In the future experiments may be run under other partial pressures, such as $1/10^{th}$ atmospheric CO_2.

The experiment running under atmospheric P_{CO_2} conditions are using four different solutions: DI water, 4 M NaCl, GWB, and ERDA-6. Each 125 ml polypropylene sample bottle includes five grams Premier Chemicals MgO and 100 ml of solution. Room air is bubbled continuously through the samples using a gas manifold. Each manifold holds 24 samples. To minimize evaporation, the air is humidified by bubbling through water prior to entering the manifold.

Samples are collected at weekly intervals and eventually will be collected on a monthly to bimonthly interval. Samples are measured for pH, filtered, dried, and crushed. The amounts of carbon incorporated into the reaction products are determined by using a UIC Inc. carbon coulometer and carbonate phases will be identified by using XRD. Based on the amounts of carbon incorporated into the reaction products, carbonate conversion rates will be assessed. New sets of samples will be added to the experiment periodically to extend the curve.

The experiments with 5% CO_2 will quantify carbonation rates in two brines, GWB and ERDA-6. There are 64 samples (two brines, four solids, eight samples). Each polypropylene bottle contains five grams of one of the following solids: Premier Chemicals MgO, Fisher Scientific MgO, pre-hydrated, crushed Premier Chemicals MgO, and pre-hydrated Fisher MgO. Hydrated samples are prepared by adding five grams of either crushed Premier Chemicals MgO, or Fisher MgO to 100 ml of brine. The bottles are placed in a 90°C oven for approximately three to four weeks. Before the pre-hydrated samples are added to the manifold, a small portion is sampled and will be analyzed for brucite. The experiments with 5% CO_2 will be sampled at a

higher frequency due to the anticipated accelerated reactions. New sets of samples will be added to the experiment periodically to extend the curve.

All samples in the experimental set using 5% CO_2 are placed in a glovebox with a controlled atmosphere. The five percent of CO_2 is controlled by delivering a mixture of 95% N_2 and 5% CO_2 into the glovebox at a fixed rate. To bring the atmosphere of the glovebox up to 5% CO_2 in a timely manner after the box is opened for sampling, dilute sulfuric acid is mixed with sodium bicarbonate within the glovebox, which releases a pre-determined amount of CO_2 to the atmosphere.

Experiments Using Brucite as Starting Material

The objectives of experiments using brucite as starting material are two-fold: (1) to determine precisely the carbonation rates, and at the same time (2) to monitor the solution chemistry in order to document the progress in carbonation processes. The second objective is mainly due to the fact that the assemblage of brucite and magnesium carbonate(s) resulting from the carbonation would influence the solution chemistry (Stumm and Morgan, 1996). While the results from the first objective would provide the firm basis for the performance assessment for the conceptual model of the WIPP, the results from the second objective would provide an important insight into (1) the reaction path when solution are in contact with brucite, (2) the identity of the solid phase that controls the solubility in terms of Mg concentrations, and (3) whether important physicochemical parameters such as pH are buffered by the assemblage of brucite and its carbonation product(s) (i.e., hydromagnesite).

In the first set of experiments, brucite powder will be added to various solutions and allowed to react with the dissolved CO_2 at fixed P_{CO_2} in polyethylene bottles and 25 mL glass vials. The volume of polyethylene bottles ranges from 25 to 1000 mL. The weight of brucite associated with experimental runs using polyethylene bottles ranges from 1.5 grams to 15 grams, and the volume of solutions employed is in the range from 25 to 1000 mL. In experimental runs using 25 mL glass vials, the weight of brucite ranges from about 1.2 grams to 2.5 grams, whereas the weight of solutions ranges from 17 grams to 25 grams. In this set of experiments, several P_{CO_2} will be employed, including $3\text{-}4 \times 10^{-4}$ atm (atmospheric CO_2). In such atmospheric CO_2 experiments, caps of polyethylene bottles and glass vials are not closed in order to allow solutions to communicate with atmospheric CO_2. DI water, and brines expected to be present at the WIPP such as GWB and ERDA-6 (Brush, 1990; Zhang *et al.*, 1999) will be used. To assess the effect of ionic strength on the carbonation rates, four solutions with different ionic strengths (0.01 M, 0.1 M, 1.0 M and 4.0 M NaCl solution) will be used. In most of the above experiments, solutions and starting materials will not be stirred, and such experiments are termed "static runs". In order to assess the effect of mass transport on carbonation rates, a subset of experiments will be conducted under the same conditions, but solutions and starting materials are continuously stirred and compressed air continuously bubbles into solutions, and such experiments are termed "dynamic runs". The results from both "static runs" and "dynamic runs" will be compared to evaluate the effect of mass transport on carbonation rates. During the experiments, an appropriate number of brine samples will be taken for the analysis of pH and Mg concentration in order to monitor changes in solution chemistry due to carbonation. Solutions will be sampled weekly. The mass of samples taken each time will be recorded. The mass of samples withdrawn

will be between 3 and 4.5 grams. Solution samples will be acidified with concentrated HNO_3 and then be diluted to 10 mL. To disturb the steady state on purpose, each experimental run will be recharged after three or four samplings with fresh matrix solutions with approximately the same amounts that have been withdrawn. In the following sampling(s), the observations of the lack of deviations in solution chemistry after recharging from the previous samplings would imply the re-equilibration. This technique has been demonstrated before (e.g., Xiong and Wood, 2001). After sufficient time (perhaps months), the solids in each bottle will be filtered, and the resulting mineral phases will be identified using Scanning Electron Microscopy (SEM) and the associated Energy Dispersive System (EDS) and Electron Backscatter Diffraction (EBSD). EBSD is able to obtain electron diffraction patterns on a scale of <1 μm and therefore provides a better mineral identification capability than the X-Ray Diffraction (XRD) technique used in the previous MgO work (TP 96-01 and TP 98-05). The contents of carbonates in solid phases will be analyzed by using a CO_2 coulometer (UIC, Inc., Model CM5014). The majority of carbonation experiments will be conducted at room temperature. Additional experiments will be conducted at 40°C, 50°C, 60°C, 70°C, 80°C, and 90°C in a manner similar to hydration experiments at these temperatures, which has been described in detail above.

To assess carbonation rates at lower CO_2 concentrations, some experiments will be set-up to allow dissolved CO_2 to diffuse into polyethylene bottles in which brucite powder is in contact with various solutions. In such diffusion experiments, caps of 250 mL polyethylene bottles will be sealed with parafilm. The weight of brucite used in such experiments will range from 4 to 6 grams, and the weight of the solutions will be from 100 to 250 grams. The sealed polyethylene bottles that contain brucite and solutions will be placed into 16 oz plastic jars filled with DI water. As the diffusivity of CO_2 through polyethylene has been established (Dietzel and Usdowski, 1996), the flux of CO_2 into polyethylene bottles by diffusion will be precisely calculated. The diffusion of CO_2 though polyethylene is expressed as:

$$\frac{dN}{dt} = FD\frac{C_s - C}{\Delta X} \qquad (3)$$

where N is the number of moles, F is the surface area of diffusion, D is the diffusion coefficient of CO_2, C_s and C are the concentrations of dissolved CO_2 in the jar and the polyethylene bottle, respectively, and ΔX is the thickness of the polyethylene. The total diffusion surface of the 250 mL polyethylene bottle is ~300 cm^2, and the thickness of the bottle is 0.2 cm. Assuming that the pressure of CO_2 delivered to the jar is 1 atm and substituting $D_{CO_2} = 10^{-7.9}$ mole cm^{-2} (Dietzel and Usdowski, 1996) into Eq. (3), the flux can be calculated to be ~8×10^{-10} mole s^{-1}. As the initial concentration of Mg in the polyethylene bottle is about 10^{-3} m controlled by brucite, the carbonate concentration required for the saturation of hydromagnesite is about 10^{-4} m. Therefore, it requires about one day for the dissolved CO_2 to diffuse into the polyethylene bottle to reach the saturation of hydromagnesite. In the actual experiments, the pressure that will be employed will be less than 1 atm, and the experiments will be conducted in a glove box. The desired pressure of CO_2 will be delivered to the glove box via a regulator. As soon as the saturation limit of hydromagnesite is reached, the fugacity of CO_2 inside the polyethylene bottle will be fixed by the formation of hydromagnesite, which is $10^{-5.14}$ bars according to the compilation of Stumm and Morgan (1996). Two temperatures, room temperature and 40°C,

which bracket the expected temperature range in the WIPP, will be employed in these experiments.

In the second set of experiments, in order to evaluate carbonation rates under conditions where aqueous media are absent, brucite powder will be allowed to react with gaseous CO_2 at various desired humidities. In this set of experiments, 100 mL beakers that contain about 4–6 grams of brucite will be placed into 16 oz plastic jars with lids filled with various saturated solutions. The saturated solutions include K_2SO_4, NaCl, NaBr, and $MgCl_2$ solutions. These saturated solutions provide relative humidities ranging from 95% to 33% (Lide, 1997, p. 15-24 to 15-25, and references therein). These saturated solutions will be prepared according to their saturated solubilities tabulated in Lide (1997, p. 8-98 to 8-105). The lids of the jars will be opened daily to allow atmospheric CO_2 to be replenished. In this set of experiments, the carbonation rates are expected to be very slow at room temperature. Therefore, in addition to experimental runs at 25°C, there will be also experimental runs at other temperatures ranging from 40°C to 90°C. These experimental runs at higher temperatures would allow extrapolations of carbonation rates under humid conditions to room temperature with confidence. For the purpose of comparison, the lids of some jars will not be opened until the termination of the experimental runs. Such comparison might provide an understanding of the carbonation rate at low P_{CO_2} as CO_2 in the experiments in which the lids will not be opened daily would rely on the diffusion of atmospheric CO_2 into the jars.

In the third set of experiments, the metastable Mg carbonate mineral phases will be incubated in various solutions at 25°C. Thermodynamically, magnesite ($MgCO_3$) is the stable phase for magnesium carbonates although its crystallization at room temperature is not kinetically favored. All other magnesium carbonates are considered as metastable phases. The metastable magnesium carbonate phases used in this set of experiments will be purchased from Ward's Natural Science Establishment (Rochester, NY) and Excalibur Mineral Company. Two major metastable phases of magnesium carbonate, hydromagnesite ($Mg_5(CO_3)_4(OH)_2{\cdot}4H_2O$) and nesquehonite ($MgCO_3{\cdot}3H_2O$), will be used. It has been demonstrated that metastable magnesium carbonates attain solubility equilibrium from the direction of undersaturation in a few days (e.g., Königsberger et al., 1992). Therefore, experimental runs will be monitored to reach solubility equilibrium from the direction of undersaturation, and solutions will be sampled periodically (bi-weekly). The metastable magnesium carbonates will be loaded in silver capsules, and then both ends of silver capsules will be crimped. This loading technique offers two advantages: (1) to prevent the solid starting material from being sampled while the capsule allows the starting material to communicate with solutions, and (2) to allow the experimental run products to be collected easily, especially when the amounts of the starting material are small, for other work such as XRD and SEM after the termination of the experimental runs. This loading technique has been successfully employed before (i.e., Xiong and Wood, 2001, and references therein). The mass of metastable magnesium carbonates will range from 0.1 grams to 0.5 grams, and the mass of solutions will be in the range from 20 grams to 35 grams. Solutions and silver capsules containing metastable magnesium carbonates will be in 35 mL plastic bottles. Caps of plastic bottles will not be closed to allow solutions to communicate with atmospheric CO_2. In order to keep the ionic strength constant and to compensate for the possible loss of

water in salt solutions, the experimental runs will be periodically monitored for possible loss of water by comparison with the original weight. If there is a loss of water, the exact amount of water will be added. These bottles will then be placed on a shaker at a constant shaking rate. These samples will be analyzed for Mg concentrations. This information will aid in interpreting which Mg carbonate phase might control the solubility in hydration experiments and carbonate rate experiments in aqueous media as mentioned before. As GWB and ERDA-6 have high matrix concentrations of Mg, in order to determine precisely concentrations of Mg resulting from the dissolution of the solubility-controlling phase, only DI water and NaCl solutions with different ionic strengths will be used in these experiments. The conversion from metastable magnesium carbonates to magnesite will be evaluated from two lines of evidence. First, the onset of the conversion will be deduced from solution chemistry by conducting EQ3/6 modeling (Wolery, 1992; Wolery and Daveler, 1992). This reasoning is based on the fact that the solubility of magnesite is orders of magnitude lower than that of metastable magnesium carbonates. If the modeling indicates the undersaturation with respect to metastable magnesium carbonate beyond the uncertainty of the thermodynamic data base, such undersaturation would imply that the conversion to magnesite is taking place. The second line of evidence will be from XRD analysis of the reaction solid product.

Task 4. Experimental determination of iron concentrations in GWB and ERDA-6 in contact with the engineered barrier owing to metal corrosion

The influence of the corrosion of metals on the chemical environment in the WIPP has been described before (Brush, 1990). The objective of this activity is to support the future EQ3/EQ6 and therefore the actinide solubility calculations. As the expected iron inventory in the WIPP is significant, the dissolved iron concentrations may influence the brine chemistry and the solid mineral assemblage of the WIPP. Siderite ($FeCO_3$) has lower solubility than that of the magnesium carbonate(s) expected in the final assemblage of the WIPP after the closure. Therefore, in addition to the engineered barrier, the precipitation of siderite may also consume some of carbon dioxide generated by microbial activity and influence the important physicochemical parameters such as pH and f_{CO_2}. It is anticipated that siderite would appear in the early stage after the closure of the WIPP if the dissolved iron concentrations reaches the level dictated by the solubility of siderite, as secondary siderite has been observed in current mine tailings (Al *et al.*, 1997).

Previous experimental studies subcontracted to Pacific Northwest National Laboratory (PNNL) determined the corrosion rate of steel (Telander and Westerman, 1993, 1997). Although they reported iron concentrations for two types of experiments (anoxic-brine seal-welded-container and brine/CO_2 seal-welded-container tests) which ranged from less than 10 mg/L to 1480 mg/L (Telander and Westerman, 1993), such chemical data cannot be used for modeling purposes based on the following facts. First, these corrosion experiments were not buffered with respect to pH dictated by the engineered barrier material (MgO) and to oxidation potentials (Eh) that may be expected at the WIPP. For example, in their brine/CO_2 seal-welded-container testes, pH varied from 3.4 to 7.3, far from the pH values expected in the WIPP (pH = 9–10). Although the expected oxidation potentials at the WIPP are not well constrained, it is likely to be buffered by the certain assemblages such as Fe-$FeCO_3$ (Brush, 1990). If it is buffered by this assemblage,

the expected Eh would be –0.62 volts at pH 10 assuming $\log f_{CO_2}$ is –5 bars. Second, when their solutions in anoxic-brine seal-welded-container testes were exposed to air prior to analysis, dissolved iron was precipitated from the solution because of the oxidation. No attempt was made to re-dissolve these precipitates. Therefore, their analyses for anoxic seal-welded-container tests significantly underestimated real iron concentrations in brines. In the follow-up corrosion experiments using ERDA-6 and GSEEP brines at PNNL (Wang et al., 2001), iron concentrations in the brines were not determined or reported.

In this study, low-carbon steel (the waste packaging material for the WIPP) will be incubated in GWB and ERDA-6 brines with Premier Chemicals MgO and pre-hydrated Premier Chemicals MgO. The weight ratio of brine to MgO will range from 0.5 to 0.8 as expected at the WIPP according to the calculations by Larry Brush (2002). The pH will be dictated by the reaction of MgO with brines. Oxygen fugacity will be buffered by various solid assemblages including the Fe-$FeCO_3$, Fe-$Fe(OH)_2$, and Zn-ZnO assemblages. Using Fe-$FeCO_3$ as an example, the half-cell reaction can be expressed as follows (Anderson and Crerar, 1993),

$$FeCO_{3\,(s)} + 2H^+ + 2e^- = Fe_{(s)} + CO_{2\,(g)} + H_2O_{(l)} \qquad (4)$$

Assuming unity for the activity of iron, siderite and water, oxidation potentials, *Eh*, for Reaction (4) can be expressed as:

$$Eh = E^o - \frac{2.303RT}{2F}\log f_{CO_2} - \frac{2.303RT}{F}pH \qquad (5)$$

Where F is Faraday constant (96485.3 C mol^{-1}), R is ideal gas constant. E^o is given by

$$\Delta G_r^o = -2\,F\,E^o \qquad (6)$$

According to the compilation of Stumm and Morgan (1996), $\Delta G_{f,\,siderite} = -666.7$ kJ mol^{-1}, $\Delta G_{f,\,CO_2,\,gas} = -394.37$ kJ mol^{-1} and $\Delta G_{f,\,H_2O,\,liquid} = -237.18$ kJ mol^{-1} at reference state (25°C and 1 bar), the free energy for Reaction (4) is 35.15 kJ $mole^{-1}$. Assuming $\log f_{CO_2}$ is –5, therefore, we have

$$Eh = -0.0325 - 0.059\,pH \qquad (7)$$

The relation between *Eh* and *pH* is plotted in Figure 1.

Similarly, for the Zn-ZnO assemblage, we have

$$ZnO_{(s)} + 2H^+ + 2e^- = Zn_{(s)} + H_2O_{(l)} \qquad (8)$$

In a manner similar to the above Fe-$FeCO_3$ assemblage and using $\Delta G_{f,\,ZnO} = -76.028$ kcal mol^{-1} at reference state from Stumm and Morgan (1996),

$$Eh = -0.42 - 0.059\,pH \qquad (9)$$

According to Eq. (9), the Zn-ZnO assemblage would provide an oxidation potential of −1.01 volts at 25°C. This assemblage has been observed to equilibrate fast and to buffer oxidation potentials in a few days (Nguyen-Trung et al., 1997). The dissolution of under the Zn-ZnO buffer would provide the lower limit of the iron concentrations. Low-carbon steel, Premier MgO or pre-hydrated Premier MgO, the oxygen fugacity buffer assemblage and brines will be placed into 250 mL plastic bottles, and then caps of plastic bottles will be well sealed with parafilm. Low-carbon steel will be used in the majority of experiments. For the sake of simplicity, pure iron will be employed in some experiments. The bottles containing the above-mentioned starting materials and brines will be placed in a glove box under N_2 atmosphere. For comparison, some experimental runs will use Premier MgO and other experimental runs will use pre-hydrated Premier MgO. A series of such experimental runs will be conducted. They will be terminated at various time scales (probably monthly). After termination of the experimental run, the solution will be filtered and be acidified with concentrated HCl, and then will be promptly analyzed using ICP-OES for Fe, Mg, Zn and other minor metals which low-carbon steel may contain by. Solid samples will be washed with DI water and dried for XRD studies.

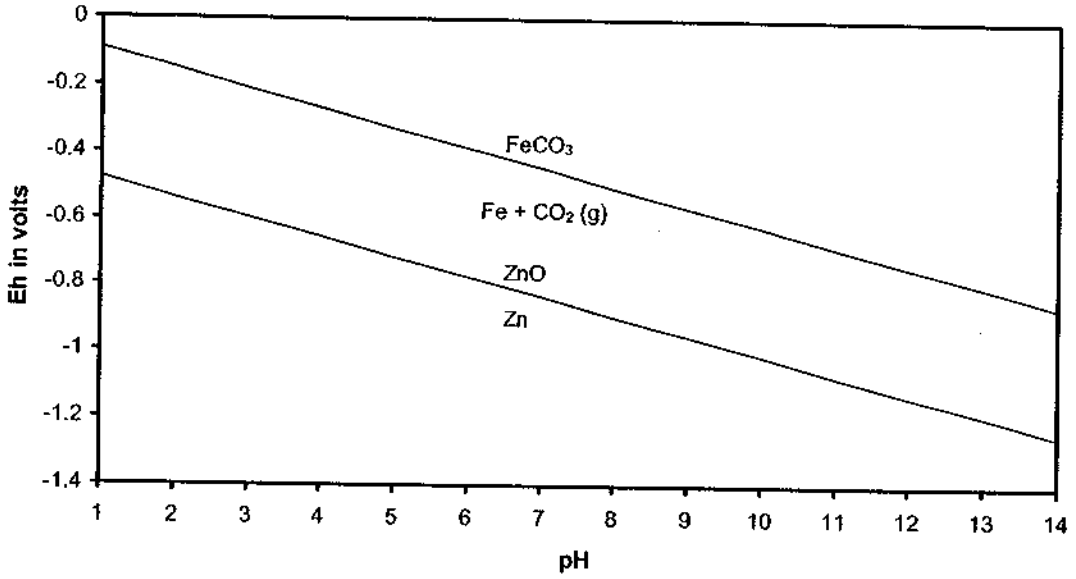

Figure 1 Oxidation potentials provided by the assemblages of Fe-$FeCO_3$ and Zn-ZnO.

4.1.2 Brine Composition

Synthetic WIPP brines are used in all the experiments except those run under humid conditions. ERDA-6 is a saturated brine that contains mainly NaCl along with minor amounts of other solutes and represents fluids from reservoirs in the Castile Formation. ERDA-6 has 4.85 M of sodium, 4.64 M of chloride, and 167 mM of sulfate. GWB is a saturated brine with 3.54 M of sodium, 1.02 M of magnesium, 467 mM of potassium, 5.61 M of chloride, and 178 mM of

sulfate, and represents intergranular brines from the Salado Formation at or near the stratigraphic horizon of the repository.

Synthetic WIPP brines are mixed following the technical operating procedure described by Robinson (1996). Brine formulas are shown below in Table 2. The ERDA-6 brine composition is from Villarreal et al. (2000). The GWB is from Zhang et al. (1999).

Table 2. Brine Formulas for Synthetic ERDA-6 and GWB.

Composition of ERDA-6

COMPOUND	GRAMS/LITER	GRAMS/10 LITERS
$MgCl_2 \cdot 6H_2O$	3.86	38.6
NaCl	261.64	2616.4
KCl	7.23	72.3
Na_2SO4	23.70	237
$Na_2B4O_7 \cdot 10H_2O$	6.00	60
$CaCl_2 \cdot 2H_2O$	1.76	17.62
NaBr	1.13	11.3

Table 2. (cont.) Brine Formulas for Synthetic ERDA-6 and GWB. Composition of GWB

COMPOUND	GRAMS/LITER	GRAMS/10 LITERS
$MgCl \cdot 6H_2O$	207.05	2070.5
NaCl	179.61	1796.1
KCl	34.84	348.4
Na_2SO_4	25.23	252.3
$Na_2B4O_7 \cdot 10H_2O$	15.06	150.6
$CaCl_2 \cdot 2H_2O$	2.03	20.3
NaBr	2.74	27.4
LiCl	0.19	1.86

4.2 Sample Control

The sample control for the work under this Test Plan will follow WIPP Nuclear Waste Management Program (NWMP) Procedure NP 13-1. Each sample will be appropriately labeled. Sample preparation, utilization, and final disposition will be documented in scientific notebooks. When samples are not in the possession of individuals designated as responsible for their custody, they shall be stored in a secure area with associated documentation (Chain of Custody).

4.3 Data Quality Control

4.3.1 Measuring and Test Equipment (M&TE)

A calibration program will be implemented for the work described in this test plan in accordance with NP 12-1, "Control of Measuring and Test Equipment." This M&TE calibration program will meet the requirements in NWMP procedure NP 12-1 for: (1) receiving and testing M&TE; (2) technical operating procedures for M&TE; (3) the traceability of standards to nationally recognized standards such as those from the National Institute of Standards and Technology; (4) maintaining calibration records. In addition, NP 13-1and SP 13-1 identify requirements and appropriate forms for documenting and tracking sample possession. The spread sheet and other computer based data handling will follow NP 9-1.

4.3.2 Data Acquisition Plan

Data collection procedures are specific to individual instruments. For details of the data acquisition for a particular instrument, see the Specific Procedures (SP) or Users Manual for that instrument. Any data acquired by a data acquisition system (DAS) will be attached directly to the Scientific Notebook or compiled in separate loose leaf binders with identifying labels to allow cross reference to the appropriate Scientific Notebook. If the instrument allows data to be recorded electronically, copies of the data disks will be submitted to the NWMP Records Center according to NWMP procedure NP 17-1 "Records." If possible, data files may be transferred to ZIP disks or CD ROM for submittal to the records center. For instruments that do not have direct data printout, the instrument readings will be recorded directly into the scientific notebook. Current versions of the DAS software will be included in the SNL WIPP Baseline Software List, as appropriate.

Quality control of the Scientific Notebooks will be established by procedures described in NWMP procedure NP 20-2 "Scientific Notebooks." Methods for justification, evaluation, approval, and documentation of deviation from test standards and establishment of special prepared test procedures will be documented in the Scientific Notebooks. Procedures including use of replicates, spikes, split samples, control charts, blanks and reagent controls will be determined during the development of experimental techniques.

The numerical data will be transferred from data printouts and scientific notebooks to Microsoft Excel (Office 97 version or later) spreadsheets. Data transfer and reduction shall be performed in such a way to ensure that data transfer is accurate, that no information is lost in the transfer, and that the input is completely recoverable. Data transfer and reduction shall be controlled to permit independent reproducibility by another qualified individual. A copy of each spreadsheet will be taped into the scientific notebook, and a second person will compare the data recorded in the notebook and that on the spreadsheet to verify that no transcription errors have occurred during technical and/or QA review of the notebook. This verification will be documented in the notebook when it is "signed off" by the reviewer.

4.3.3 Data Identification and Use

All calculations performed as part of the activities of TP 00-07 will be documented in a scientific notebook. The notebook will be technically reviewed periodically by a second person, who will note concurrence by co-signing the examined material. If a discrepancy is found, that discrepancy and its resolution will be documented in the notebook. In addition, there will be periodic quality assurance reviews of the notebook to ensure that the requirements of NWMP procedure NP 20-2, "Scientific Notebooks" are addressed.

4.4 Equipment

A variety of measuring and analytical equipment will be used for the work described in this test plan. This equipment includes that listed below, as well as equipment not yet purchased. A complete equipment list, including serial numbers, will be maintained in the scientific notebook. Much of the instrumentation to be used for this project is newly purchased, and operating procedures have not yet been developed or written. Scientific notebooks will be used to record all laboratory work activities.

4.4.1 Weighing Equipment

Several balances are present in the facility and may be used for this project. These include a Mettler AT-261 five-decimal place electronic balance, an ANC three-decimal place balance, and top loading balances and scales with maximum ranges of 2 to 30 kilograms. Balance calibration checks will be performed routinely using the following NBS-traceable weight sets, which, in turn, are calibrated by the SNL Calibration Laboratory every 3 years:

- Troemner Calibration weight set, ASTM Class 1, Serial number 22803, 1 mg – 100 g, calibration expires 12/16/02.
- *Troemner Calibration weight*, NBS-Class 1, Serial number 42795, 100 g, calibration expires 11/19/02.
- *Troemner Calibration weight*, NBS-Class 1, Serial number 42797, 100 g, calibration expires 11/19/02.
- *Troemner Calibration weight*, NBS-Class 1, Serial number 42799, 100 g, calibration expires 11/19/01.
- *Troemner Calibration weight*, NBS-Class 1, Serial number 42800, 100 g, calibration expires 11/19/01.
- *Troemner Calibration weight*, ASTM-Class 1, Serial number 47824, 200 g, calibration expires 11/19/02.
- *Troemner Calibration weight*, ASTM-Class 1, Serial number 55335, 1000 g, calibration expires 11/19/02.
- *Troemner Calibration weight*, ASTM-Class 2, Serial number I-12, 10 kg, calibration expires 12/17/02.

Balance accuracy and precision will be checked daily or prior to use (whichever is less frequent), using the calibration weight sets listed above. Calibration checks will be recorded in the scientific notebook.

4.4.2 Liquid Measuring Equipment

Standard Laboratory Class A glassware (pipettes, volumetric flasks, etc.) will be used at all times. In addition, several adjustable Eppendorf pipettes are available for use in the laboratory. The calibration of pipettes will be checked routinely against a calibrated balance, and will be recorded in the scientific notebook.

4.4.3 Other Analytical Equipment

- *Ovens and Furnace*- Six Precision Telco Lab ovens are being used to hold samples at elevated temperatures. Temperature is monitored, maintained, and recorded on a weekly to biweekly schedule. A Fisher Isotemp furnace is used to determine LOI.
- *pH Meters and Autotitrators* – Solution pH may be measured using pH meters and/or autotitrators. A *Mettler Model MA235 pH/Ion Analyzer* and a *Mettler Model DL25 Autotitrator* will be used for this purpose. The range for all pH meters is 0.00 to 14.00. Electrodes will be calibrated before each use or daily (whichever is less frequent) with pH 4, 7, and 10 buffers manufactured by Fisher Scientific with unique lot numbers and expiration dates; traceable to the National Institute of Standards and Technology (NIST). The accuracy of the buffers is ±0.01 pH units; buffer values will be adjusted for laboratory temperatures as per buffer instruction sheets if necessary. Calibration checks will be recorded in the scientific notebook. Measuring pH in concentrated brines is difficult, and a procedure will be developed to calibrate pH meters.
- *Equipment for Chemical Analysis* – Three instruments may be used for chemical analyses. The first is a Perkin Elmer Optima 3300 DV Inductively-Coupled Plasma Optical Emission Spectrometer (ICP-OES); the second is a Cary 300 UV-Visible Spectrophotometer; and the third, is a UIC, Inc. Carbon Analyzer, consisting of an acidification module, a furnace module, and a CO_2 coulometer. These instruments will be user-calibrated each time they are used and documented in the scientific notebook.
- *Equipment for Mineralogical, and Textural Characterization* – The mineralogy and texture may be characterized using either an Olympus BX60 Polarizing Microscope or a JEOL JSM 5900LV scanning electron microscope (SEM). Calibration standards will be used to verify instrument magnification when these instruments are used. Bulk sample mineralogy will be determined using a Bruker AXS D-8 Advance X-Ray Diffractometer (XRD). A mineral standard will be run periodically to verify diffraction line positions. Calibration results will be documented in the scientific notebook.

NMWP Activity/Project Specific Procedures (SPs) will be written for these instruments as necessary. Until that time, detailed procedure descriptions will be documented in laboratory notebooks.

5.0 Training

All personnel involved in the experiments described in this Test Plan will be trained and qualified for their assigned work. This requirement will be implemented through NWMP procedure NP 2-1, "Qualification and Training." Evidence of training to assigned NPs, SPs, TOPs, TP 00-07, ES&H procedures, and any other required training will be documented through Form NP 2-1-1 *Qualification and Training.* Annual Refresher QA training will ensure on-site personnel are trained to the NWMP QA Program. Specifically, the following Nuclear Waste Management Program Procedures (NPs) and Activity/Project Specific Procedures (SPs) are applicable:

- SOP-C001 – "Standard Operating Procedure for Activities in the SNL/Carlsbad Laboratory Facility."
- SP 13-1 – "Chain of Custody"
- NP 6-1 – "Document Review Process"
- NP 13-1 – "Sample Control"
- NP 12-1 – "Control Of Measuring And Test Equipment"
- NP 20-2 – "Scientific Notebooks"
- NP 2-1 – "Qualification and Training"
- NP 17-1 – "Records"

In addition, SPs will be written for use of the ICP, SEM, XRD, Carbon analyzer, UV-Vis spectrophotometer, and assorted balances and scales used in the laboratory. Sample preparation procedures, which may vary from sample to sample as work scope evolves, will be detailed in Scientific Notebooks, in accordance with NWMP procedure NP 20-2.

6.0 Health and Safety

All of the health and safety requirements relevant to the work described in this Test Plan and the procedures that will be used to satisfy these requirements are described in ES&H standard operating procedures. SOP-C001 describes the non-radiological hazards associated with these experiments and describes the procedures to deal with those hazards, including all the training requirements for personnel involved in conducting the experiments. In addition, a Radiological Work Permit (RWP) will be written for procedures involving use of the X-Ray Diffractometer. Additional SPs and RWPs may be mandated by SNL ES&H requirements and their issuance will not require revision of this Test Plan.

7.0 Permitting/Licensing

There are no special licenses or permit requirements for the work described in this Test Plan.

8.0 References

Al, T.A., Blowes, D.W., Martin, C.J., Cabri, L.J., and Jambor, J.L. (1997) Aqueous geochemistry and analysis of pyrite surfaces in sulfide-rich mine tailings. *Geochim. Cosmochim. Acta,* 61, 2353–2366.

Brush L. H. (1990) *Test Plan for Laboratory and Modeling Studies of Repository and Radionuclide Chemistry for the Waste Isolation Pilot Plant.* SAND90-0266, Sandia National Laboratories, Albuquerque, NM.

Bynum R. V., Stockman, Papenguth H. W., Wang Y., Peterson A. C., Krumhansl J. L., Nowak E. J., Cotton J., Patcher S. J., and Chu M. S. Y. (1998) Identification and evaluation of appropriate backfills for the Waste Isolation Pilot Plant (WIPP). *International Workshop on the Uses of Backfill in Nuclear Waste Repositories*, Carlsbad, New Mexico, US, May 1998. p.2-178–2-187.

Dietzel M. and Usdowski E. (1996) Coprecipitation of Ni^{2+}, Co^{2+}, and Mn^{2+} with galena and covellite, and Sr^{2+} with calcite during crystallization via diffusion of H_2S and CO_2 through polyethylene at 20°C: Power law and Nernst law control of trace element partitioning. *Chemical Geology*, 131, 55–65.

Kolthoff, I. M., and Sandell, E. B. (1961) Textbook of Quantitative Inorganic Analysis, 3rd Ed., The Macmillan Company, New York.

Königsberger E., Königsberger L. C., and Gamsjäger H. (1999) Low-temperature thermodynamic model for the system Na_2CO_3–$MgCO_3$–$CaCO_3$–H_2O. *Geochimica et Cosmochimica Acta*, 63, 3105–3119.

Königsberger E., Schmidt, P., and Gamsjäger H. (1992) Solid-solute phase equilibrium in aqueous solution. VI. Solubilities, complex formation, and ion-interaction parameters for the system Na^+—Mg^{2+} —ClO_4^-—CO_2—H_2O. *Journal of Solution Chemistry*, 21, 1195–1216.

Lide, D.R. (1997) Handbook of Chemistry and Physics, 78th Ed., CRC Press, New York.

Nguyen-Trung, C., Palmer, D.A., and Giffaut, E. (1997) Solubility and complex formation of TcO_2 in aqueous solution up to 70°C, 0.1 Mpa (extended abstract). In Palmer D.A., and Wesolowski, D.J. (Eds.), Proceedings of the 5th International Symposium on Hydrothermal Reactions, Oak Ridge National Laboratories, p.293–294.

Papenguth H. W., Krumhansl J. L., Bynum R. V., Wang Y., Kelly J. W., Anderson H. A., and Nowak E. J. (1998) Status of research on magnesium oxide backfill. *International Workshop on the Uses of Backfill in Nuclear Waste Repositories*, Carlsbad, New Mexico, US, May 1998. p.3-43 to 3-63.

Robinson, K. (1996) Preparing Synthetic Brines for Chemical Retardation and Transport Experiments. Sandia National Laboratories TOP-544

Stumm, W., and Morgan, J.J. (1996) Aquatic Chemistry (3rd edition). John Wiley & Sons, Inc., New York, 1022 p.

Telander, M.R., and Westerman, R.E. (1993). Hydrogen generation by metal corrosion in simulated Waste Isolation Pilot Plant environments: Progress report for the period November 1989 through December 1992. SAND92-7347.

Telander, M.R., and Westerman, R.E. (1997). Hydrogen generation by metal corrosion in simulated Waste Isolation Pilot Plant environments. SAND96-2538.

Wang, L.-W., Wang, Z.-C., Yang, H., Yang, G.-L. (1999). The study of thermal stability of the SiO_2 powders with high specific surface area. *Materials Chemistry and Physics*, 57, 260–263.

Wang, Z., Moore, R.C., Felmy, A.R., Mason, M.J., Kukkadapu, R.K. (2001). A study of the corrosion products of mild steel in high ionic strength brines. *Waste Management*, 21, 335–341.

Wolery T. J. (1992) *EQ3NR, A Computer Program for Geochemical Aqueous Speciation-Solubility Calculations: Theoretical Manual, User's Guide, and Related Documentation (Version 7.0)*. Lawrence Livermore National Laboratory, UCRL-MA-110662 PT III (1992).

Wolery T. J. and Daveler S. A. (1992*) EQ6, A Computer Program for Reaction Path Modeling of Aqueous Geochemical Systems: Theoretical Manual, User's Guide, and Related Documentation (Version 7.0)*. Lawrence Livermore National Laboratory, UCRL-MA-110662PTIV (1992).

Xiong, Y.-L., Wood, S.A. (2001) Hydrothermal transport and deposition of rhenium under subcritical conditions (up to 200°C) in light of experimental studies. *Economic Geology and the Bulletin of The Society of Economic Geologists*, 96, 1429–1444.

Zhang, P.-C., Anderson, H.L.Jr., Kelly, J.W., Krumhansl, J.L., Papenguth, H.W., 1999, Kinetics and mechanisms of formation of magnesite from hydromagnesite in brine. SAND99-1946J.

Hydration of Magnesium Oxide in the Waste Isolation Pilot Plant[1]

Anna C. Snider
Carlsbad Programs Group, Sandia National Laboratories
Carlsbad, NM 88220, U.S.A.

ABSTRACT

Magnesium oxide (MgO) is the only engineered barrier being emplaced in the Waste Isolation Pilot Plant (WIPP), a U.S. Department of Energy repository for transuranic waste. MgO will control actinide solubilities by consuming CO_2 from possible microbial activity, by buffering the pH between 8.5 and 9.5, and by reducing the amount of free water in the repository. This paper discusses results from experiments measuring the hydration of MgO. Results suggest that periclase (MgO) hydrates rapidly to brucite ($Mg(OH)_2$) in de-ionized water and 4 M NaCl solution at 90°C; the hydration rate decreases significantly as temperature decreases. In ERDA-6, a NaCl-rich WIPP brine, MgO hydrates directly to brucite; in GWB, a high-Mg brine, periclase hydrates to magnesium chloride hydroxide hydrate(s) until the dissolved Mg^{2+} concentration decreases sufficiently to form brucite. Under humid conditions MgO fully hydrates at higher humidities. All data are consistent with diffusion-limited hydration reactions.

INTRODUCTION

The Waste Isolation Pilot Plant (WIPP) is a U.S. Department of Energy repository designed for the disposal of defense-related transuranic waste. The WIPP is located in southeast New Mexico at a depth of 655 m in the Salado, a Permian bedded salt formation. Magnesium oxide (MgO) is currently the only engineered barrier certified by the U.S. Environmental Protection Agency. The MgO currently being emplaced is supplied by Premier Chemicals of Gabbs, Nevada. MgO emplaced in the WIPP will reduce actinide solubilities by consuming CO_2 from possible microbial degradation of organic material (cellulose, plastic, and rubbers, and buffer the system between pH 8.5 and 9.5 and P_{CO_2} at $10^{-5.5}$ atm. MgO will reduce the amount of water in the repository if subsequent carbonation produces hydrous magnesium carbonates, however formation of magnesite ($MgCO_3$) would release water. Water (brine) within the WIPP is postulated to derive from the surrounding Salado Formation or from human drilling intrusion penetrating underlying brine pockets of the Castile formation.

Investigations on the efficacy of MgO are underway at Sandia National Laboratories' Carlsbad Programs Group. Experiments include possible repository conditions. The ambient temperature of the Salado Formation. at the depth of the repository (655 m) is 28 °C [1]. Studies focus on hydration and carbonation rates, and characterization of the products formed under humid and inundated conditions. This paper describes chemical and mineralogical characterization of MgO and the hydration experiments. These experiments help determine hydration rates and pathways, and whether the reaction products passivate MgO.

---

[1] This work is covered by WBS #1.3.5.4.3.1

EXPERIMENTS

Characterization of Premier Chemicals MgO by physical and chemical analyses determined mineralogy and quantity or impurities. Bulk MgO and uncrushed sieved fractions were analyzed. Physical analyses utilized a JEOL 5900LV scanning electron microscope (SEM) and a Brucker X-ray diffractometer (XRD). The SEM was used to identify major and minor mineral phases and to document grain textures, such as the physical distribution of minerals and intergranular porosity. SEM analysis was performed under backscatter electron mode at 15 kV in order to emphasize compositional differences. Chemical analyses included gravimeteric determination of silica coupled with analysis by a Perkin Elmer Optima 3300 DV inductively coupled plasma optical emission spectrometer (ICP-OES) [2]. These analyses determine the amount of unreactive silicates and aluminates present in Premier Chemicals MgO.

Inundated hydration experiments are currently being run, under agitated conditions, to evaluate the effects of various factors on MgO hydration rates. In the first series of hydration experiments, 5 g of Premier MgO was placed in 125-mL polypropylene bottles, each containing either deionized (DI) water or one of three solutions: 4 M NaCl, ERDA-6 (a synthetic Castile brine), or Generic Weep Brine (GWB a synthetic Salado brine). The first two liquids were included in an effort to help develop a mechanistic understanding of the hydration process. Samples were aged in ovens at 25, 50, 70, or 90 °C, and were agitated frequently. Sample agitation was performed to eliminate the formation of lithified hydration products, minimizing the likelihood that cake formation would inhibit hydration by limiting brine access to unhydrated MgO. The effects of cake formation are being examined in a separate series of experiments, not presented here. However, hydration products may still inhibit hydration by coating individual particles, or by plugging the internal pores in the MgO grains.

Periodically, samples are removed from the ovens, cooled, and the pH measured. The solid fraction is then filtered using Whatman #40 filters, rinsed with DI water to remove any remaining brine, and then dried, crushed, and characterized by XRD and SEM. The loss on ignition (LOI) at 500 °C (brucite dehydrates at ~350 °C) is used to calculate the amount of hydrated material in each sample.

The humid hydration samples consist of uncrushed Premier Chemicals MgO and are being reacted at temperatures of 25, 40, 60, and 80 °C and relative humidities of 35, 50, 75, and 95%. Samples of MgO are contained in six-well polycarbonate trays, with 3 g of MgO in each well. Four trays are stacked in sealed polypropylene containers. Each container holds a saturated salt solution providing the desired relative humidity. Relative humidity will vary a few percent with temperature, the exception being solutions of $NaBr{\cdot}2H_2O$, which may vary as much as 8% at 25 °C [3]. The trays in each container are elevated on plastic blocks above the salt solution. Holes have been drilled in the bottom and top of each tray; and the upper lip of each well is notched. The holes and notches allow air circulation through each sample well.

Samples were periodically collected over a period of months to years. Each sample is dried and analyzed by LOI and a few entirely reacted samples by XRD. We assume that MgO hydration is the only reaction that occurs to a significant extent during these experiments because MgO will only be in contact with water vapor. Analysis by XRD will test this assumption.

RESULTS

XRD patterns show that Premier Chemicals MgO is dominated by periclase (MgO) and contains other minor phases such as forsterite (Mg_2SiO_4), lime (CaO), monticellite ($CaMgSiO_4$), spinel ($MgAl_2O_4$), and ulvospinel ($FeTi_2O_4$). In sieved batches of MgO the larger size fractions contain relatively more impurities than the smaller particle fractions.

Quantitative mineral analysis results are shown in Table 1. Reactive minerals (MgO + CaO) constitute approximately 90 wt %, whereas the unreactive constituents constitute the remaining 10 wt %.

Analysis of SEM images reveals that MgO grains are angular and highly fractured. Each individual grain contains subrounded MgO grains surrounded by Ca-Mg silicates or lime.

Results from the inundated hydration experiments are expressed as hydration (mol % brucite or wt % LOI) vs. time (Figures 1 and 2). In DI water, 4 M NaCl, and in ERDA-6, XRD studies indicate that brucite ($Mg(OH)_2$) is the only hydration phase present. In GWB a magnesium chloride hydroxide hydrate (probably $Mg_3(OH)_5Cl{\cdot}4H_2O$) precipitates initially; brucite becomes the stable hydration phase only at higher degrees of hydration. Because the magnesium chloride hydroxide hydrate and brucite lose different amounts of water upon ignition, the extent of hydration is expressed as wt % loss on ignition.

Table I. Mineral constituents of Premier Chemicals MgO

	A				B			
Premier MgO	wt % MgO (Periclase)	wt % Mg_2SiO_4 (Forsterite)	wt % CaO (Lime)	wt % $MgAl_2O_4$ (Spinel)	wt % MgO (Periclase)	wt % $MgCaSiO_4$ (Monticellite)	wt % CaO (Lime)	wt % $MgAl_2O_4$ (Spinel)
Results	86.86	5.027	2.386	2.071	88.73	5.756	1.273	2.071
Standard Deviation	0.05	0.092	0.040	0.043	0.53	0.105	0.059	0.043

Data complied from ICP-OES and gravimetric silica method results. Scenario (A) is calculated assuming Mg_2SiO_4 is the only silicate present, (B) assumes $MgCaSiO_4$ is the only silicate occuring in the sample.

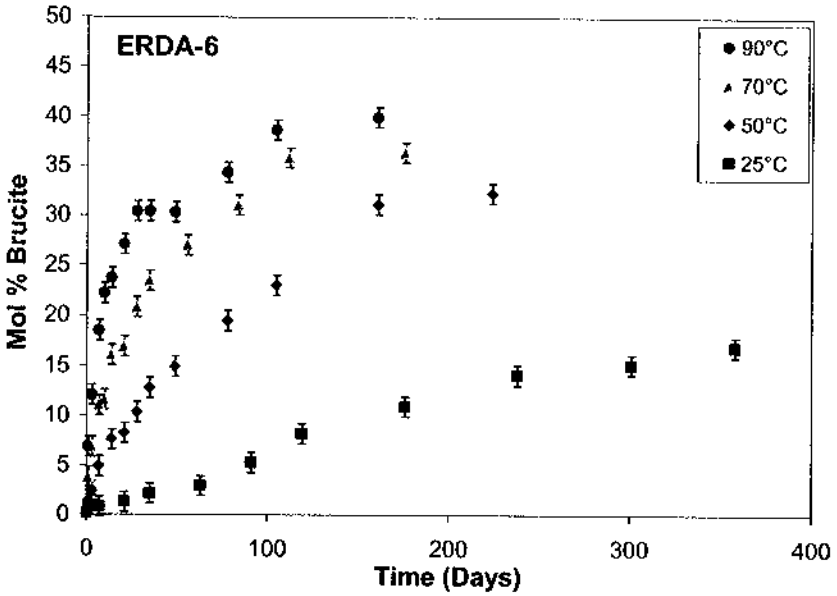

Figure 1. Hydration as a function of time of samples from ERDA-6.

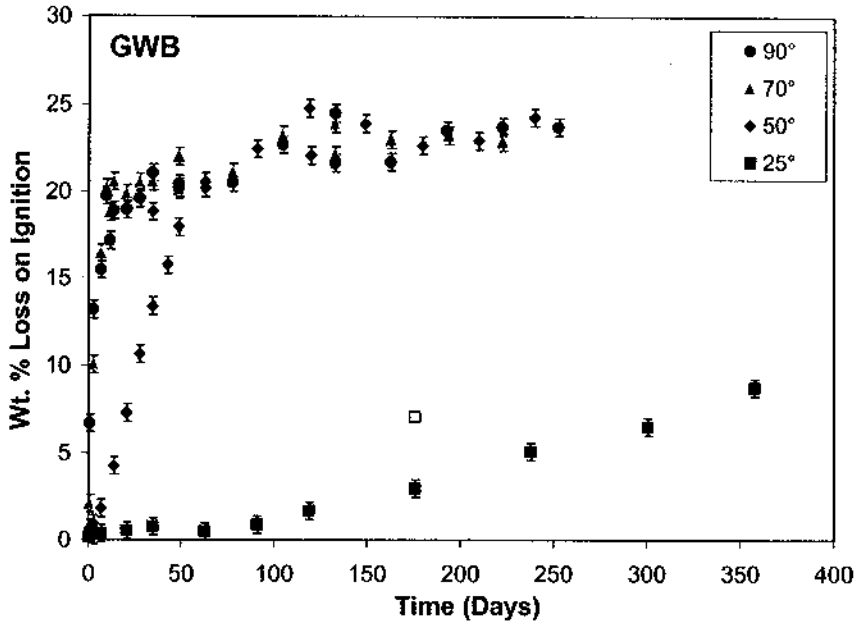

Figure 2. Hydration as a function of time of samples from GWB.

Hydration proceeded to completion in DI water at 90 and 70 °C and in 4 M NaCl at 90 °C. After 14 days, 90 °C samples in DI water reached 82–85 mol % hydration. XRD patterns indicate that no periclase remains. After 160 days, ERDA-6 samples at 90 °C hydrated to 40 mol % (Figure 1). GWB behaves somewhat differently (Figure 2). The 70 and 90 °C samples in GWB behave similarly, rising very rapidly initially, and after 10 days the rate of hydration slows and appears to flatten to approximately 23 wt % LOI. The samples at 50 °C initially hydrate at a slower rate than the 70 and 90 °C samples. After 50 days the 50 °C samples converge with the higher temperatures and continue to follow the same trend at approximately 23 wt % LOI. If the

GWB hydration product was entirely brucite then 23 wt % LOI would be equivalent to approximately 80 mol % hydration. If magnesium chloride hydroxide hydrate was the only hydration product then 23 wt % LOI would be equivalent to approximately 33 mol %.

XRD analysis of GWB samples across the plateau indicates that periclase is continuing to decrease, while brucite peaks are increasing in intensity. The rate of hydration is most likely linked to changes in mineral phases between magnesium chloride hydroxide hydrate and brucite. It is not evident how magnesium chloride hydroxide hydrate behaves over time. The mineral is thought to be an amorphous phase at higher temperatures and thus was not detected by XRD. However, its existence is inferred from SEM images coupled with Energy Dispersive System (EDS, that identify Mg-Cl phases) at all temperatures and XRD patterns from 25 °C samples. GWB contains high concentrations of Mg (1 M). MgO dissolves and reprecipitates as magnesium chloride hydroxide hydrate. This reaction, which consumes excess Mg in the brine, continues until the Mg concentration drops to ~0.7 M, according to EQ6 calculations. At this point, brucite becomes the stable hydroxide phase.

Mol % conversion plots for humid hydration data show that hydration is relatively slow at lower temperatures and humidities, but occurs readily at elevated temperatures. After four weeks, the degree of hydration reached over 80% in 95 and 75% relative humidity samples at 80 °C (Figure 3). XRD patterns from 80 °C and 95% relative humidity after 30 days confirm that brucite is the only hydration product present. No periclase peaks are evident. At 60 °C, the experiments at higher humidities slowed and appear to level out around 70 mol % conversion. There is evidence of hydration at 25 °C and 50% and 75% relative humidity, a range that includes the expected relative humidity in WIPP disposal rooms after filling and sealing, about 70%. The experiments at 35% relative humidity have not shown any evidence of hydration at 25, 40, 60, or even 80°C. An interesting point to note is that MgO in DI water at 90 °C and MgO exposed to high relative humidities at 80 °C behave similarly. They both are completely hydrated by 37 days.

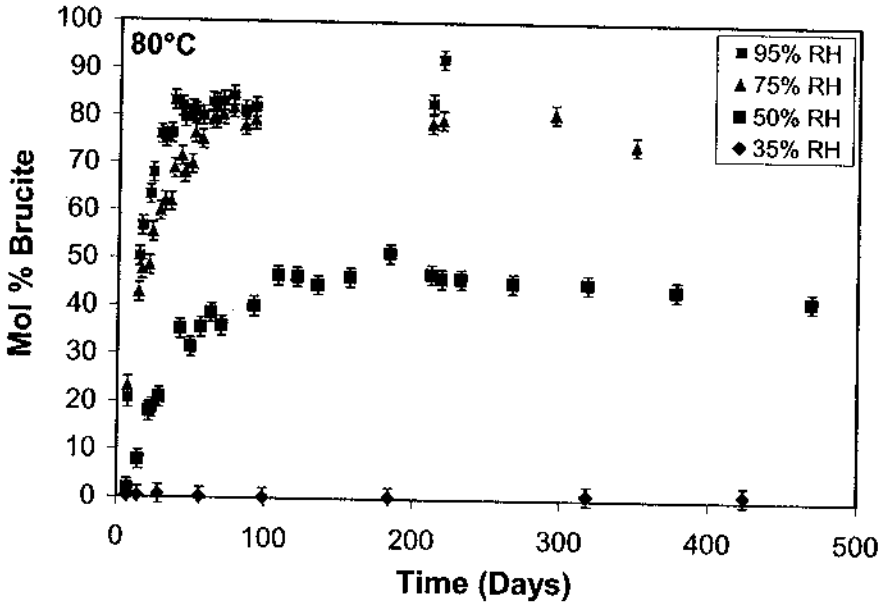

Figure 3. Hydration as a function of time for humid experiments at 80 °C.

CONCLUSION

Premier Chemicals MgO comprises approximately 90 wt % periclase and 10 wt % silicates, aluminates, and lime. Permier MgO hydrates under inundated environments relevant to predicted WIPP conditions (28 °C). Brucite is the reaction product formed in DI water, 4 M NaCl and ERDA-6 systems. In GWB, magnesium chloride hydroxide hydrate forms initially. Magnesium chloride hydroxide hydrate has been identified by XRD at 25 °C and inferred at higher temperatures by SEM and LOI. Brucite becomes the stable hydration phase, once the concentration of Mg in solution drops below ~0.7 M. ERDA-6 and GWB experiments continue to hydrate as testing progresses. Humid hydration samples exposed to higher relative humidities behave in a similar manner to samples inundated in DI water.

ACKNOWLEDGEMENTS

Sandia National Laboratories is a multi-program laboratory operated by Sandia Corporation, a Lockheed Martin Company, for the United States Department of Energy under contract DE-AC04-94AL85000.

REFERENCES

1. D.E. Munson, R.L. Jones, D.L. Hoag, and J.R. Ball, Report No. SAND87-2488, Sandia National Laboratories,1987.
2. L. Greenspan, Journal of Research of the National Bureau of Standards – Physics and Chemistry, **81A** (1), 89-96 (1977).
3. I. M. Kolthoff and E.B. Sandell, *Textbook of Quantitative Inorganic Analysis* (The Macmillan Company, New York, 1961).

4.3 Carbonation Rates of the Magnesium Oxide Hydration Product Brucite in Various Solutions

Yongliang Xiong and Anna C. Snider
Sandia National Laboratories, MS 1395
4100 National Parks Hwy.
Carlsbad, NM 88220

Abstract

Sandia National Laboratories' Carlsbad Programs Group is investigating several aspects of the efficacy of MgO under expected repository conditions. Previous work has been described in detail in status reports to the DOE by Bryan and Snider (2001a, 2001b), Snider (2002) and Snider and Xiong (2002a). This report focuses on the kinetics of carbonation of the MgO hydration product brucite ($Mg(OH)_2$), in various solutions at ambient laboratory temperature (referred to hereafter as "room temperature") and ambient laboratory CO_2 pressure (referred to as "atmospheric CO_2 pressure").

In the previous status report (Snider and Xiong, 2002a), the reaction path at room temperature and atmospheric CO_2 pressure has been described as periclase (MgO) → magnesium chloride hydroxide hydrate (presumably $Mg_3(OH)_5Cl{\cdot}4H_2O$) → brucite → hydromagnesite ($Mg_5(CO_3)_4(OH)_2{\cdot}4H_2O$). Therefore, the carbonation of brucite is fundamentally important to the performance of the repository. Should CO_2 be produced by possible microbial degradation of organic materials in the repository, it would be sequestered by the carbonation of brucite.

The conversion rate of brucite to hydromagnesite in low-ionic-strength H_2O (de-ionized, or DI, H_2O with small quantities of dissolved Ca, CO_2, Mg, etc.) at room temperature and atmospheric CO_2 pressure is 1.3×10^{-5} h^{-1}. Measured conversion rates in 4 M NaCl, ERDA-6, and GWB are 7.3×10^{-6} h^{-1}, 5.4×10^{-6} h^{-1}, and 2.3×10^{-6} h^{-1}, respectively. These rates are strongly correlated with ionic strength.

The uptake rates of CO_2 by brucite in various solutions at room temperature and atmospheric CO_2 pressure are also being determined experimentally. Measured uptake rates of CO_2 in low-ionic-strength H_2O, 4 M NaCl, ERDA-6, and GWB are 2.75×10^{-7} mol g^{-1} h^{-1} (2409 μmol g^{-1} $year^{-1}$), 1.55×10^{-7} mol g^{-1} h^{-1} (1358 μmol g^{-1} $year^{-1}$), 1.15×10^{-7} mol g^{-1} h^{-1} (1007 μmol g^{-1} $year^{-1}$), and 4.9×10^{-8} mol g^{-1} h^{-1} (430 μ g^{-1} $year^{-1}$), respectively. These rates are also strongly correlated with ionic strength. The uptake rates of CO_2 by brucite are orders of magnitude higher than the CO_2 production rates predicted for possible microbial degradation of the organic materials in transuranic waste (cellulosics, plastics, and rubbers) based on experimental studies (~1 to ~25 μmol g^{-1} $year^{-1}$). Therefore, it is unlikely that microbial degradation of organic materials will result in high partial pressures of CO_2 in the repository.

Introduction and Objectives

In the Compliance Certification Application, the U.S. Department of Energy (DOE) asserted that MgO, along with panel closures, shaft seals, and borehole plugs, would help meet the requirement for multiple natural and engineered barriers (U.S. DOE, 1996), one of the assurance requirements in the regulations for the radioactive constituents of transuranic (TRU) waste (U.S Environmental Protection Agency, 1993). In May 1998, the EPA certified that the WIPP complies with these regulations (U.S. EPA, 1998). In its certification, the EPA recognized MgO as the only engineered barrier in the Waste Isolation Pilot Plant (WIPP) disposal system, and agreed that MgO will prevent or delay the movement of radionuclides toward the accessible environment. MgO will sequester CO_2 generated by possible microbial degradation of organic materials (cellulosics, plastics, and rubbers) in the TRU waste in the repository. Thus, the engineered barrier will maintain the pH and CO_2 fugacity in the repository within favorable ranges, in which actinide solubilities in brine are minimized.

Early work on the engineered barrier conducted at Sandia National Laboratories in Albuquerque was summarized in Papenguth et al. (1997, 1999). This early work was conducted at a CO_2 pressure of 1 atm. Since the opening of the laboratory at Sandia in Carlsbad, experimental work has been conducted at much lower partial pressures of CO_2 ($P_{CO_2} \approx 10^{-3.5}$ atm and $P_{CO_2} = 10^{-1.3}$ atm). In the previous status report (Snider and Xiong, 2002a), the reaction path at ambient laboratory temperature (referred to hereafter as "room temperature") and ambient laboratory CO_2 pressure (referred to as "atmospheric CO_2 pressure") has been established as periclase (MgO) $\rightarrow$ magnesium chloride hydroxide hydrate (presumably $Mg_3(OH)_5Cl{\cdot}4H_2O$) $\rightarrow$ brucite ($Mg(OH)_2$) $\rightarrow$ hydromagnesite ($Mg_5(CO_3)_4(OH)_2{\cdot}4H_2O$). Therefore, the carbonation of brucite (the hydration product of periclase) is fundamentally important to the performance of the repository. As described in our previous status report (Snider and Xiong, 2002a), there are to our knowledge no previous experimental studies on the carbonation rates of periclase or brucite under conditions relevant to the WIPP. Therefore, carbonation experiments under WIPP-relevant conditions must be conducted.

The objectives of the current experiments are multifold: (1) continued characterization of Premier Chemicals MgO; (2) determination of hydration rates and pathways; (3) quantification of carbonation rates and identification of the metastable mineral(s) produced; (4) quantification of the effect(s) of possible lithification on hydration and carbonation rates and pathways. These experiments are being run in accordance with Snider and Xiong (2002b). This report focuses on the carbonation rates of brucite in various solutions at room temperature and atmospheric CO_2 pressure.

Carbonation Rate Experiments

CONVERSION RATES OF BRUCITE TO CARBONATES

Experimental design and procedures regarding carbonation-rate experiments have been described in detail by Snider and Xiong (2002b). The carbonation of brucite as hydromagnesite can be expressed as the following reaction:

$$5Mg(OH)_2(s) + 4CO_2(aq \text{ or } g) \rightleftharpoons Mg_5(CO_3)_4(OH)_2 \cdot 4H_2O \quad (1)$$

As suggested by Reaction 1, carbonation can take place under both aqueous (inundated) and humid conditions. In carbonation experiments using Fisher brucite as starting material, experiments are designed to investigate carbonation rates in both inundated and humid scenarios. This report concentrates on the carbonation rates in aqueous media.

In carbonation experiments under inundated conditions, samples are continually monitored for changes in pH, and solutions are periodically sampled for chemical analysis of elements such as Ca and Mg with an inductively coupled plasma optical emission spectrometer (ICP-OES). After the termination of runs, reaction products are filtered, dried and analyzed for the quantities of C that have been incorporated into solid phase(s) with a UIC carbon coulometer, and the carbonate phase(s) are determined with an X-ray diffractometer (XRD) and scanning electron microscope (SEM).

Figure 1 illustrates the conversion of brucite to carbonate as a function of time at room temperature and atmospheric CO_2 pressure. From Figure 1, it is obvious that experiments in de-ionized (DI) H_2O have the highest conversion rates, whereas those in GWB have the lowest conversion rates. The conversion rates in 4 M NaCl and ERDA-6 are similar, although the rates in 4 M NaCl are slightly higher than those in ERDA-6. In the calculations that led to these conclusions, the conversion in DI H_2O and 4 M NaCl is calculated as the conversion to hydromagnesite because the initial concentrations of Ca in these solutions are negligible. The conversion rates in ERDA-6 and GWB are calculated as the conversion to carbonates (including calcite, $CaCO_3$, and hydromagnesite) because the initial concentrations of Ca in these solutions are 0.012 M and 0.014 M, respectively. The precipitation of calcite by the reaction

$$Ca^{2+} + CO_2(aq) + H_2O(l) \rightleftharpoons CaCO_3(s) + 2H^+ \quad (2)$$

may also contribute to the total C incorporated into the reaction solid product. However, 1 mol of Ca will consume 1 mol of CO_2. In the conversion of brucite to hydromagnesite by Reaction 1, 5 moles of brucite will consume 4 moles of CO_2. Therefore, the conversion rate calculated using the molar ratio suggested by Reaction 1 would provide the minimum conversion rates for ERDA-6 and GWB.

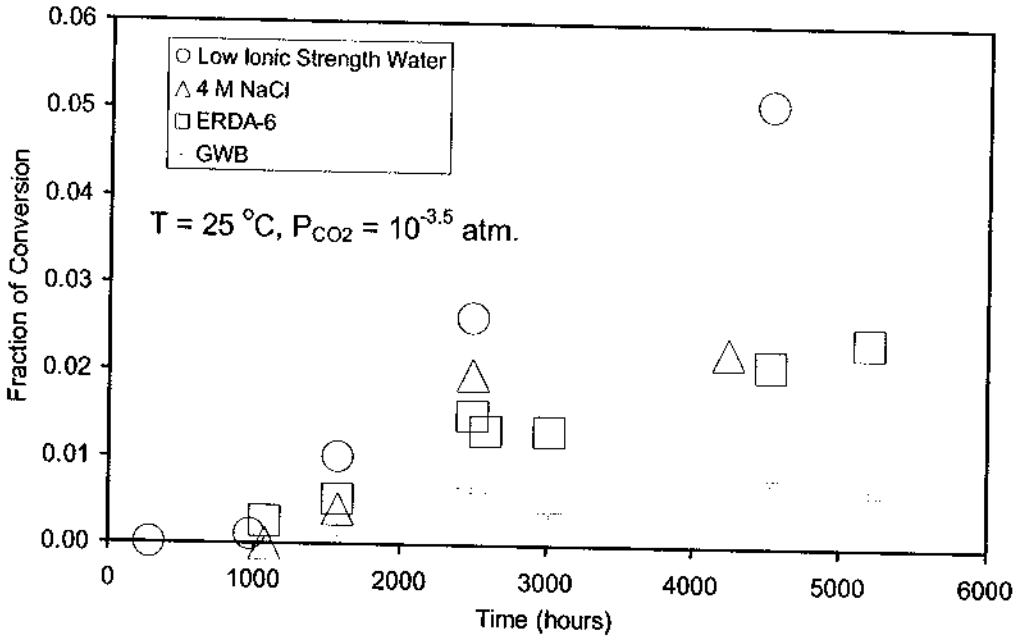

Figure 1. Conversion of burcite to carbonate(s) vs. time at room temperature and atmospheric CO_2 pressure.

As experiments started with DI H_2O have the lowest ionic strength ($I \approx 0.005$ M, referred to hereafter as "low-ionic-strength H_2O") among these solutions, and those in GWB have the highest ionic strength ($I = 7.2$ M), the above results imply that the conversion is strongly correlated with ionic strength. To further explore this, fractions of conversion for experiments terminated at the same time are plotted against ionic strength. Figure 2 displays the relation between the fraction of conversion and ionic strength for experiments terminated after 3019 h. From Figure 2, it is apparent that fraction of conversion has a negative linear relation with ionic strength. Such a correlation may be related to the solubility of CO_2 in solutions as a function of ionic strength. A detailed treatment of this relation will be presented in a future report.

To further demonstrate this dependence, Figure 3 shows conversion for runs simultaneously terminated at 3790 h in solutions with six different ionic strength at 40 °C and atmospheric CO_2 pressure. Figure 3 also displays a strong linear relationship between ionic strength and conversion, consistent with the relationship observed for experiments at room temperature.

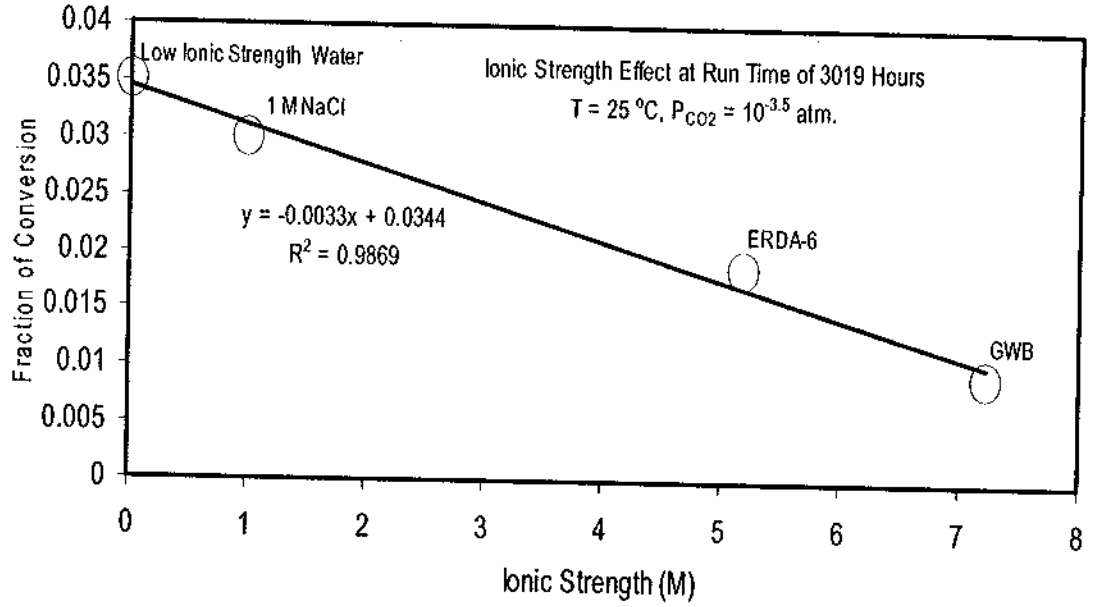

Figure 2. Conversion of brucite to carbonate(s) vs. ionic strength at room temperature and atmospheric CO_2 pressure, 3019-h runs.

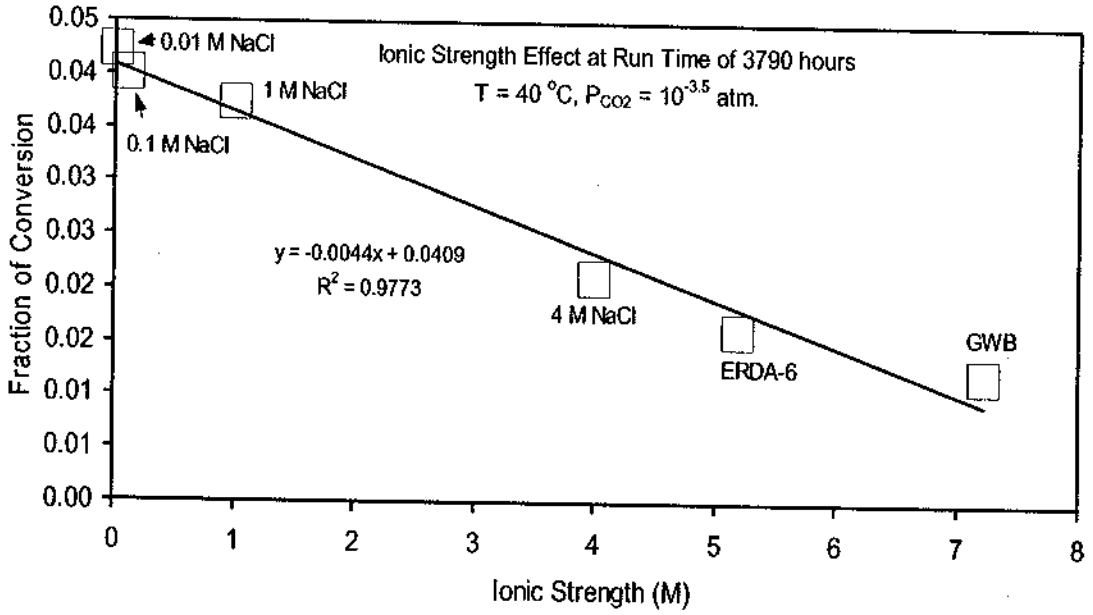

Figure 3. Conversion of brucite to carbonate(s) vs. ionic strength at 40 °C and atmospheric CO_2 pressure, 3790-h runs.

Based upon linear regression, the conversion rates in different solutions are presented in Table 1.

Table 1. Conversion Rate of Brucite to Carbonate(s) in Various Solutions

Solutions	Ionic Strength (M)	Conversion Rate (h^{-1})
Low-ionic-strength H_2O	~0.005	$(1.29 \pm 0.18) \times 10^{-5}$
4 M NaCl	4.0	$(7 \pm 3) \times 10^{-6}$
ERDA-6	5.2	$(5.37 \pm 0.64) \times 10^{-6}$
GWB	7.2	$(2.29 \pm 0.62) \times 10^{-6}$

From Table 1, it is apparent that ionic strength has a strong effect on conversion rates. The conversion rate in low-ionic-strength H_2O is almost 6 times higher than that in GWB. The conversion rate in ERDA-6 is about twice that in GWB. The conversion rate in 4 M NaCl solution is similar to that in ERDA-6. In Figure 4, conversion rates are plotted against ionic strength, demonstrating that conversion rates have a good linear relation with ionic strength. The linear relation can be described as:

$$k = (1.34 \pm 0.09) \times 10^{-5} - (1.70 \pm 0.19) \times 10^{-6} I \ (r^2 = 0.9744), \quad (3)$$

in which k is conversion rate in h^{-1} and I is ionic strength in M. Using such a relation, we can predict conversion rates of brucite to carbonates over a wide range of ionic strength should ERDA-6 or GWB change ionic strength due to reaction with the engineered barrier. However, experimental studies in solutions with ionic strength higher than that of GWB should be conducted to determine rates if the ionic strength significantly exceeds that of GWB. Reaction-path calculations using EQ6, Version 7.2 (Wolery and Daveler, 1992) suggest that the reaction of GWB with MgO could increase the ionic strength to values higher than that of GWB.

The above conversion rates are preliminary rates at a CO_2 partial pressure of about $10^{-3.5}$ atm. When the conversion rates at other partial pressures of CO_2 become available and the dependence of conversion rates on the CO_2 partial pressure is determined, we will be able to assess the time scale required for about 62.5% conversion of brucite to carbonate(s) (fraction of conversion = 0.625) in ERDA-6 or GWB. Carbonation of 62.5% of the engineered barrier is required because of the fact that the molar ratio of the MgO to be emplaced in the WIPP to the total C in organic materials in the TRU waste to be emplaced is 1.6 (Snider and Xiong, 2002a). This molar ratio means that after 62.5% carbonation of the engineered barrier, all of the CO_2 that could be produced by microbial degradation of organic materials in the waste will be sequestered.

Therefore, when the relation between conversion rates and partial pressures of CO_2 is quantitatively determined, we can evaluate with confidence the time scale required for carbonation of 62.5% of the engineered barrier at various partial pressures of CO_2. This will then lead to increased confidence with the performance assessment of the WIPP.

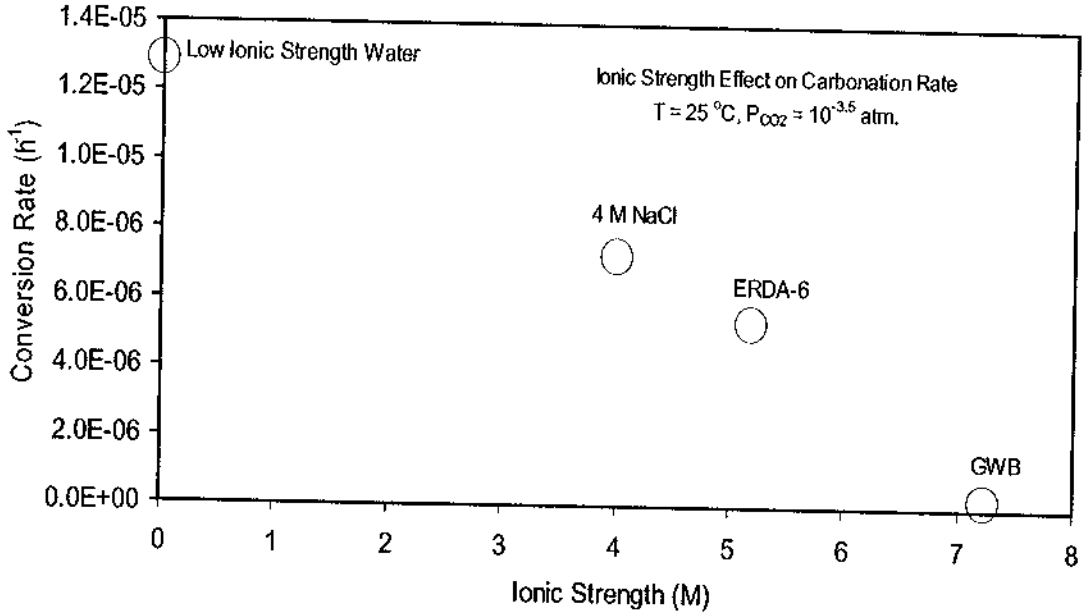

Figure 4. Conversion rate of brucite to carbonates vs. ionic stength at room temperature and atmospheric CO_2 pressure.

UPTAKE RATES OF CO_2

It is necessary to quantify the rate of CO_2 uptake by MgO to determine if CO_2 produced by possible microbial degradation of organics could be consumed in the WIPP.

Figure 5 illustrates the consumption of CO_2 as a function of time. Notice that the consumption of CO_2 is normalized to the mass the starting material brucite. The units of uptake rates determined from this plot are in mol g^{-1} h^{-1}. It is certainly preferable to express uptake rates in terms of surface area of the starting material instead of its mass. However, the apparatus used to determine specific surface area in our laboratory is undergoing repairs. Therefore, the specific surface area of the starting material cannot be determined at this time. As soon as the specific surface area of the starting material is determined, the above units will be converted to mol cm^{-3} h^{-1}.

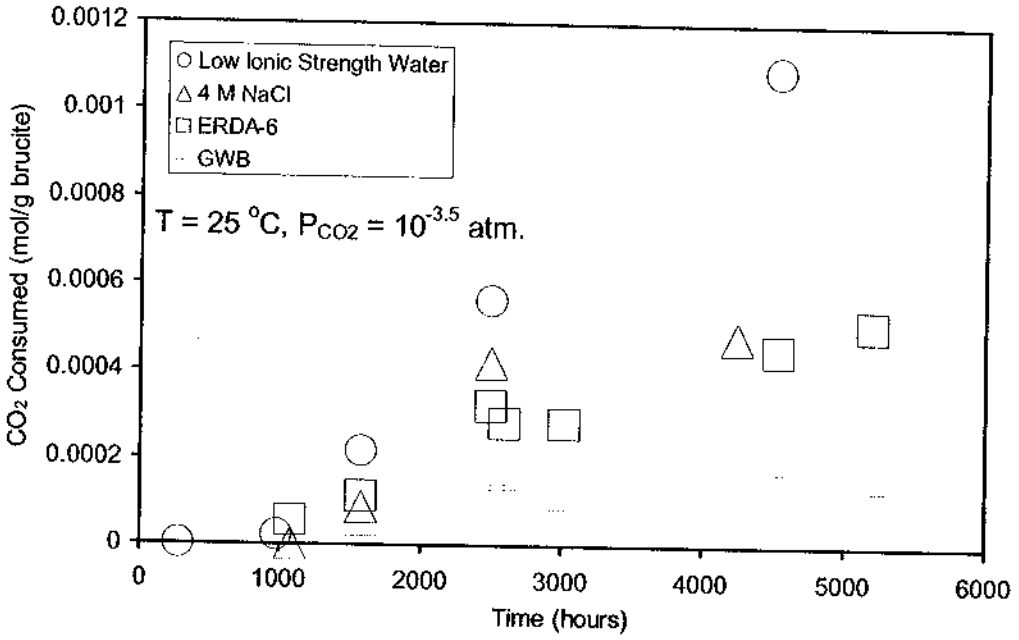

Figure 5. CO_2 consumed by brucite vs. time at room temperature and atmosheric CO_2 pressure.

In Table 2, the CO_2 uptake rates of MgO in various solutions are listed. It is clear from Table 2 that ionic strength also has a strong effect on the CO_2 uptake rate. Figure 6 illustrates the relation of ionic strength to CO_2 uptake rate. The linear relation of ionic strength to the uptake rate is described by the following equation:

$$k = (2.81 \pm 0.21) \times 10^{-7} - (2.99 \pm 0.43) \times 10^{-8} I \ (r^2 = 0.9649), \quad (4)$$

in which k is in mol g^{-1} h^{-1} and I is ionic strength in M.

Table 2. Uptake Rates of CO_2 by Brucite in Various Solutions

Solutions	Ionic Strength (M)	Uptake Rate (mol g^{-1} h^{-1})
Low ionic strength H_2O	~0.005	$(2.75 \pm 0.38) \times 10^{-7}$
4 M NaCl	4.0	$(1.55 \pm 0.78) \times 10^{-7}$
ERDA-6	5.2	$(1.15 \pm 0.14) \times 10^{-7}$
GWB	7.2	$(4.9 \pm 1.3) \times 10^{-8}$

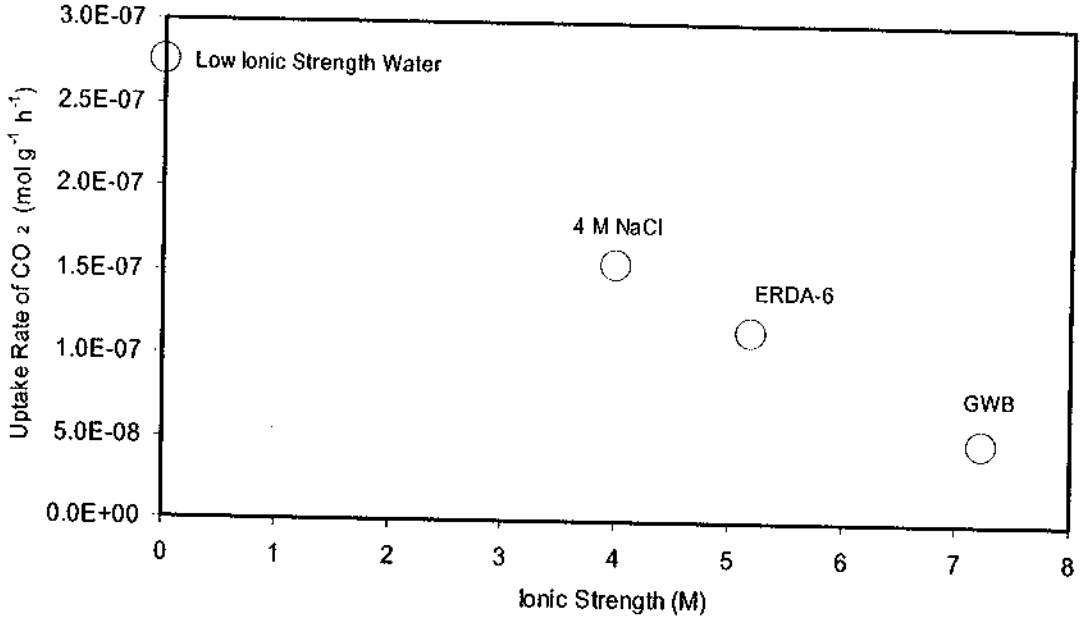

Figure 6. Uptake rate of CO_2 vs. ionic strength at room temperature and atomospheric CO_2 pressure.

We can compare these CO_2 uptake rates with the CO_2 production rates based on experimentally measured rates of microbial degradation of cellulosics similar to those in TRU waste (Wang et al., 2002). Experimental results indicate that the CO_2 production rates range from ~1 to ~25 μmol g^{-1} $year^{-1}$ under inundated conditions, and 0 to ~4 μmol g^{-1} $year^{-1}$ under humid conditions (Wang et al., 2002). When converted to mol g^{-1} $year^{-1}$, the above uptake rates of CO_2 in ERDA-6 and GWB are 1007 μmol g^{-1} $year^{-1}$ and 429 μmol g^{-1} $year^{1}$, respectively. These uptake rates are orders of magnitude higher than the CO_2 production rates. Therefore, it is highly unlikely that microbial activity would produce high CO_2 partial pressures in the WIPP disposal system, even if significant microbial activity occurs. Thus, MgO appears to be an effective engineered barrier in the WIPP.

Summary

The carbonation of brucite is fundamentally important to the long-term performance of the WIPP and its compliance with regulations for TRU waste (U.S. EPA, 1993). Should CO_2 be generated by microbial degradation of organic materials in TRU waste, it would be sequestered by this carbonation process. Therefore, kinetic data on carbonation is crucial. This paper reports the preliminary kinetic data obtained at Sandia National Laboratories' Carlsbad facility.

The conversion rates from brucite to hydromagnesite in low ionic strength H_2O, 4 M NaCl, ERDA-6, and GWB at room temperature and atmospheric CO_2 pressure are 1.3×10^{-5} h^{-1}, 7.3×10^{-6} h^{-1}, 5.4×10^{-6} h^{-1}, and 2.3×10^{-6} h^{-1}, respectively. The

carbonation rates are strongly correlated with ionic strength. When the conversion rates at other partial pressures of CO_2 become available and the dependence of conversion rates on CO_2 partial pressure is established, we will be able to calculate the time scale required for about 62.5% conversion of brucite to carbonate(s) (fraction of conversion = 0.625) in ERDA-6 or GWB. Such information will lead to the increased confidence in the WIPP engineered barrier.

The uptake rates of CO_2 by brucite in various solutions at room temperature and atmospheric CO_2 pressure have also been experimentally determined. The uptake rates of CO_2 by brucite also correlate strongly with ionic strength. The uptake rates of CO_2 in low-ionic-strength H_2O, 4 M NaCl, ERDA-6 and GWB are 2.75×10^{-7} mol g^{-1} h^{-1}, 1.55×10^{-7} mol g^{-1} h^{-1}, 1.15×10^{-7} mol g^{-1} h^{-1}, and 4.9×10^{-8} mol g^{-1} h^{-1}, respectively. These CO_2 uptake rates by brucite are orders of magnitude higher than the CO_2 production rates predicted for possible microbial degradation of organic materials in TRU waste based upon experimental studies, which are ~1 to ~25 μmol g^{-1} $year^{-1}$. Therefore, it is unlikely that microbial degradation of organic materials will result in high partial pressures of CO_2 in the repository.

References

Bryan, C.R., and A.C. Snider. 2001a. "MgO Hydration and Carbonation at SNL/Carlsbad," "Sandia National Laboratories Technical Baseline Reports, WBS 1.3.5.4, Repository Investigations, Milestone RI010, January 31, 2001." Carlsbad, NM: Sandia National Laboratories. 66-83.

Bryan, C.R., and A.C. Snider. 2001b. "MgO Experimental Work Conducted at SNL/CB: Continuing Investigations with Premier Chemicals MgO," "Sandia National Laboratories Technical Baseline Reports, WBS 1.3.5.4, Repository Investigations, Milestone RI020, July 31, 2001." Carlsbad, NM: Sandia National Laboratories. 5-1 to 5-15.

Papenguth, H.W., J.L. Krumhansl, R.V. Bynum, E.J. Nowak, Y. Wang, J.W. Kelly, and N.J. Linarez-Royce. 1997. "Chemical Conditions Model: Results of the MgO Backfill Efficacy Investigation." Unpublished report to the WIPP Conceptual Models Peer-Review Panel, April 23, 1997. Carlsbad, NM: Sandia National Laboratories.

Papenguth, H.W., J.L. Krumhansl, R.V. Bynum, Y. Wang, J.W. Kelly, H.L. Anderson, and E.J. Nowak. 1998. "Status of Research on Magnesium Oxide Backfill," *International Workshop on the Uses of Backfill in Nuclear Waste Repositories, Carlsbad, New Mexico, US, May 1998.* Eds. D.G Bennett, H.W. Papenguth, M.S.Y. Chu, D.A. Galson, S.L. Duerden, and M.L. Matthews. Bristol, United Kingdom: Environment Agency. R&D Technical Report P178, 3-43 to 3-63.

Snider, A.C. 2002. "MgO Studies: Experimental Work Conducted at SNL/Carlsbad. Efficacy of Premier Chemicals MgO as an Engineered Barrier," "Sandia National Laboratories Technical Baseline Reports, WBS 1.3.5.3, Compliance Monitoring; WBS 1.3.5.4, Repository Investigations, Milestone RI110, January 31, 2002." Carlsbad, NM: Sandia National Laboratories. 3.1-1 to 3.1-18.

Snider, A.C., and Y.-L. Xiong. 2002a. "Carbonation of Magnesium Oxide," "Sandia National Laboratories Technical Baseline Reports, WBS 1.3.5.3, Compliance Monitoring; WBS 1.3.5.4, Repository Investigations, Milestone RI130, July 31, 2002." Carlsbad, NM: Sandia National Laboratories. 4.1-1 to 4.1-28.

Snider, A.C., and Y.-L. Xiong. 2002b. "Experimental Study of WIPP Engineered Barrier MgO at Sandia National Laboratories Carlsbad Facility." TP 00-007, Rev. 2. Carlsbad, NM: Sandia National Laboratories.

U.S. Department of Energy. 1996. *Title 40 CFR Part 191 Compliance Certification Application for the Waste isolation Pilot Plant, Vol. 1-21.* Carlsbad, NM: U.S. Department of Energy Carlsbad Area Office.

U.S. Environmental Protection Agency. 1993. "40 CFR Part 191 Environmental Radiation Protection Standards for the Management and Disposal of Spent Nuclear Fuel, High-Level and Transuranic Radioactive Wastes; Final Rule. *Federal Register*, Vol. 58, 66398-66416. Washington, DC: U.S. Environmental Protection Agency Office of Radiation and Indoor Air.

U.S. Environmental Protection Agency. 1998. "40 CFR 194, Criteria for the Certification and Recertification of the Waste Isolation Pilot Plant's Compliance with the Disposal Regulations: Certification Decision: Final Rule," *Federal Register*. Vol. 63, 27354-27406.

Wang, Y., L.H. Brush, J.B. Gillow, A.J. Francis, R.W. Westerman, and M.R. Telander. 2002. "Gas generation studies for WIPP long-term performance assessments." Presentation to the International Workshop on How to Treat Gas in Safety Assessments of a Radioactive Waste Repository, Cologne, Germany, November 12-14, 2002. Carlsbad, NM: Sandia National Laboratories.

Wolery, T.J., and S.A. Daveler. 1992. *EQ6, A Computer Program for Reaction Path Modeling for Aqueous Geochemical Systems: Theoretical Manual, User's Guide, and Related Documentation (Version 7.0).* UCRL-MA-110662 PT III. Livermore, CA: Lawrence Livermore National Laboratory.

Sandia National Laboratories
Waste Isolation Pilot Plant (WIPP)
Test Plan, TP 00-06

Experimental Work to Develop a Model for Cement/Brine Interactions at the WIPP Site

TASK 1.3.5.4.3

Rev. 1

Effective Date: 12/19/02

Prepared by:
Charles R. Bryan, 6822
Yifeng Wang, 6822

Sandia National Laboratories
Albuquerque, NM

WIPP:1.2.01.09.02.02:TD:QA:DPRP1:NF: Test Plan for Cement Borehole Plug Degradation Studies, TP 00-06, Rev. 1

1.0 APPROVAL PAGE

Author:	*Original signed by Charles R. Bryan* Charles R. Bryan, 6822	*12/17/02* Date
Author:	*Original signed by Yifeng Wang* Yifeng Wang, 6823	*12/17/02* Date
Technical Reviewer:	*Original signed by Donald Wall* Donald Wall, 6822	*12/17/02* Date
Management Reviewer:	*Original signed by Paul E. Shoemaker for FDH* Frank Hansen, 6822	*12/18/02* Date
QA Reviewer:	*Original signed by M.J. Mitchell* Martha Mitchell, 6820	*17 Dec 02* Date
SNL Safety Reviewer:	*Original signed by Diane G. Gibson* Diane Gibson, 6800 ES&H Coordinator, Nuclear Waste Management Programs Center	*12/18/2002* Date

2.0 TABLE OF CONTENTS

3.0 REVISION HISTORY

This is the first revision of this test plan (TP). Changes to TP 00-06, other than those defined as editorial changes per Nuclear Waste Management Program (NWMP) procedure NP 20-1, "Test Plans," shall be reviewed and approved by the same level of responsibility of persons that performed the original review and approval. All TP 00-06 revisions will follow the same distribution as the original document.

4.0 DEFINITION OF ABBREVIATIONS AND ACRONYMS

ACI	American Concrete Institute
API	American Petroleum Institute
ASTM	American Society for Testing and Materials
CAH	Calcium aluminum hydrate
CAS	Calcium aluminum sulfate
CSH	Calcium silicate hydrate
CCA	Compliance Certification Application
DAS	Data acquisition system
DOE	Department of Energy
EBSD	Electron backscatter diffraction
ICP-OES	Inductively-coupled plasma optical emission spectrometery
ICP-MS	Inductively-coupled plasma mass spectrometery
GC-MS	Gas chromatograph mass spectrometry
JCPDS-ICDD	Joint Committee on Powder Diffraction Standards – International Center for Diffraction Data
M&TE	Measuring and Test Equipment
MOC	Management and Operations Contractor
MSH	Magnesium Silicate Hydrate
NIST	National Institute of Standards and Technology

NAS	National Academy of Sciences
NBS	National Bureau of Standards
NP	Nuclear Waste Management Program Quality Assurance Procedure
NWMP	Nuclear Waste Management Program
OPC	Ordinary portland cement
P&A	Plugging and abandonment
PA	Performance assessment
PNNL	Pacific Northwest National Laboratories
RWP	Radiological Work Permit
SEM	Scanning electron microscope
SNL	Sandia National Laboratories
SP	Activity Specific Procedure
TP	Test Plan
USI	Ultrasonic well-logging instrument
WID	[Westinghouse] Waste Isolation Division
WIPP	Waste Isolation Pilot Plant
XRD	X-ray diffraction

5.0 PURPOSE AND SCOPE

Upon reviewing the technical and scientific data gathered by Sandia National Laboratories (SNL) for the Waste Isolation Pilot Plant (WIPP) site characterization study, a National Academy of Sciences (NAS) review panel concluded that the only credible scenarios resulting in significant releases from the site involve human intrusion. Oil and gas deposits are common in the rock units underlying the repository formation (the Salado Formation), and currently active oil and gas wells are present within hundreds of meters of the site boundary (WIPP Compliance Certification Application (CCA), Appendix DEL). Inadvertent and intermittent drilling for resources was assumed to be the most severe human intrusion scenario. Estimates based on current and previous Delaware Basin drilling rates suggest that, over the next 10,000 years, 46.8 boreholes/km^2 will be drilled to a depth great enough to intersect the WIPP repository (CCA, Appendix DEL, Section 7.4).

Oil wells drilled within the Delaware Basin are plugged using several different plug configurations. These plug configurations are discussed in detail in the CCA, Appendix MASS, Section 16. The three most prevalent types of plug configurations are:

1) A two-plug configuration, with one plug at the top of the Salado, between the brine-bearing Rustler units and the stratigraphic level of the repository, and the other at the base of the evaporite sequence, below the Castile. The plugs are on average 40 m long, and are located at casing step-downs.

2) A three-plug configuration, that includes the two-plug configuration described in (1), plus a third plug in the Salado, either above or below the repository level. The plugs beneath the repository level are of particular importance, as they would serve to isolate the repository from brine pockets in the Castile.

3) A single-plug, extending through much or all of the evaporite section.

In the CCA, failure of borehole plugs was assumed to be a function of two processes—corrosion of the steel casing and degradation of the cementitious materials in the concrete comprising the plugs. Factors affecting the rate of plug failure include depth of emplacement and the length of the plug. Plugs emplaced above the Salado were assumed to fail in less than 200 years due to rapid casing corrosion under the oxidizing conditions present in the shallow subsurface. The resulting lack of radial confinement and radial infiltration of reactive brines into the concrete plug would then lead to fracturing, spalling and failure.

Concrete plugs extending through the entire evaporite sequence were assumed to behave as confined systems. Alteration products produced by brine/cement reactions build up in the plug, resulting in decreased porosity and permeability. Plug failure was not predicted to occur within time spans relevant to the repository.

Shorter concrete plugs emplaced at depths below the repository horizon were treated as open systems. At these depths, casing corrosion—assumed to be occurring as oxidation to goethite (α–FeOOH), with an accompanying generation of H_2 gas—was assumed to be inhibited by buildup of hydrogen gas. The porosity and permeability of the concrete plugs was assumed to remain constant until a "critical volume" of brine—assumed from work by Berner (1990) to be 100 pore volumes—passed through the plug. At that point, cementitious components would be degraded significantly by leaching and dissolution, and unconstrained microfracturing and physical failure would occur. Failure was estimated to occur very slowly, with plugs maintaining integrity for 5,000 to 50,000 years – the breadth of the range indicating the large uncertainties in the model. While the lower part of the range was ½ the regulatory period (10,000 years), the bulk of the range was much larger. On the basis of these calculations, units beneath the Castile were screened out as sources of brine for repository influx.

Since boreholes provide the only credible conduits for brine access to the repository, accurate estimates of borehole plug failure rates, especially for plugs below the repository, are critical to performance assessment (PA) modeling of releases at the WIPP site. The estimates of plug failure rates in the CCA are based upon experimental work done using cements and groundwaters that are not specific to the WIPP site. The Castile and Salado brines are considerably more complex than the electrolyte that Berner (1990) used in his experiments. Cement degradation may be slower than predicted, if precipitated minerals inhibit cement/brine reactions (Krumhansl, 1993). Carbonate-rich Castile brines may be especially effective at promoting calcite precipitation and sealing cement porosity. Alternatively, cement plug degradation may be faster than predicted in the CCA, if the "critical volume" estimate, based upon

work with dilute solutions (Berner, 1990), is smaller for the complex, high ionic strength Castile and Salado brines. Formation formation of expansive alteration products (Atkinson and Hearne, 1990; Havlica and Sahu, 1992; Xie and Beaudoin, 1992) might also shorten plug lifetimes, by causing spalling of partially reacted or unreacted material from the end of the plug, or by splitting the casing, allowing radial inflow of brine.

SNL proposes to develop a more rigorous model for borehole plug failure at the WIPP site. Two approaches will be used. The first is collection of casing and concrete samples from boreholes at the WIPP site during plugging and abandonment (P&A). Current schedules for borehole P&A at the WIPP site are described in Richardson and Crawley (1999). The samples collected during P&A will establish casing corrosion and cement degradation products and mechanisms relevant to WIPP conditions, and test plug failure assumptions in the CCA. Casing and cement sampling during borehole P&A is described in detail in a separate test plan—TP 00-02, "Collection and Analysis of Downhole Cement and Steel Samples During Borehole Plugging and Abandonment."

The second approach, which is described in this test plan, will be an experimental program to determine cement alteration reactions and mechanisms in Salado and Castile brines, and to develop a thermodynamically-based model for borehole plug degradation under conditions relevant to the WIPP. Using this model, more accurate cement plug failure rates will be determined for performance assessment (PA) analysis. This is the second revision of this test plan, and, as well as describing planned experimental work, describes and references work that has already been carried out.

The work performed under this test plan is largely intended to confirm conceptual models used in WIPP certification and recertification. Development of a new borehole plug degradation model supports assumptions of plug failure rates in radionuclide release scenarios, and will affect several parameters used in PA calculations. Evaluating the effects of cement on repository chemistry could impact estimates of actinide solubilities in WIPP brines, influencing predicted radionuclide releases in repository failure scenarios.

5.1 General Scope of the Experimental Work

A robust, versatile model for cement/brine reactions, able to incorporate effects of changing brine and solid compositions with continued reaction, and of variations in initial compositions, will incorporate equilibrium thermodynamic speciation modeling, kinetic effects due to both reaction kinetics and diffusion, and the effects of changing porosity/permeability or cement accessibility. The basic information required for the equilibrium thermodynamic model includes Pitzer binary interaction coefficients for the solution species present, and thermodynamic data (e.g. formation constants) for the solid phases present. Pitzer parameters for major components in WIPP brines have been determined, but good data do not exist for Si and Al at high pH values, such as those expected in concrete pore waters. These two components are important when considering the solubility of cement phases, which include calcium silicate hydrate (CSH), calcium aluminate hydrate (CAH), and calcium aluminum sulfate (CAS).

The first step of the experimental program will be to carry out solubility experiments with simple Si and Al phases — amorphous silica, crystalline silica, and gibbsite ($Al(OH)_3$)— in single and multi-component electrolytes covering a range of concentrations. From these data, Pitzer interaction parameters will be determined.

The second round of experiments will be aimed at determining the mineral phases present under WIPP conditions. In these batch experiments, crushed or powdered cement and cement coupons will be aged in synthetic WIPP brines, and the cement alteration phases that form will be identified. If thermodynamic data are unavailable for some phases, thermodynamic parameters may be measured experimentally using solubility experiments, or data for mineral analogs may be used. The mode of alteration will also be documented.

The third round of experiments will involve use of cement cores. Brine will be pumped through (synthetically) fractured and unfractured cement cores, and chemical changes in both the effluent brine and the cement will be measured. Changes in the cement porosity, permeability, and texture will be monitored. As opposed to the batch systems, the cement will constantly be exposed to fresh brine. These experiments will yield information on the mode of cement failure under flow-through conditions; local expansion and fracturing would result in more rapid and extensive degradation than diffusion-limited alteration. Successful modeling of the brine effluent composition will be a measure of the thermodynamic model performance.

5.2 Previous Work

It is beyond the scope of this document to review the huge body of literature on the degradation of cement in various environments. However, a review of previous studies examining cement degradation in WIPP-related brines, and previous thermodynamic modeling, is appropriate.

Previous cement studies involving WIPP-related materials are summarized in Krumhansl (1995). Several studies document degradation of the concrete waste shaft liner due to interactions with Mg-rich brine at the Rustler-Salado Contact (Lambert et al., 1992; Wakely et al., 1992). The liner is composed of ASTM Type V (sulfate-resistant) cement that was mixed with fresh water. Microscopy and X-ray diffraction studies determined that the degraded liner showed surficial spalling and extensive microfracturing and contained brucite, gypsum, magnesium hydroxychloride hydrate, and locally calcium aluminum chloride. Wakely et al. (1994), and Poole et al. (1994) performed experimental work to explain the observed shaft liner degradation and to examine the chemical stability of concrete developed for the repository panel closures. Batch experiments were carried out using cement wafers aged in Mg-sulfate rich brine. After several months to a year, most specimens had developed surface coatings of precipitated minerals, and showed alteration of the underlying cement. Formation of a Mg-rich silicate phase was predicted, but not observed, and the authors postulated that the alteration process was driven by precipitation of brucite on the cement surface, lowering the activity of OH^- in solution. This caused dissolution of $Ca(OH)_2$ and ultimately, of CSH gel, in the cement matrix. The mineralogy of the alteration assemblage was very sensitive to the brine composition, and included phases not observed in altered cement samples collected from the shaft liner.

Krumhansl and Lambert (1992) and Krumhansl (1993) examined the degradation of salt-saturated cement at elevated temperatures, by a Mg-sulfate-rich brine formulated to represent a composite of Rustler groundwaters, and by synthetic Salado brine. They used batch systems with cement coupons or prisms, aged at temperatures of 100°C to 250°C to speed reactions. Surface coatings of brucite and calcium sulfate phases (anhydrite, gypsum, or bassanite, depending upon temperature) were observed. These phases, as well as Mg and Mg-Al hydroxychlorides, were also observed in the altered cement matrix. In contrast to the experimental work done by Wakely et al. (1994) and Poole et al. (1994), Ca was quantitatively replaced in CSH with Mg to form magnesium silicate hydrate (MSH). The mineralogy and texture of the surface coatings varied with brine composition and temperature, and that these coating properties had a strong influence the continued conversion of CSH to MSH in the cement matrix.

Krumhansl (1995) examined possible failure rates for cement shaft liners in the Culebra and Salado, and panel seals within the repository. He developed a thermodynamic model to examine cement stability in Culebra and Salado brines. Because of the lack of available thermodynamic data for actual cement phases, he used thermodynamic data for mineral analogs of cement and alteration phases. In addition, because of the unavailability of data for a Pitzer activity coefficient model, Krumhansl could only estimate the activities of species in solution. He concluded that dominant phases present in ordinary Portland cement (OPC) are unstable in all of the WIPP brines examined in the study. Krumhansl also estimated cement degradation rates in synthetic Culebra and Salado brines, using two different models. The first, the "shrinking core model," estimated the rate at which the alteration front would move into the cement, by assuming that diffusion of Ca and hydroxide out of the cement is the rate-limiting step. The second model was based upon mass balance arguments; cement degradation was assumed to be a function of the rate at which Mg could be delivered to the cement surface, and hence to be controlled by brine availability and inflow rates. Shaft liners (50 cm thick) were found to fail in hundreds to thousands of years, depending upon model assumptions; the 12-meter-thick panel seals were not significantly degraded over thousands of years. Krumhansl also evaluated the effect of microfracturing induced by expansive alteration products, and concluded that it could potentially increase failure rates by orders of magnitude. He concluded that accurate modeling of cement degradation rates at the WIPP was not possible with available models, due to several factors: 1) the lack of material-specific properties, such as thermodynamic data, on WIPP-relevant cement and alteration phases, requiring the use of mineral analog data and simplifying assumptions; 2) inability to incorporate the effects of microfracturing and mineral precipitation on brine accessibility to cement beneath the altered rim; 3) the lack of kinetic information for alteration reactions, and the potential formation of metastable phases; and 4), the lack of site-specific information, such as brine distribution and availability.

Bonen (1996) examined 9-year-old cement (Type H, salt saturated) from the WIPP repository, and found little evidence for alteration, other than minor carbonation along the salt/cement contact. He also examined 20-year-old cement grout (initial composition unknown) from a nearby potash mine. The grout, which had been in contact with Mg-rich formation waters, showed widespread alteration, with precipitation of brucite and conversion of CSH to MSH. In laboratory studies, Bonen examined the reactivity of American Petroleum Institute (API) Type H (equivalent of ACI type 2) salt-saturated cement with Mg-sulfate-rich brines similar in composition to those from the base of the Rustler Formation. The

cement showed massive alteration, with precipitation of brucite and gypsum coatings and conversion of CSH to MSH.

To summarize, previous experimental work has consisted largely of characterization of liner samples collected from the waste handling shaft, and laboratory studies to determine the stability of liner cement or proposed panel seal cement in brines similar to that found in the Rustler or Salado Formations. No work has been done to examine cement interactions with sulfate-rich Castile brine. Only Krumhansl (1995) attempted to predict failure rates for cement materials, and he recognized that only crude modeling was possible with the available data.

5.3 Modeling cement degradation

A great deal of thermodynamic data are available on cement and alteration phases, and thermodynamic models for cement degradation in dilute solutions have been formulated. The information needed to expand those existing models to cover WIPP conditions can be summarized as follows:

1. Parameters for a Pitzer model for the activities of aqueous species in the brines. Pitzer parameters for the dominant species present in WIPP brines are summarized in Harvie et al. (1984) and Pitzer (1987). Some solubility data and Pitzer interaction coefficients are available for Si and Al in concentrated electrolytes at low to intermediate pH and in some cases, at high pH (Marshall, 1980; Chen and Marshall, 1982; Gasteiger, et al., 1992; Palmer and Wesolowski, 1992; Wesolowski, 1992; Wesolowski and Palmer, 1992, 1994; Felmy et al., 1994a,b; Azaroual et al., 1997; Richter et al., 2000). However, a complete data set of the necessary Pitzer parameters is not available for Si and Al at pH values and brine compositions relevant to the WIPP or to cement pore fluids (pH 9-13).

2. Identification of the initial hydrated cement phases, cement alteration phases, and alteration pathways. The phases that are present in hydrated cement are well known, and can be calculated modally from the initial composition of the cement blend (Atkins et al., 1992a; Macphee et al., 1989). These phases are listed in Table 1. Degradation of both salt-free and salt-saturated cement in different electrolytes has been widely studied (Atkinson and Hearne, 1990; Bonen, 1992; Bonen and Cohen, 1992; Havlica and Sahu, 1992; Krumhansl 1993, 1995; Krumhansl and Lambert, 1992; Lambert et al., 1992; Wakely et al., 1992, 1994; Poole et al., 1994; ; Neall, 1994, 1996; Bonen, 1996; Pfingsten and Shiotsuki, 1998), and possible alteration phases that are likely to form have been identified, and have also been listed in Table 1. Although several studies have been done with synthetic WIPP brines, the actual alteration phases that form will have to be determined experimentally, for several reasons. In previous studies, the results varied from study to study, and were in some cases inconsistent. In addition, no experiments have been run with simulated Castile brine, one of the most WIPP-relevant brines with respect to borehole plug degradation. Also, the alteration phases that form are dependent upon the initial composition of the cement. Most alteration studies have been done with American Cement Institute (ACI) Type 1 portland cement or API Type H oilfield cement mixed with fresh water, in some cases with NaCl added to make it salt-saturated. In the Delaware Basin, oilfield cements may be mixed with "formation fluids" or with locally mined "salt", that may contain

Table 1. Phases Likely to Occur in Fresh and Altered Cement

Initial Cement Phases (assuming 100% hydration)	
Calcium Silicate Hydrate (CSH)	$xCaO{\cdot}SiO_2{\cdot}yH_2O$
($0.8 \leq x \leq 1.8$, generally 1.4–1.8 for Portland cements)	
Calcium aluminum ferrite hydrate ("hydrogarnet")	$3CaO{\cdot}(Al_2O_3, Fe_2O_3){\cdot}6H_2O$
Calcium aluminum silicate hydrate	$2CaO{\cdot}Al_2O_3{\cdot}SiO_2{\cdot}8H_2O$
Calcium aluminate monosulfate	$3CaO{\cdot}Al_2O_3{\cdot}CaSO_4{\cdot}12H_2O$
Ettringite (high sulfate)	$3CaO{\cdot}Al_2O_3{\cdot}3CaSO_4{\cdot}32H_2O$
Gibbsite	$Al(OH)_3$
Gypsum	$CaSO_4{\cdot}2H_2O$
Hydrotalcite	$4MgO{\cdot}Al_2O_3{\cdot}10H_2O$
Portlandite	$Ca(OH)_2$
Secondary (alteration) Phases	
Brucite	$Mg(OH)_2$
Calcite	$CaCO_3$
Calcium aluminum chloride hydrate (I)	$3CaO{\cdot}Al_2O_3{\cdot}CaCl_2 * 12\ H_2O$
CSH (depleted in Ca)	
Gypsum	$CaSO_4{\cdot}2H_2O$
Ettringite (high sulfate)	$3CaO{\cdot}Al_2O_3{\cdot}3CaSO_4{\cdot}32H_2O$
Magnesite	$MgCO_3$
Magnesium silicate hydrate	$xMgO{\cdot}SiO_2{\cdot}yH_2O$
Magnesium hydroxychloride	$Mg_3(OH)_5Cl * 4\ H_2O$
Magnesium sulfate hydrate	$Mg_6O_5SO_4 * 8H_2O$

significant amounts of K, Mg, or SO_4^{-2}. These species will significantly affect the initial mineralogical composition of the cement and of the alteration phases that form as it degrades.

3. Once the important phases have been identified, thermodynamic data must be compiled, and an equilibrium thermodynamic model will be generated. Thermodynamic data are available for cement phases, alteration phases, and naturally-occurring mineral analogs (Goto et al., 1979; Gartner and Jennings, 1987; Glasser et al., 1987; Atkinson et al, 1989; Atkins et al., 1991a, 1991b, 1992b; Damidot and Glasser, 1992, 1993; Taylor, 1992; Xie and Beaudoin, 1992). Where possible, data for the actual cement phases will be used, as mineral analogs are commonly more crystalline than the cement phases, and are not compositionally identical. Finally, the model will be compared to existing thermodynamic models for cement degradation (Berner, 1987, 1988; Atkins et al., 1992a; Bennett, et al., 1992; Neall, 1994, 1996; Krumhansl, 1995; Pfingsten and Shiotsuki, 1998).

4. A complete equilibrium thermodynamic model for brine/cement interactions is still insufficient for describing cement plug degradation, as it is not an equilibrium process. Reaction kinetics may inhibit

formation of specific phases; coatings may form on cement/brine interfaces or precipitated phases may reduce porosity and permeability, inhibiting further reaction; or expansive alteration phases may fracture the cement, resulting in spalling of partially reacted cement from the end of the core and reducing the amount of brine access necessary for plug failure. In addition to developing the thermodynamic model, column experiments with cement cores will be performed to evaluate the impact of these non-equilibrium processes. Finally, a more comprehensive degradation model, incorporating these non-equilibrium processes, will be implemented with EQ3/6 (Wolery, 1992; Wolery and Daveler, 1992) using a mixing tank approach (Berner, 1987, 1988, 1990; Neall, 1994, 1996). Reactive transport simulations will be conducted using activity coefficients calculated from EQ3/6. It is expected that the activity coefficients for a given brine composition will remain more or less constant along a flow path. Version 7.2a of EQ3/6 is currently qualified for WIPP use.

6.0 EXPERIMENTAL PROCESS DESCRIPTION

6.1 Planning Overall Strategy and Process

Developing the cement degradation model will be done in several steps. First, Pitzer parameters applicable to Si and Al in WIPP brines will be determined. Simultaneously, completely hydrated cement wafers and crushed or powdered cement will be exposed to synthetic Culebra and Salado brines to determine the alteration phases that form in those solutions. Once the important cement phases and alteration phases have been identified, a survey will be made of the thermodynamic data available for those phases and for mineral analogs. This information will be used to develop an equilibrium thermodynamic model for cement alteration. In addition, column experiments will be performed using cement cores. Brines will be pumped through whole and synthetically fractured cement cores, and geometric effects on cement alteration (e.g., the formation of low-porosity mineral coatings or changes in matrix porosity due to plugging of existing porosity or expansion and fracturing) will be observed and documented. Finally, a comprehensive model, incorporating both the equilibrium model and the empirically measured disequilibrium effects, will be developed.

6.1.1 Brines

Two synthetic brines, representative of those occurring in the Salado and the Castile formations at the WIPP, will be used in this study. These brines are GW brine, and ERDA-6 brine, respectively, and will be prepared using the recipes given in Table 2, and following the procedures described in NWMP Technical Operating Procedure (TOP) TOP-544, "Preparing Synthetic Brines for Chemical Retardation and Transport Experiments."

Table 2. Composition of synthetic Salado and Castile Brines

Compound	Salado generic weep (GW) brine[1] (g/L)	Castile (ERDA-6) brine[2] (g/L)
$MgCl_2 \cdot 6\,H_2O$	207.05	3.86
NaCl	179.61	261.64
KCl	34.84	7.23
Na_2SO_4	25.23	23.7
$Na_2B_4O_7 \cdot 10H_2O$	15.06	6.00
$CaCl_2 \cdot 2H_2O$	2.03	1.76
NaBr	2.74	1.13
LiCl	0.186	--
Component	**M, GW brine**	**M, ERDA-6 brine**
Na	3.536	4.854
K	0.467	0.097
Li	0.004	--
Ca	0.014	0.012
Mg	1.018	0.019
Cl	5.609	4.636
Br	0.027	0.011
SO_4	0.178	0.167
B_4O_7	0.039	0.016

[1] Zhang et al., 1999

[2] Villareal et al, 1999

6.1.2 Cement types used

In order to determine the type of cement used in the oilfield for borehole plugging operations, borehole plugging logs for wells in the Delaware Basin were examined. The results for 52 boreholes are summarized in Table 3. Type C sulfate-resistant cement is the most common type specified. Type H cement is also used—it is sulfate resistant and is chemically similar to Type C, but cures more slowly because it is coarsely ground. It is mostly used in deeper holes (>7000 ft) where higher temperatures accelerate curing and a slow-hardening cement is required. The borehole plugs were poured "neat"—without aggregate, and additives to accelerate or retard curing were rarely used (in three instances, 2% $CaCl_2$ was used as an accelerant, and in one instance, 2% KCl).

Schlumberger/Dowell, an oilfield service company, was also contacted. They confirmed that "neat" Type C cement is the most common type used for borehole plugs, and that aggregate is not used under normal circumstances. The cement is mixed at the surface, adding water equivalent to 44% of the dry weight of the cement. Only 27% water is necessary for complete hydration—the excess is added to thin the cement for pumping purposes. If the plug is to be emplaced in an evaporite section, the cement must be salt-saturated. To accomplish this, an amount of dry NaCl, equal to 37 wt% of the water added, is added to the mix.

Because Type C cement is commonly used at WIPP-relevant depths, and because there is little difference, other that initial grain size, between Type C and Type H cement, only Type C cement is being

Table 3. Summary of borehole plug cement types, extracted from 52 borehole plugging logs.

Cement type used	Number of boreholes
Type C	21
Type H	5
Type C and Type H	2
Not specified in log	24

used in the borehole plug degradation experiments described in this test plan. Both salt-free and salt-saturated cement are being used in powdered cement, cement wafer, and cement core experiments.

The cement used to mix cementitious waste forms is commonly ordinary Portland cement (OPC). Type C cement, because it is sulfate-resistant, is a poor analog for OPC. Thus, in order to evaluate the effects of cement on repository chemistry, salt-free OPC is also being used in the experiments with powdered cement and cement wafers.

Approximately 25 kg of both Type C cement and OPC were obtained from Lone Star Industries, Inc., a cement company that supplies oilfield service companies in the Delaware Basin. These materials are being used in the experimental work performed under this test plan.

In the oilfield, cement is mixed on the surface, using whatever water is available, and then pumped into the boreholes. The conditions for mixing cementitious waste forms vary widely, but air exposure during mixing is likely. Thus, no effort was made to exclude CO_2 when the cements were prepared, and all cement types are expected to contain some calcium carbonate. The cements were mixed in the proportions described above for oilfield use, and sealed into one liter rectangular plastic containers to cure for two weeks. It is recognized that cement does not fully hydrate in two weeks—full hydration can take decades or even centuries. However, accelerating the hydration process by autoclaving would affect the crystallinity and mineralogy of the hydration products, and is not desirable. After two weeks, the hardened cement "bricks" were removed from the containers, and different fractions of each were crushed to <100 mesh (150 μm), cut into 25mm square by 3mm thick wafers, and cored to produce 1" diameter by 2-3" long cement cores. All materials were stored in sealed plastic bottles or bags until use.

6.1.3 Atmospheric conditions

Within the repository, CO_2 fugacities will be controlled by the presence of brucite and a magnesium carbonate mineral, probably hydromagnesite. This corresponds to a P_{CO_2} of $10^{-5.5}$, or about 3 ppm. In the presence of cement, calcite/portlandite are the expected controlling phases (Novak, 1997) and will limit the P_{CO_2} to even lower values. Significant calcite will initially be present in the systems

because the cements will be mixed under atmospheric P_{CO2}, simulating oilfield conditions for mixing cement for borehole plugs, and conditions for solidifying cementitious waste forms. Rather than attempting to maintain such low CO_2 fugacities in a glovebox, samples will be kept sealed, and higher levels of CO_2 will be excluded as much as possible from the experimental setup. If diffusion of CO_2 into the systems is minimized, then the presence of calcite and portlandite will maintain the desired P_{CO_2}. Diffusion of CO_2 into the systems will only affect the P_{CO_2} if it occurs more rapidly than carbonate can precipitate, or if the amount diffusing in overwhelms the amount of portlandite available. For these reasons, all brines will be sparged with Ar or N_2 (industrial grade, >99.99% pure) prior to use to render them carbonate-free, and all experiments will be carried out in inert atmosphere in a glove box to minimize carbonation reactions. To ensure that the atmosphere in the glovebox is carbonate-free, Ar or N_2 will be slowly bled into the chamber to maintain a positive pressure with respect to the external atmosphere. In addition, a small pump will recirculate the atmosphere in the glove box through a bubbler (0.1 M NaOH + 0.05 M $BaCl_2$) at a rate of ~2 liters/minute to remove CO_2. The solution in the bubbler scavenges CO_2 from the glovebox atmosphere by precipitation of barium carbonate ($BaCO_3$), and will be replaced on a monthly cycle. The atmosphere in the glove box will be sampled and analyzed by gas chromatography–mass spectrometry (GC-MS) on a regular basis to monitor the amount of CO_2 present.

Some experiments may be run under higher P_{CO2} conditions—probably atmospheric—in order to evaluate the changes in pH and alteration product mineralogy as the portlandite is consumed through precipitation of calcite.

6.1.4 Measuring Si and Al Pitzer parameters

Pitzer binary interaction coefficients for the major ions in WIPP brines—H^+, Na^+, Mg^{2+}, Ca^{2+}, OH^-, Cl^-, SO_4^{2-}, and CO_3^{2-}—are known for most conditions of medium and high pH. However, interaction coefficients between Si and Al and some of these ions (Mg^{2+}, Ca^{2+}, and SO_4^{2-}) are not known, especially at high pH. Experimental work to determine some interaction parameters for silica is currently being carried out at by Andrew Felmy at Pacific Northwest National Laboratories (PNNL). (This work is not being funded by the WIPP Project.) The silica system is complex at high pH because multiple aqueous chain and ring silica polymers may form. Al–containing systems are less complex, as only monomeric and dimeric Al species are stable in solution. We will use batch experiments to examine Al solubilities and identify the solid phases present at equilibrium. In collaboration with Felmy, we will interpret pH-solubility curves to determine Pitzer parameters.

It is anticipated that the concentrations of both Si and Al in solution will be pH-dependent, as the silicon phase in solution is a weak acid (H_4SiO_4), which will progressively deprotonate and polymerize with increasing pH, and aluminum will be present as monomeric and dimeric aqueous hydroxide species. Thus, solubilities will be measured over a pH range starting at 7 and extending to higher values. The upper pH limit will vary with the salt used and the electrolyte concentration—care must be taken to avoid precipitation of such large volumes of hydroxide that the electrolyte concentration is affected. Initial experiments will be run with crystalline $Al(OH)_3$ (gibbsite); solids present at equilibrium will be determined by XRD. Solubilities will be measured over a range of ionic strengths, typically in 4-6 steps, from 0.1 M to saturation for the salt involved. For example, the suite of $MgCl_2$ concentrations to be used

to determine Pitzer interaction parameters for Al and Mg will be 0.1, 0.2, 0.5, 1.0, 2.0, and 3.7M, where 3.7M is saturation for the salt involved.

The solubility experiments will be run in polyethylene or polycarbonate Oak Ridge style screw-cap centrifuge tubes, with 0.1 to 0.5 gram of gibbsite in each tube, and 25-30 ml of electrolyte. The system pH will be adjusted with NaOH, and will be checked and readjusted as necessary over the first few weeks of the experiment. Samples will be aged in temperature-regulated orbital-mixing water baths. Two sets of samples will be run for each electrolyte concentration. One will be aged at 25°C, and will approach equilibrium from an undersaturated state. The other set will be aged at 50°C and allowed to re-equilibrate at 25°C. Thus, it will approach equilibrium from an oversaturated state. Samples of the electrolyte will be collected at the end of the experiment, and analyzed to determine the Al concentration and to check if hydroxide precipitation has significantly affected the concentration of the binary electrolyte. To be acceptable, the electrolyte concentration must be within 5% of the nominal value. Coincidence of the two data sets will provide evidence for equilibrium.

Although electrolytes will be degassed by sparging with N_2 to remove CO_2, the samples will not be aged in a glove box. Other than keeping the samples tightly closed, no effort will be made to keep out CO_2. This is because the carbonate concentration, even up to one-tenth molar quantities, has little effect on Al solubility (Felmy, personal communication).

The concentration of Al in solution will be measured using several methods, including inductively-coupled plasma optical emission spectroscopy (ICP-OES), using a Perkin Elmer Optima 3300, colorimetric methods, using a Cary 300 UV-visible spectrophotometer, and possibly ICP-mass spectrometry (ICP-MS). The solids present will be identified by X-ray Diffraction (XRD).

6.1.5 Cement-brine equilibration experiments

Cement brine equilibration experiments are being run with both powdered cement and cement wafers, and are summarized in Table 4. Experiments with powdered cement include 1) equilibration rate experiments, to determine how long systems will have to be mixed in order to see significant generation of cement alteration products; 2) long-term equilibration experiments, to generate enough alteration products for identification and analysis; and 3) leaching experiments, to evaluate the effect of introducing fresh brine on alteration product mineralogy and cement degradation. The cement wafer experiments will evaluate the effects of disequilibrium processes (mineral precipitation, fracturing due to expansive mineral growth, etc.) on cement degradation. In all of these experiments, both OPC and API Type C cement are being used.

6.1.5.1 Reaction rate experiment

The goal of this experiment was to determine, in a general sense, the rate of reaction between the powdered cement and brine. This information was used to plan longer-term cement/brine equilibration experiments, in order to guarantee that sufficient reaction products formed for analysis.

Table 4. Experimental matrix for cement/brine equilibration experiments

Reaction rate experiment

Brines (2)	Cements (3)	Cement/brine ratios (2)
GW	OPC	1g/110ml
ERDA-6	Salt-free Type C	5g/110ml
	Salt-sat. Type C	

Total number of systems: 12, each sampled 10 times over a period of 3.5 months.

Conditions: Systems agitated. Containers sealed and stored in a N_2-purged glovebox.

Long-term cement/brine equilibration experiment

Brines (2)	Cements (3)	Cement/brine ratios (6)
GW	OPC	0.1g/30ml
ERDA-6	Salt-free Type C	0.2g/30ml
	Salt-sat. Type C	0.5g/30ml
		1.0g/30ml
		2.0g/30ml
		5.0g/30ml

Total number of systems: 36 (first experiment), sampled after 3.5 months. 24(second experiment).

Conditions: Systems agitated. Containers sealed and stored in a N_2-purged glovebox. A second set has been initiated using only OPC and salt-free Type C cement.

Cement leaching experiment

Brines (2)	Cements (3)	Cement/brine ratios (1)
GW	OPC	1g/30ml
ERDA-6	Salt-free Type C	
	Salt-sat. Type C	

Total number of systems: 36 (6 per cement/brine combination).

Conditions: Systems agitated. Containers sealed and stored in a N_2-purged glovebox.

Cement wafer experiment

Brines (2)	Cements (3)	Cement/brine ratios (1)
GW	OPC	1 wafer(~3g) /250ml
ERDA-6	Salt-free Type C	
	Salt-sat. Type C	

Total number of systems: 60 (10 per cement/brine combination). Sampled every 1-2 months

Conditions: Systems not agitated. Containers sealed and stored in a N_2-purged glovebox.

In this experiment, powdered cement was aged in GW and ERDA-6 brines, and brine pH and composition was monitored over several months to monitor reaction progress. Three types of cement were used—salt-free and salt-saturated Type C cement, and OPC cement. Experiments were run in 250 ml polypropylene bottles, using cement/brine ratios of 1g/110 ml and 5g/110 ml. Brines were degassed prior to use, and samples were stored as described in section *6.1.2* above, to control the P_{CO_2}.

During aging, the bottles were agitated constantly on a rotary mixing platform. Brine samples were collected at intervals for 3.5 months, and analyzed by inductively-coupled plasma optical emission spectroscopy (ICP-OES). Results of this experiment are presented in Bryan (2002). To summarize, brine chemistry changed rapidly initially, and then more slowly over the entire sampling period, indicating that equilibrium was not reached. A longer-term rate experiment will be initiated.

6.1.5.2 LONG-TERM EQUILIBRATION EXPERIMENTS

In these experiments, cement-brine systems of varying cement/brine ratio will be aged for extended periods of time (the reaction rate experiment was designed to provide guidance on the length of time necessary), and then sampled. Brine compositions and reaction product mineralogy will be analyzed by pH meter, ICP-OES, and ICP-MS, and the solids will be identified by SEM and XRD. The purpose of this experiment is two-fold. First, identification of the alteration products produced by brine/cement reactions is necessary for development of the thermodynamic model. Second, each pair of brine compositions and corresponding alteration minerals will provide a data point for validation of the thermodynamic model.

In the first phase of these experiments, reported by Bryan (2002), three cements were used—OPC and both salt-saturated and salt-free Type C. As there was no discernable difference in brine composition or alteration products between the salt-saturated and salt-free Type C cement systems, in the second set of experiments, only OPC and salt-free Type C cement were used.

These experiments are being carried out in polycarbonate and polypropylene screw-cap Oak Ridge-style centrifuge tubes (40-50ml), using 30 ml of brine, and 0.1 to 5 grams of powdered cement. The amount of cement in the system affects the brine composition (especially the pH and the Mg^{2+}, Ca^{2+}, and SO_4^{2-} contents), and thus influences the reaction products that form. The systems are prepared with degassed brine, sealed tightly, and aged in a nitrogen-sparged glovebox, as described in section 6.1.2. They are constantly agitated on hematology mixers or rotary mixers. The initial experiment was sampled after 3.5 months—a new experiment has been started, and will be sampled after 6 months. Both brine and solid samples are collected at sampling. The brine samples are filtered through 0.2μm syringe filters, and are then acidified to 1% HNO_3 to prevent precipitation. The remaining material is vacuum filtered through 0.2μm membrane filters to separate the solids, which are lightly washed with deionized water to remove the last of the brine. Care is taken to limit the deionized water contact time, to minimize dissolution of gypsum, portlandite and other cement phases.

Following collection, brine compositions are measured by pH meter, ICP-OES, and ICP-MS, and the solids identified by SEM and XRD. The results of the initial experiment, reported by Bryan (20002), indicate that other than gypsum and portlandite, well-crystallized alteration phases are restricted to the systems containing smaller amounts of cement. Systems with more cement have higher pH values, which may stabilize CSH and MSH relative to crystalline materials. It is not clear whether longer aging times will affect this.

6.1.5.3 CEMENT LEACHING EXPERIMENT

In the cement leaching experiments, mixtures of brine and powered cement will be aged for extended periods of time, and then the brine will be centrifuged off and replaced. Several samples will be run simultaneously, and at each step, one of the samples will be sacrificed to analyze the solids. This experiment is intended to measure the volume of brine necessary to completely leach components out of the cement, and serves two purposes. The first is to provide electrolyte/solid data pairs to validate the thermodynamic model. The second is to provide information for a simpler borehole plug degradation model based on mass balances, similar to that used in the CCA. The CCA model assumes that 100 pore volumes of brine will leach sufficient components out of the cement to cause complete failure of the plug. This was based on reactions between cement and low ionic strength waters (Berner, 1990). A similar model, based on interactions with actual WIPP brines, might be more readily instituted than a thermodynamic model. For instance, the results collected from the cement wafer experiment (section 6.1.5.1) during the first several months suggest that one criterion of cement plug failure might be complete replacement of CSH with MSH, which causes shrinkage and fracturing in the wafer. Alternatively, in Berner's (1990) experiments, failure was described as crumbling of the cement, after nearly everything but silica had been leached out. If analysis of the solids in the cement leaching experiment indicates that all Ca has been replaced by Mg, or that only silica remains after exposure to a given volume of brine, then a mass balance model, involving predicted brine flow rates, can be developed.

Six systems, each containing 1g powdered cement and 30ml degassed brine, have been prepared for each cement/brine combination. The samples will be aged in a glove box as described in section 6.1.2, and will be constantly agitated. Every 6 months, each sample will be centrifuged and the brine will be decanted off and collected for analysis. The solids in one sample will be retained for analysis. Fresh brine will be added to the remaining samples, which will be returned to the glove box to re-equilibrate.

6.1.5.4 CEMENT WAFER EXPERIMENT

In the cement wafer experiment, thin wafers of cement are being aged in brine for extended periods of time. In the experiments with cement powders, the goal was to react the cement and brine as quickly and completely as possible, in order to reach equilibrium or steady state conditions. The wafer experiments examine the effects of non-equilibrium processes—the formation of mineral coatings, diffusion-limited reactions, the formation of expansive alteration phases (e.g., ettringite)—on the rate of cement reaction, and on the alteration products that form.

Salt-saturated Type C cement, salt-free Type C cement, and OPC were used. The wafers are 25 mm square by 3 mm thick and weigh about 3 grams. Each is aged in 250 ml of degassed brine (GW or ERDA-6) in a sealed polycarbonate wide-mouth bottle, stored in a N_2-sparged glove-box. Both brines and wafers are being sampled periodically (monthly/bimonthly) to observe the mineral coatings that form, and the possible effects these may have on the alteration mineral assemblage that forms in the underlying cement. It is possible that formation of low-porosity mineral coatings will significantly deplete cement pore waters in some aqueous species, resulting in formation of different alteration products than those observed in the crushed cement systems.

The results of SEM analyses of samples collected over the first 5 months of the experiment are discussed in Bryan (2002).

6.1.6 Column experiments with cement

Cured salt-free Type H cement was dry-cored using a 1" diamond core drill, and cores 2"–3" long were recovered. These will be used in core-column flow experiments, in which fresh brine will be pumped through the cores. The brine will not be degassed; rather, the GW brine will be mixed with the appropriate carbonate concentration for equilibrium with brucite/hydromagnesite, and the ERDA-6 brine will contain the same carbonate content as was measured in field samples. The brines will be sealed in a Hastalloy C accumulator to prevent degassing. An ISCO model 500D syringe pump will pump deionized water into the accumulator, pushing a piston which forces the brine through the core. The core will be encased in an ISCO RCH-type (radial confining pressure) core holder, with a Viton rubber core sleeve. The pump, accumulator, and core sleeve are capable of maintaining a pressure of greater than 2500 psi. Initially, the pumping pressure will be low, and the confining pressure a few hundred psi (just enough to seal the core sleeve against the core), but as minerals precipitate at the cement/brine interface and in the cement pore space, the pumping pressure and the confining pressure will be raised. A differential of 200 psi will be maintained between the pumping pressure and the confining pressure, to avoid leakage around the core. If the confining pressure reaches 2000 psi, the experiment will be terminated.

The core effluent will be collected using a fraction collector, and analyzed for pH, major elements, Si, and Al. Following the termination of the experiment, the core will be removed from the core holder and sliced in half. One half of the core will be impregnated with epoxy and characterized texturally and petrographically by optical microscopy and SEM imaging. Material from the other half will be crushed and analyzed by XRD to determine the alteration phases present, or digested and chemically analyzed to determine the chemical changes associated with alteration.

In addition to pumping brine through intact cores, the cores will be sliced to simulate a fracture, and the brine pumped through the fracture. In this case, the fracture surface is continuously exposed to fresh brine, and cement and brine components can diffuse into and out of the cement matrix, accelerating the rate of degradation.

6.2 Sample Control

Samples created routinely in the laboratory will be handled following the procedures described in NP 13-1 "Sample Control." They will be labeled with a unique sample number, as described and recorded in the scientific notebook. Any necessary handling and storage requirements will be stated in the scientific notebooks. Failure to meet those requirements will result in the data being disqualified and the experiment repeated; this will be documented and the appropriate action taken, as described in NP 13-1 "Sample Control."

No samples will be collected at the WIPP site for this project. Should offsite sample transfer be necessary, it will be accomplished following the procedures outlined in NP 13-1 "Sample Control," and SP 13-1 "Chain-of-Custody".

6.3 Data Control

A calibration program will be implemented for the work described in this test plan in accordance with NP 12-1, "Control of Measuring and Test Equipment." This M&TE calibration program will meet the requirements in NP 12-1 for: (1) receiving and testing M&TE; (2) technical operating procedures for M&TE; (3) the traceability of our standards to nationally recognized standards such as those from the National Institute of Standards and Technology (NIST); (4) maintaining calibration records. In addition, NP 13-1 and SP 13-1 identify requirements and appropriate forms for documenting and tracking sample possession.

6.3.1 Data Quality Control

Data collection procedures are specific to individual instruments. For details of the data acquisition for a particular instrument, see the specific SP or Users Manual for that instrument. A list of the relevant SPs is provided in Section 7.0. If no SP exists, or the analysis procedure listed in the SP is modified, the new procedure will be recorded in the scientific notebook. Any data acquired by a data acquisition system (DAS) will be attached directly to the scientific notebook or compiled in separate loose leaf binders with identifying labels to allow cross reference to the appropriate Scientific Notebook. If the instrument allows data to be recorded electronically, copies of the data disks will be submitted to the NWMP Records Center. For instruments that do not have direct data printout, the instrument readings will be recorded directly into the scientific notebook. Current versions of the DAS software will be included in the SNL WIPP Baseline Software List, if appropriate.

Quality control of the Scientific Notebooks will be established by procedures described in NP 20-2 "Scientific Notebooks." Methods for justification, evaluation, approval, and documentation of deviation from test standards and establishment of special prepared test procedures will be documented in the scientific notebooks. General procedures, goals and quality assurance controls for TP 00-06 are described below. Procedures including use of replicates, spikes, split samples, control charts, blanks and reagent controls will be determined during the development of experimental techniques as described in Section 5.1 above and documented in the scientific notebooks.

6.3.2 Data Acquisition Plan

The approach for collecting data varies for each instrument being used. Equipment data printouts will be attached directly to the scientific notebook or submitted to the SNL WIPP Record Center. For instruments that do not have direct data printout (balances, pH meters), the instrument reading will be directly recorded in the scientific notebook. The numerical data will be transferred from data printouts and scientific notebooks to Microsoft Excel (Office 97 version) spreadsheets. Data transfer and reduction shall be performed in such a way to ensure that data transfer is accurate, that no information is lost in the transfer, and that the input is completely recoverable. Data transfer and reduction shall be controlled to permit independent reproducibility by another qualified individual. A copy of each spreadsheet will be taped into the scientific notebook, and a second person will compare the data recorded in the notebook and that on the spreadsheet to verify that no transcription errors have occurred during technical and/or QA review of the notebook. This verification will be documented in the notebook when it is "signed off" by the reviewer.

6.3.3 Data Identification and Use

All calculations performed as part of the activities of TP 00-06 will be documented in a scientific notebook. The notebook will be technically reviewed periodically by a second person, who will note concurrence by co-signing the examined material. If a discrepancy is found, that discrepancy and its resolution will be documented in the notebook. In addition, there will be periodic quality assurance reviews of the notebook to ensure that the requirements of NP 20-2 "Scientific Notebooks" are addressed.

Data generated under this TP will be used to evaluate the casing corrosion and cement alteration models used in the CCA, and to develop a more robust borehole plug degradation model for conditions at the WIPP site.

6.4 Equipment

A variety of measuring and analytical equipment will be used for the work described in this test plan. This equipment includes that listed below, as well as equipment not yet identified. A complete, up-to-date, equipment list, including serial numbers, will be maintained in the scientific notebook. Scientific notebooks will be used to record all laboratory work activity.

Measuring and analytical equipment to be used for this project include:

6.4.1 Weighing Equipment.

Several balances are present in the facility and may be used for this project. These include a Mettler AT-261 five-decimal place electronic balance, an ANC three-decimal place balance, and top loading balances and scales with maximum ranges of 2 to 150 kilograms. Balance calibration checks will

be performed routinely using NIST-traceable weight sets, which are calibrated by the SNL Calibration Laboratory every 3 years. These weight sets include, but are not limited to, the following:

- *Troemner Calibration weight set*, ASTM Class 1, Serial number 22803, 1 mg – 100 g, calibration expires 12/16/02.
- *Troemner Calibration weight*, NBS-Class 1, Serial number 42795, 100 g, calibration expires 11/19/02.
- *Troemner Calibration weight*, NBS-Class 1, Serial number 42797, 100 g, calibration expires 11/19/02.
- *Troemner Calibration weight*, NBS-Class 1, Serial number 42799, 100 g, currently being re calibrated.
- *Troemner Calibration weight*, NBS-Class 1, Serial number 42800, 100 g, currently being recalibrated.
- *Troemner Calibration weight*, ASTM-Class 1, Serial number 47824, 200 g, calibration expires 11/19/02.
- *Troemner Calibration weight*, ASTM-Class 1, Serial number 55335, 1000 g, calibration expires 11/19/02.
- *Troemner Calibration weight*, ASTM-Class 2, Serial number I-12, 10 kg, calibration expires 12/17/02.

Balance accuracy and precision will be checked daily or prior to use (whichever is less frequent), using the calibration weight sets listed above. Calibration checks will be recorded in a scientific notebook.

6.4.2 Liquid Measuring Equipment

Standard Laboratory Class A glassware (pipettes, volumetric flasks, etc.) will be used at all times. In addition, several adjustable Eppendorf pipettes are available for use in the laboratory. The calibration of pipettes will be checked routinely against a calibrated balance, and will be recorded in the scientific notebook.

6.4.3 Other Analytical Equipment

- *Glass and digital thermometers* – Solution and oven temperatures will be measured using either: 1) NIST-traceable liquid-in-glass or digital thermometers, calibrated on an annual or biannual schedule as determined by the calibration service provider; or 2) thermometers which have been calibration-checked against the NIST-traceable thermometers described above. Such calibration checks will be recorded in the scientific notebook.
- *pH Meters and Autotitrators* – solution pH may be measured using pH meters and/or autotitrators. The range for all pH meters is 0.00 to 14.00. Electrodes will be calibrated before each use or daily (whichever is less frequent) with pH 4, 7, and 10 buffers manufactured by Fisher Scientific with unique lot numbers and expiration dates; traceable to the National Institute of Standards and Technology (NIST). The accuracy of the buffers is

±0.01 pH units; buffer values will be adjusted for laboratory temperatures as per buffer instruction sheets if necessary. Calibration checks will be recorded in the scientific notebook.

- *Equipment for Chemical Analysis* – Several instruments may be used to chemically characterize crushed or digested samples of cement or brines. These include a Perkin Elmer Optima 3300 DV Inductively-Coupled Plasma Optical Emission Spectrometer (ICP); a Cary 300 UV-Visible Spectrophotometer; and a UIC, Inc. Carbon Analyzer, consisting of an acidification module, a furnace module, and a CO_2 coulometer. These instruments will be user-calibrated according to the manufacturers specifications each time they are used and the calibration documented in the scientific notebook. Other instruments may be used as required.

- *Equipment for Petrographic, and Textural Characterization* – Several instruments will be used for physical characterization of the cement samples. The mineralogy and texture may be characterized using either an Olympus BX60 Polarizing Microscope or a JEOL JSM 5900LV scanning electron microscope. Bulk sample mineralogy will be determined using a Bruker AXS D-8 Advance X-Ray Diffractometer.

NMWP Activity/project-Specific Procedures may be written for these instruments if necessary. Until that time, detailed procedure descriptions will be documented in laboratory notebooks.

6.5 Location and Personnel

All experimental work related to TP 00-06 will be performed at the SNL Carlsbad Operations laboratory facility located in Carlsbad, NM. Sandia Personnel, including but not limited to Charles Bryan, Yifeng Wang, and Huizhen Gao will carry out the work. Users of identified equipment have received appropriate training by virtue of advanced technical degrees and years of laboratory experience.

7.0 NUCLEAR WASTE MANAGEMENT QUALITY ASSURANCE PROGRAM PROCEDURES (NPS), AND NWMP ACTIVITY SPECIFIC PROCEDURES (SPS)

The following project documents cover the work described in this Test Plan.

NP 2-1 – *Qualification and Training.* Rev 5, effective date 10/28/02.

NP 4-1 – *Procurement.* Rev 4, effective date 03/01/02.

NP 6-1 – *Document Review Process.* Rev 3, effective date 02/15/02.

NP 9-1 – *Analyses.* Rev 4, effective date 08/29/01.

NP 12-1 – *Control Of Measuring And Test Equipment.* Rev. 3, effective date 11/06/02.

NP 13-1 – *Sample Control.* Rev 1, effective date 04/14/99.

NP 16-1 – *Corrective Action.* Rev 2, effective date 11/23/99

NP 17-1 – *Records.* Rev. 2, effective date 05/14/01.

NP 19-1 – *Software Requirements.* Rev 9, effective date 06/12/02

NP 20-2 – *Scientific Notebooks.* Rev 1, effective date 04/26/99.

SP 1-1 – *QA Grading.* Rev. 3, effective date 03/01/02.

SP 12-1 – *Use of Laboratory Balances and Scales.* Rev. 0, effective date 08/08/00.

SP 12-2 – *Use and Maintenance of the UIC, Inc. Model CM5014 CO_2 Coulometer, CM5130 Acidification Module and CM5120 Furnace Apparatus.* Rev 0, effective date 12/05/00.

SP 13-1 – *Chain of Custody.* Rev. 2, effective date 06/13/00.

TOP 544 – *Preparing Synthetic Brines for Chemical Retardation and Transport Experiments.* Rev 0, effective date 01/05/96.

Any revisions in the above technical work documents that occur during the course of this project will be implemented, and do not require modification of this test plan. Current versions of the documents listed above are maintained at the following SNL NWMP web site:

http://www.nwmp.sandia.gov/onlinedocuments

In addition, procedures for use of the ICP, SEM, XRD, and UV-Vis spectrophotometer will be recorded in the scientific notebooks until such time as SP's are written for these instruments. Cement mixing and sample preparation procedures, which may vary from sample to sample as work scope evolves, will be detailed in Scientific Notebooks, in accordance with NP 20-2.

8.0 RECORDS, REPORTS, AND AUDITS

All records providing evidence of quality, including but not necessarily limited to personnel qualification and training forms, lists of M&TE and software, electronic data, technical procedures, laboratory notebooks, calibration records and certificates, and reports, will be QA records. These records will be maintained in accordance with NP 17-1, "Records." To the maximum extent possible, the format of the enclosed WIPP Records Package will be used to organize QA records. All records will be accurate, complete, identifiable, and legible, and will be inspected to ensure they satisfy these requirements prior to submittal to the SNL/WIPP Records Center. Two copies of all QA records will be submitted.

Documents will be prepared for review and approval in accordance with NP 6-1, "Document Review Process." NP 6-1 requires that the author(s) and reviewer(s): (1) use the DRC Form NP 6-1-1,

(see Appendix A in NP 6-1) in some, but not all, cases; (2) resolve all of the comments; (3) return this form with all signatures to the SNL/WIPP Records Center.

9.0 TRAINING

All personnel involved in the experiments described in TP 00-06 will be trained and qualified for their assigned work. This requirement will be implemented through NP 2-1 Qualification and Training. Evidence of training to assigned NPs, SPs, TOPs, TP 00-06, ES&H procedures, and any other required training will be documented through Form NP 2-1-1 *Qualification and Training Form.* Annual Refresher QA training will ensure on-site personnel are trained to the SNL/WIPP QA Program.

10.0 HEALTH AND SAFETY

All of the health and safety requirements relevant to the work described in TP 00-06 and the procedures that will be used to satisfy these requirements are described in a SNL ES&H standard operating procedure (SOP-C001, "Activities in the SNL/Carlsbad Laboratory Facility"). This document describes the hazards associated with these experiments and the procedures to deal with those hazards, including all the training requirements for personnel involved in conducting the experiments. In addition, a Radiological Work Permit (RWP-1617) and Radiological Work License (RWL 6000-16, "Use of the XRD Unit Located in the Carlsbad Laboratory Facility") covers activities involving use of the X-Ray Diffractometer. Additional SPs and RWPs may be mandated by SNL corporate ES&H requirements and their issuance will not require revision of this Test Plan.

11.0 PERMITTING/LICENSING

RWL and RWP documents are in place for use of the X-ray diffractometer in the Carlsbad Laboratory Facility. There are no other special licenses or permit requirements for the work described in TP 00-06.

12.0 REFERENCES

Atkins, M., D.G. Bennett, A.C. Dawes, F.P. Glasser, A. Kindness, and R. Read. 1992a. "A Thermodynamic Model for Blended Cements," *Cement and Concrete Research.* Vol. 22, no. 3, 497-502.

Atkins, M., F.P. Glasser, and A. Kindness. 1992b. "Cement Hydrate Phases; Solubility at 25 °C," *Cement and Concrete Research*, Vol. 22, no. 3, 241-246.

Atkins, M., F.P. Glasser, and A. Kindness, A. 1991a. "Phase Relations and Solubility Modelling in the CaO-SiO_2-Al_2O_3-MgO-SO_3-H_2O System: for Application to Blended Cements," *Materials Research Society Symposium Proceedings*, Vol. 212, 387-394.

Atkins, M., D. Macphee, A. Kindness, and F.P. Glasser, 1991b. "Solubility Properties of Ternary and Quaternary Compounds in the CaO-Al_2O_3-SO_3-H_2O System," *Cement and Concrete Research*, Vol. 21, no. 6, 991-998.

Atkinson, A., and J.A. Hearne. 1990. "Mechanistic Model for the Durability of Concrete Barriers Exposed to Sulphate-bearing Groundwaters," *Materials Research Society Symposium Proceedings*, Vol. 176, 149-156.

Atkinson, A., J.A. Hearne, and C.F. Knights. 1989. *Aqueous Chemistry and Thermodynamic Modelling of CaO-SiO2-H2O Gels at 80°C*, DOE Report # DOE/HMIP/RR/91/045.

Azaroual, M., C. Fouillac, and J.M. Matray. 1997. "Solubility of Silica Polymorphs in Electrolyte Solutions, I. Activity Coefficient of Aqueous Silica from 25 °C to 250 °C, Pitzer's Parameterization," *Chemical Geology*, Vol. 140, 155-165.

Bennett, D.G., D. Read, M. Atkins, and F.P. Glasser. 1992. "A Thermodynamic Model for Blended Cements II: Cement Hydrated Phases; Thermodynamic Values and Modelling Studies," *Journal of Nuclear Materials*, Vol. 190, 315-325.

Berner, U.R. 1987. "Modelling Porewater Chemistry in Hydrated Portland Cement," *Materials Research Society Symposium Proceedings*, Vol. 84, 319-330.

Berner, U.R.. 1988. "Modelling the Incongruent Dissolution of Hydrated Cement Minerals," *Radiochim. Acta*, Vol. 44/45, 387-393.

Berner, U. 1990. *A Thermodynamic Description of the Evolution of Pore Water Chemistry and Uranium Speciation During the Degradation of Cement*, Technical Report 90-12, Paul Scherrer, Villigen, Switzerland.

Bonen, D. 1992. "Composition and Appearance of Magnesium Silicate Hydrate and its Relation to Deterioration of Cement-Based Materials," *Journal of the American Ceramics Society*, Vol. 75, 2904-2906.

Bonen, D., and M.D. Cohen. 1992. "Magnesium Sulfate Attack on Portland Cement Paste II. Chemical and Mineralogical Analysis," *Cement and Concrete Research*, Vol. 22, 707-718.

Bonen, D. 1996. "Petrographic Analyses of Concrete and Grout Recovered from the Waste Isolation Pilot Plant," The Technological Institute, Northwestern University, Interim Report to SNL dated January 15, 1996.

Bryan, C.R. 2002. "Experimental Work to Develop a Model for Cement-Brine Interactions," "Sandia National Laboratories Technical Baseline Reports, WBS 1.3.5.3, Compliance

Monitoring; WBS 1.3.5.4, Repository Investigations, Milestone RI130, July 31, 2002." Carlsbad, NM: Sandia National Laboratories. 4.2-1 to 4.2-15.

Chen, C.A., and W.L. Marshall. 1982. "Amorphous Silica Solubilities IV. Behavior I Pure Water and Aqueous Sodium Chloride, Sodium Sulfate, Magnesium Chloride, and Magnesium Sulfate Solutions up to 350 °C," *Geochimica et Cosmochimica Acta*, Vol. 46, 279-287.

Damidot, D., and F.P. Glasser. 1992. "Thermodynamic Investigation of the CaO-Al_2O_3-$CaSO_4$-H_2O System at 50°C and 85°C," *Cement and Concrete Research*, Vol. 22, 1179-1191.

Damidot, D., and F.P. Glasser. 1993. "Thermodynamic Investigation of the CaO-Al_2O_3-$CaSO_4$-H_2O System at 25°C and the Influence of Na_2O," *Cement and Concrete Research*, Vol. 23, 221-238.

Felmy, A.R., C.C. Schroeder, and M.J. Mason. 1994a. *A Solubility Model for Amorphous Silica in Concentrated Electrolytes*, DOE Report # PNL-SA-25345.

Felmy, A.R., J.R. Rustad, M.J. Mason, and R. de la Bretonne. 1994b. *A Chemical Model for the Major Electrolyte Components of the Hanford Waste Tanks: the Binary Electrolytes in the System: Na-NO_3-NO_2-SO_4-CO3-F-PO_4-OH-Al$(OH)_4$-H_2O,* DOE Report # PNL-SA-23952.

Gartner, E.M., and H.M. Jennings. 1987. "Thermodynamics of Calcium Silicate Hydrates and Their Solutions," *Journal of the American Ceramics Society*, Vol. 70, no. 10, 743-749.

Gasteiger, H.A., W.J. Frederick, and R.C. Streisel. 1992. "Solubility of Aluminosilicates in Alkaline Solutions and a Thermodynamic Equilibrium Model," *Ind. Eng. Chem. Res.*, Vol. 31, 1183-1190.

Glasser, F.P., E.E. Lachowski, and D.E. MacPhee. 1987. "Compositional Model for Calcium Silicate Hydrate (C-S-H) Gels, their Solubilities and Free Energies of Formation," *Journal of the American Ceramics Society*, Vol. 70, no. 7, 481-485.

Goto, S., M. Tsunetani, and R. Kondo. 1979. "Free Energy of Formation of $3CaO{\cdot}Al_2O_3{\cdot}CaCl_2{\cdot}12H_2O$ in Connection with Durability of Hardened Cement Immersed in Sea Water," *Ann. Chim. Fr.*, Vol. 4, 425-429.

Harvie, C.E., N. Møller, and J.H. Weare. 1984. "The Prediction of Mineral Solubilities in Natural Waters: The Na-K-Mg-Ca-H-Cl-SO_4-OH-HCO_3-H_2O System to High Ionic Strengths at 25 °C," *Geochimica et Cosmochimica Acta*, Vol. 44, 981-997.

Havlica, J., and S. Sahu. 1992. "Mechanism of Ettringite and Monosulfate Formation," *Cement and Concrete Research*, Vol. 22 no. 4, 671-677.

Krumhansl, J.L. 1993. "The Accelerated Testing of Cement in Brines" *Proceedings of the American Ceramics Society, Cement-Based Materials*, April 19-22, 1993, Cincinnati, OH, 153-154.

Krumhansl, J.L. 1995. *Brine-Concrete Interactions and their Implications for WIPP Seal Performance*, unpublished SNL letter report, dated Oct. 25, 1995. Available from NWMP Records Center, WPO# 418229, records package # 247886.

Krumhansl J.L., and S.J. Lambert. 1992. "Degradation of Portland Cements Exposed to Evaporite Brine at Hydrothermal Temperatures," *Materials Research Society Symposium Proceedings,* Vol. 245, 123-128.

Lambert, S.J., E.J. Nowak, L.D. Wakely, and T.S. Poole. 1992. "Interactions between Concrete and Brine at the Waste Isolation Pilot Plant (WIPP) Site, New Mexico," in *Advanced Cementitious Systems: Mechanisms and Properties, Materials, Research Society Symposium Proceedings*, Vol. 245, 111-122.

Marshall, W.L. 1980. "Amorphous Silica Solubilities — I. Behavior in Aqueous Sodium Nitrate Solutions; 25-300°C, 0-6 molal*," *Geochimica et Cosmochimica Acta*, Vol. 44, 907-913.

Macphee, D.E., M. Atkins, and F.P. Glasser. 1989. "Phase Development and Pore Solution Chemistry in Ageing Blast Furnace Slag-Portland Cement Blends," in *Scientific Basis for Nuclear Waste Management XII, Materials Research Society Symposium Proceedings,* Vol. 127, 475-480.

Neall, F.B. 1994. *Modelling of the Near-Field Chemistry of the SMA Repository at the Wellenberg Site: Application of the Extended Cement Degradation Model*, Paul Scherrer Institute Paper # 94-03.

Neall, F.B. 1996. *Modelling the Long-Term Chemical Evolution of the Near-Field of a Cementitious Repository Using SEQDISSOLVE – Model, Assumptions, and Results*, Paul Scherrer Institute Paper # TM 44-95-08.

Novak, C.F. 1997. "Calculation of Actinide Solubilities in WIPP SPC and ERDA-6 Brines under MgO Backfill Scenarios Containing either Nesquehonite or Hydromagnesite as the Mg-CO3 Solubility-Limiting Phase." Unpublished memorandum to R.V. Bynum, April 21, 1997. WPO 46124. Carlsbad, NM: Sandia National Laboratories.

Palmer, D.A., and D.J. Wesolowski. 1992. "Aluminum Speciation and Equilibria in Aqueous Solution: II. The Solubility of gibbsite in Acidic Sodium Chloride Solutions from 30-70 °C," *Geochimica et Cosmochimica Acta*, Vol. 56, 1093-1111.

Pfingsten, W., and M. Shiotsuki. 1998. "Modelling a Cement Degradation Experiment by a Hydraulic Transport and Chemical Equilibrium Coupled Code," *Materials Research Society Symposium Proceedings,* Vol. 506, 805-812.

Pitzer, K.S. 1987. "A Thermodynamic Model for Aqueous Solutions of Liquid-like Density," in *Thermodynamic Modeling of Geological Materials: Minerals, Fluids, and Melts*, I.S.E. Carmichael and H.P. Eugster (eds), Mineralogical Society of America Reviews in Mineralogy, Vol. 17, 97-142.

Poole, T.S., L.D. Wakely, and C.L. Young. 1994. *Individual and Combined Effects of Chloride, Sulfate, and Magnesium Ions on Hydrated Portland Cement Pastes*, SAND93-7040 (Contractor Report; Army Waterways Experiment Station, Vicksburg, Miss.).

Richardson, R.G., and M.E. Crawley. 1999. *Waste Isolation Pilot Plant Borehole Plugging and Abandonment Program Plan*, Westinghouse.

Richter, U., P. Brand, K. Bohmhammel, and T. Könnecke. 2000. "Thermodynamic Investigations of Aqueous Solutions of Aluminium Chloride," *Journal of Chemical Thermodynamics*, Vol. 32, 145-154.

Taylor, H.F.W. 1992. "Tobermorite, Jennite, and Cement Gel," *Zeitschrift für Kristallographie*, Vol. 202, 41-50.

Villareal, R., A. Trujillo, C. Scherer, and A. Morzinski. 1999. *A Study of STTP Pyrochemical Salt Tests and Results Featuring L25, 26, 27, and 28*, Los Alamos National Labs Interim Report.

Wakely, L.D., T.S. Poole, and J.P. Burke. 1992. *Deteriorated Concrete from Liner of WIPP Waste Shaft*, Technical Report SL-92-14, Army Waterways Experiment Station, Vicksburg, MS.

Wakely, L.D., T.S. Poole, and J.P. Burke. 1994. *Individual and Combined Effects of Chloride, Sulfate, and Magnesium Ions on Hydrated Portland Cement Paste*, SAND93-7040, Sandia National Laboratories, Albuquerque, NM.

Wesolowski, D.J. 1992 "Aluminum Speciation and Equilibria in Aqueous Solution: I. The Solubility of Gibbsite in the System Na-K-Cl-OH-Al$(OH)_4$ from 0 to 100 °C," *Geochimica et Cosmochimica Acta*, Vol. 56, 1065-1091.

Wesolowski, D.J., and D.A. Palmer. 1992. "Experimental Studies of Aluminum Solubility and Speciation in Brines," in *Water-Rock Interaction*, Kharaka and Maes (eds), Balkema, Rotterdam.

Wesolowski, D.J., and D.A. Palmer. 1994. "Aluminum Speciation and Equilibria in Aqueous Solution: V. Gibbsite Solubility at 50 °C and pH 3-9 in 0.1 Molal NaCl Solutions (a General Model for Aluminum Speciation; Analytical Methods," *Geochimica et Cosmochimica Acta*, Vol. 58, no. 14, 2947-2969.

Wolery, T.J. 1992. *EQ3NR, A Computer Program for Geochemical Aqueous Speciation-Solubility Calculations: Theoretical Manual, User's Guide, and Related Documentation (Version 7.0)*, Lawrence Livermore National Laboratories, UCRL-MA-110662 PT III.

Wolery, T.J., and S.A. Daveler. 1992. *EQ6, A Computer Program for Reaction Path Modeling of Aqueous Geochemical Systems: Theoretical Manual, User's Guide, and Related Documentation (Version 7.0)*, Lawrence Livermore National Laboratories, UCRL-MA-110662 PT IV.

Xie, P., and J.J. Beaudoin. 1992. "Mechanism of Sulphate Expansion. I. Thermodynamic Principle of Crystallization Pressure," *Cement and Concrete Research*, Vol. 22 no. 4, 631-640.

Zhang, P., H.L. Anderson, J.W. Kelley, J.L. Krumhansl, and H.W. Papenguth. 1999. *Kinetics and Mechanisms of Formation of Magnesite from Hydromagnesite in Brine*, SAND2000-1946J.

4.5 Temperature Measurements in Support of the WIPP Salado Mass Concrete Test Program[1]

T. W. Pfeifle, T. L. MacDonald, and E. F. Schaub
Sandia National Laboratories, MS 1395
4100 National Parks Hwy.
Carlsbad, NM USA 88220

Abstract

The U.S. Department of Energy (DOE) Carlsbad Field Office authorized Washington TRU Solutions LLC, the Management and Operating Contractor of the Waste Isolation Pilot Plant (WIPP), to design and conduct a large-scale Salado Mass Concrete (SMC) test program in anticipation of installing the first Panel Closure System in Panel 1 of the WIPP repository. The objectives of the test were to: (1) locate and procure raw materials consistent with the SMC mix design; (2) conduct laboratory bench-scale tests to verify target properties of both fresh and cured SMC samples; (3) conduct two small-scale field tests to demonstrate pumpability of the SMC; (4) conduct a large-scale (30-yd^3) test to demonstrate SMC workability, transportability, and placement techniques; (5) evaluate SMC physical, hydrological, and thermal properties during the large-scale test.

To support the overall objectives of the SMC test program, the DOE directed Sandia National Laboratories' Carlsbad Programs Group to acquire heat-of-hydration temperature increase data during the placement and curing of the large-scale 30-yd^3 test. In response to this directive, Sandia designed and assembled a data acquisition system (DAS) comprising temperature sensors and a stand-alone measurement and control unit capable of interfacing and communicating with the sensors. The validated system was then used to measure temperatures in the 30-yd^3 (10-ft by 10-ft by 8-ft) monolith cast during the large-scale test. Data were acquired within the monolith using a three-dimensional orthogonal array of sensors and steel-rope support wire having its origin centered at the midpoint of the monolith. Boundary condition temperatures (i.e., below and in the air adjacent to the monolith) were also acquired. This report presents a description of the DAS, the procedures used to acquire the temperature data, and the results from the large-scale and two small-scale field tests.

[1]This work is covered by WBS #1.3.5.4.3.1.

Introduction

BACKGROUND

The U.S. Department of Energy (DOE), through its Carlsbad Field Office, manages the Waste Isolation Pilot Plant (WIPP) located near Carlsbad, NM, as a geologic repository for the safe disposal of transuranic radioactive and hazardous wastes generated as by-products of various U.S. defense-related activities. Waste is (or will be) stored in eight waste panels or disposal units excavated at a depth of 655 m in bedded salt of the Permian Salado Formation. Each panel contains seven disposals rooms serviced by two access drifts for waste emplacement and air circulation. The access drifts are typically referred to as the air-intake and air-exhaust drifts and have nominal cross-sectional dimensions (width by height) of 20 ft by 13 ft (6.1 m by 4 m) and 14 ft by 12 ft (4.3 m by 3.7-m), respectively.

Because the WIPP accepts mixed wastes, it is subject to two sets of regulatory requirements: (1) U.S. Environmental Protection Agency (1993) and U.S. EPA (1996) for the radioactive constituents of the waste, and (2) U.S. Code (1976) for the hazardous component of the waste. The EPA is responsible for ensuring compliance of the WIPP with both requirements, but has delegated its responsibility for the Resource Conservation and Recovery Act (RCRA) requirements to the state of New Mexico. In turn, the state of New Mexico has enacted laws consistent with and in lieu of RCRA, authorizing the New Mexico Environment Department (NMED) to promulgate and enforce regulations for hazardous waste disposal.

As part of its respective applications to EPA and NMED for a certification and hazardous waste facility permit (HWFP) for the WIPP, DOE presented four detailed design options and engineering specifications for the construction, emplacement, and interface grouting associated with panel closure systems (PCS) to be installed in the access drifts (air-intake and exhaust) of each waste panel after the panel was filled with waste. The primary purpose of the PCS is to meet RCRA requirements for limiting the migration of volatile organic compounds found in the waste. The PCS must also safely contain a hypothetical methane explosion during repository operations. The four PCS options ranged from the simplest design, in which a freshwater concrete barrier and construction-isolation wall are placed directly in the access drifts, to the most robust design, which comprises a massive freshwater concrete monolith (keyed into the native rock by removing the disturbed rock zone in the vicinity of the seal) and an explosion wall. The various options were presented to provide flexibility for the range of ground conditions likely to be encountered in the underground repository.

Both the EPA certification (U.S. EPA, 1998) and the NMED HWFP (NMED, 1999) required the DOE to install the most robust PCS (referred to as Option D), and to substitute Salado Mass Concrete (SMC) for the freshwater concrete to ensure that the compatibility of the concrete monolith and the host environment (Salado Formation). In addition, the HWFP established schedules for initiation (60 days after filling a panel) and completion (180 days after filling) of the PCS and a requirement to demonstrate that the SMC meets target properties for slump, compressive strength, heat rise, heat of hydration, concrete set time, thermal diffusivity, and water permeability.

Following EPA certification of the WIPP in 1998 and issuance of a HWFP by NMED in 1999, the DOE initiated disposal of waste in Panel 1 and has continued operations for more than three years. With an accelerated rate of waste shipments to the WIPP, the DOE anticipates that Panel 1 will be filled sometime during Fiscal Year (FY) 2003 and, thus, will need to initiate the construction and emplacement of the first set of PCS monoliths in the access drifts of Panel 1. Therefore, the DOE authorized Washington TRU Solutions LLC (WTS), the WIPP Management and Operating Contractor (M&OC), to design and conduct a SMC test program. The objectives of the test program were to: (1) locate and procure raw materials consistent with the specified SMC mix design; (2) prepare bench-scale SMC batches using procured raw materials to verify target properties of both fresh and cured test samples; (3) mix a 5-yd^3 SMC batch to demonstrate pumpability; (4) mix and place a 30-yd^3 SMC batch to demonstrate workability, transportability, and placement techniques; (5) collect appropriate data for fresh and cured properties of the 30-yd^3 SMC batch to evaluate physical, mechanical, hydrological, and thermal properties, as appropriate; (6) prepare a final report documenting all results.

Based on the results of the 5-yd^3 batch (i.e., observation of a low slump value of approximately 1.5 in instead of the specified slump of 8 in), the M&OC modified the test program to include the mixing of a third field batch, one with a volume of approximately 1 yd^3, before the mixing of the 30-yd^3 batch. In comparison to the 5-yd^3 batch, the 1-yd^3 batch was mixed by using: (1) different sequencing when adding the various batch ingredients, and (2) a lower initial batch temperature.

In concert with the M&OC test activities, the DOE also authorized Sandia National Laboratories' Carlsbad Programs Group, the WIPP Scientific Advisor, to support the SMC test program through the collection of temperature-increase data during the various field tests. This report documents Sandia's efforts consistent with this directive. Quantification of the temperature increase served to: (1) verify that the SMC is a low heat-of-hydration concrete, and (2) validate assumptions in seal design analyses related to the magnitude of thermally-induced tensile strains. An accuracy of $\pm$ 1 °C was established for the temperature measurements, proved to be easily obtainable, and satisfied the general requirements for the test program.

TECHNICAL APPROACH AND SCOPE

In supporting the SMC test program, Sandia developed a technical approach (MacDonald, 2002) that included: (1) design, assembly, and calibration of an instrumentation system to collect temperature data; (2) installation and monitoring of temperature sensors placed in samples of SMC obtained from the 5-yd^3 and 1-yd^3 batches to evaluate and verify the

operation of the selected instrumentation system; (3) installation of the framework used to position the temperature sensors in the formwork for containing the 30-yd^3 SMC batch mix; (4) installation and performance testing of temperature sensors used for the 30-yd^3 SMC batch mix; (5) collection and documentation of temperature-increase data during curing of the 30-yd^3 SMC batch mix.

The instrumentation system designed and assembled for the test included temperature sensors (thermocouples and thermistors) and a programmable, fully-automated data acquisition system (DAS) powered by a solar panel and rechargeable battery. The sensors and DAS were calibrated against standards traceable to the National Institute of Standards and Technology (NIST) at Sandia's Primary Standards Laboratory in Albuquerque, NM.

Two separate performance evaluation tests of the instrumentation system were conducted before the 30-yd^3 test was performed. The tests were conducted by: (1) placing fresh SMC from the 5-yd^3 and 1-yd^3 batches into drums; (2) inserting temperature sensors into the SMC at the center of the drums; (3) monitoring SMC and ambient temperature over several weeks using the DAS.

To monitor temperatures in the 30-yd^3 field test, temperature sensors were secured to a framework of stainless-steel wire rope installed inside a steel-reinforced plywood box (10-ft-length by 10-ft-width by 8-ft-height) erected on a 9-inch-thick, steel-reinforced concrete slab. The wire rope volume was small relative to the concrete mass so thermal conduction along the rope was assumed to be small. In addition, the sensor tips were located approximately one inch from the rope to minimize any influence of the rope on the temperature measurements. The steel rope and sensors formed a three-dimensional orthogonal array with the origin of the array located at the center of the box (Figure 1). The array consisted of two horizontal axes, aligned approximately north-south (y axis) and east-west (x axis), and a single vertical axis (z axis). Sensors were secured to the wire rope at predetermined and, in some cases, redundant locations to ensure that the maximum temperature increase could be determined during the test and to identify the existence of any temperature gradients. Temperature sensors were also placed under the steel-reinforced concrete slab forming the foundation of the box and in the ambient air (i.e., above the box, on the outside surfaces of the box, and at the DAS location). Electrical instrumentation cables were run from the sensors to the DAS mounted on the outside of the plywood box. Operations checks were performed on each sensor. A system performance evaluation was conducted by initiating the data acquisition protocol at the DAS and monitoring the output of each sensor over a 4-day period before any SMC was placed in the box.

During the 30-yd^3 field test, 26 temperature sensors (22 thermocouples and 4 thermistors) were monitored and data were logged at ten-minute intervals. Of this total, 17 were located in the SMC, 4 were located below the steel-reinforced slab, and 5 (including the one placed near the DAS) were located in air. Four other thermocouples were also installed along the vertical axis as spares, but were not monitored during the test. Monitoring and logging of active sensors continued for 65 consecutive days. Temperature data were plotted as a function of time to determine the maximum temperature recorded by each sensor and to determine the peak temperature increase and its location within the 30-yd^3 test monolith.

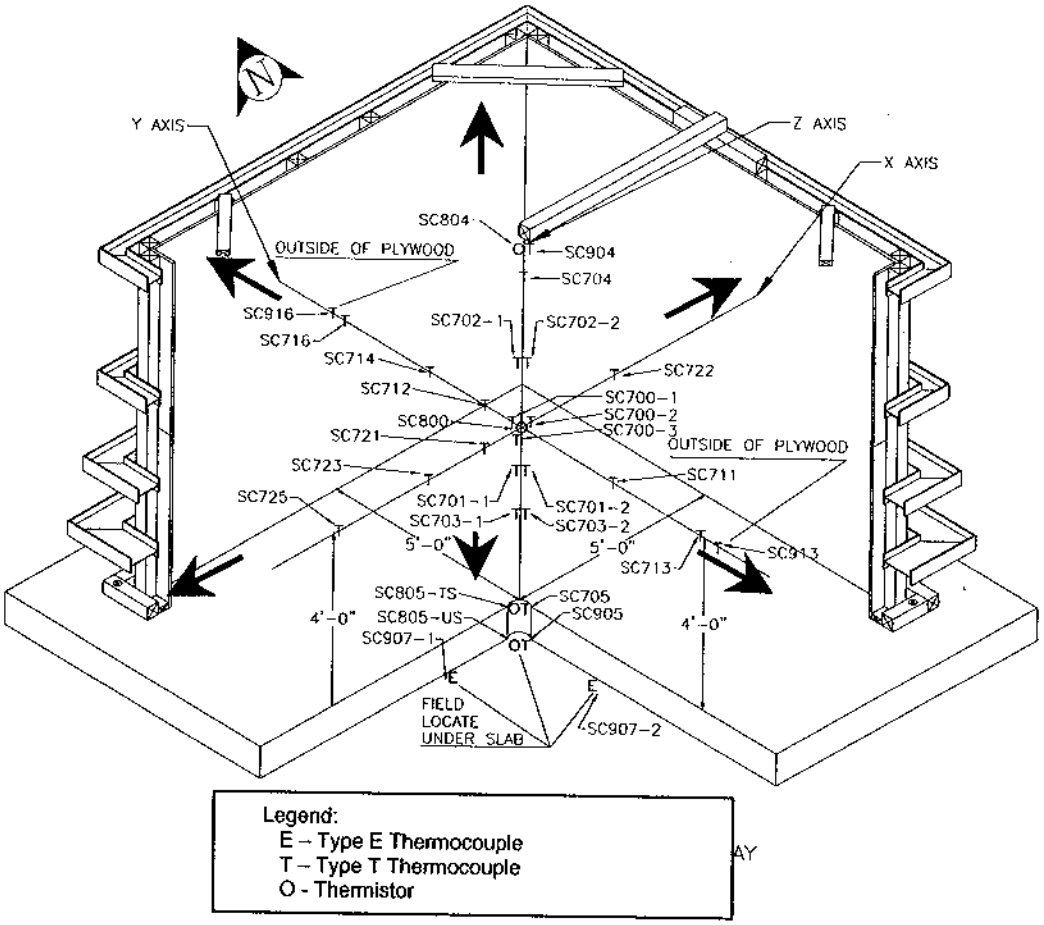

Figure 1. Isometric view of 30-yd^3 SMC plywood form depicting temperature sensor instrumentation array.

All Sandia support activities were documented through use of a Scientific Notebook.

Measurement and Test Equipment

The measurement and test equipment used to monitor temperatures during the SMC program comprised a DAS and temperature sensors (thermocouples and thermistors). All quality-affecting equipment was calibrated against standards traceable to the NIST at Sandia's Primary Standards Laboratory. A brief description of the equipment and calibration techniques is provided below under separate headings.

DATA ACQUISITION SYSTEM

The DAS used to collect data automatically during the SMC test consisted of a Geomation, Inc., model 2380 measurement and control unit (MCU), a solar panel kit, and a portable (laptop) personal computer (PC) loaded with GEONET Suite™ software also supplied by Geomation, Inc. Dimensional measurements made to locate sensors and sensor support wires were acquired manually using standard tapes.

The 2380 MCU™ is "off-the-shelf," stand-alone hardware that includes: (1) power supplies for supplying sensor excitation voltage, signal conditioners to modify and amplify sensor output; (2) a 16-bit processor and analog-to-digital (DA) and digital-to-analog (AD) converter modules to acquire and process sensor signals; (3) on-board memory cards to store acquired data locally; (4) a rechargeable battery to power the MCU circuitry, internal clock and calendar to synchronize data acquisition; (5) input-output (IO) ports for communication with the portable PC and other peripherals. The on-board battery was continuously recharged during daylight hours using a 20-W solar panel kit connected directly to the MCU. The portable PC and GEONET Suite™ software were used to create/modify test protocol tables and access data stored on the MCU. The protocol tables, prepared by the DAS operator before test initiation, included information on sensor calibration constants, sensor channel assignments, logging frequency, measurement units, alarm limits, etc. After the protocol tables were downloaded from the PC to the MCU, the MCU executed the programmed instructions as a stand-alone operation and acquired data according to these instructions. Periodically during the test, the portable PC was reconnected to the MCU to upload and view the acquired data and to modify any protocols, as necessary.

The Geomation GEONET Suite™ software is an "off-the-shelf" product and was treated as acquired software in accordance with the requirements established under Sandia's Nuclear Waste Management Program (NWMP) (Chavez, 2002). Temperature data uploaded from the MCU to the PC using GEONET were subsequently transferred electronically to Microsoft Excel for plotting and trend evaluation.

TEMPERATURE SENSORS

Temperature sensors used in the 1-yd^3, 5-yd^3, and 30-yd^3 tests included Watlow-Gordon Type E and Type T thermocouples and Watlow-Gordon thermistors. General specifications for the sensors are provided in Table 1. The thermocouples provided the principal temperature measurements, while the thermistors provided redundant measurements. A total of 38 sensors were installed during the three tests including a single thermocouple that was always placed in the air adjacent to the DAS.

Most of the 38 sensors were placed directly in the SMC to measure the heat-of-hydration temperature response in the 30-yd^3 test or to evaluate the capabilities and response of the DAS in the 5-yd^3 and 1-yd^3 tests. Other sensors were also placed in the air near the SMC and under the reinforced concrete slab used as the foundation for the 30-yd^3 test to quantify boundary temperatures during the curing of the SMC.

Table 1. General Specifications for Temperature Sensors Used in the SMC Tests

Sensor Type[a]	Range and Accuracy (°C)	Sheath Specification[b]	Leadwire Specification[b]
'E' TC	-200 to 870 / ± 1.0	OD = 0.125 in, L = 55 in, Alloy 600, ungrounded	L = 11 ft, FEP solid overbraid construction
'T' TC	-200 to 370 / ± 0.5	OD = 0.125 in, L = 12 in, 316 Stainless Steel, ungrounded	L = 30 ft, FEP solid standard construction
TM	-60 to 150 / ± 0.3	OD = 0.188 in, 316 Stainless Steel, 10,000 ohms	L = 30 ft, TFE stranded standard construction

a TC = thermocouple; TM = thermistor
b OD = outside diameter; L = length

Table 2 identifies each sensor used in the three SMC tests and also provides information on sensor type, serial number, and placement location. As shown, four thermocouples and a thermistor were installed at the mid-height of a 96-gal drum filled with SMC from the 5-yd^3 test, while two thermocouples were installed at the mid-height of a 55-gal drum filled with SMC from the 1-yd^3 test. In addition, 26 thermocouples and 4 thermistors were installed in the 30-yd^3 test including 22 sensors placed in the SMC, 4 sensors placed below the reinforced concrete slab, and 4 sensors placed in the air near the monolith. Four of the thermocouples installed in the 30-yd^3 test were treated as spares and thus were not connected to the DAS. These spare sensors were added to ensure that SMC midpoint temperature could be monitored should the DAS and/or active sensors be corrupted or destroyed by natural events or vandalism. The locations of all sensors placed in the 30-yd^3 test are provided in Table 2 and shown schematically in Figure 1.

Table 2. Temperature Sensors Used in SMC Tests

SMC Test	Sensor Type[a]	Instrument Number	Serial Number	Date Calibrated	Installation Location
5 yd^3	'E' TC	SS700-AE	1	02/02/02	Midheight of 96-gal drum
	'T' TC	SS700-AT	1	03/02/02	Midheight of 96-gal drum
	'E' TC	SS700-BE	2	02/08/02	Midheight of 96-gal drum
	'T' TC	SS700-BT	2	03/02/02	Midheight of 96-gal drum
	TM	SS800A	1	03/05/02	Midheight of 96-gal drum
	'T' TC	SS900-AT	3	03/02/02	Air adjacent to DAS
1 yd^3	'E' TC	SS701-AE	6	02/08/02	Midheight of 55-gal drum
	'E' TC	SS701-BE	7	02/08/02	Midheight of 55-gal drum
	'T' TC	SS900-AT	3	03/02/02	Air adjacent to DAS
30 yd^3	'E' TC	SC907-1	9	02/08/02	Below reinforced concrete slab, 1 ft NW of center
	'E' TC	SC907-2	8	02/08/02	Below reinforced concrete slab, 1 ft SE of center
	'T' TC	SC700-1	7	03/02/02	Monolith midpoint
	'T' TC	SC700-2	12	03/02/02	Monolith midpoint
	'T' TC	SC700-3	21	03/02/02	Monolith midpoint, spare
	'T' TC	SC701-1	19	03/02/02	Vertical axis, ~ 3 ft above top of reinforced concrete slab
	'T' TC	SC701-2	20	03/02/02	Vertical axis, ~ 3 ft above top of reinforced concrete slab, spare
	'T' TC	SC702-1	22	03/02/02	Vertical axis, ~ 5.5 ft above top of reinforced concrete slab
	'T' TC	SC702-2	23	03/02/02	Vertical axis, ~ 5.5 ft above top of reinf. concrete slab, spare
	'T' TC	SC703-1	17	03/02/02	Vertical axis, ~ 2 ft above top of reinforced concrete slab
	'T' TC	SC703-2	18	03/02/02	Vertical axis, ~ 2 ft above top of reinforced concrete slab, spare
	'T' TC	SC704	24	03/02/02	Vertical axis, ~ 7 ft above top of reinforced concrete slab
	'T' TC	SC705	16	03/02/02	Vertical axis, top of reinforced concrete slab
	'T' TC	SC711	6	03/02/02	N-S axis, ~2.5 ft south of monolith midpoint
	'T' TC	SC712	8	03/02/02	N-S axis, ~ 1 ft north of monolith midpoint
	'T' TC	SC713	5	03/02/02	N-S axis, inside face of south plywood form
	'T' TC	SC714	9	03/02/02	N-S axis, ~ 2.5 ft north of monolith midpoint
	'T' TC	SC716	10	03/02/02	N-S axis, inside face of north plywood form
	'T' TC	SC721	13	03/02/02	E-W axis, ~ 1 ft west of monolith midpoint

Table 2. Temperature Sensors Used in SMC Tests (cont.)

SMC Test	Sensor Type[a]	Instrument Number	Serial Number	Date Calibrated	Installation Location
	'T' TC	SC722	11	03/02/02	E-W axis, ~2.5 ft east of monolith midpoint
	'T' TC	SC723	14	03/02/02	E-W axis, ~ 2.5 ft west of monolith midpoint
30-yd^3	'T'TC	SC725	15	03/02/02	E-W axis, inside face of west plywood form
	TM	SC800	4	03/05/02	Monolith midpoint
	TM	SC804	5	03/05/02	Air, above monolith
	TM	SC805-TS	6	03/05/02	Vertical axis, top of reinforced concrete slab
	TM	SC805-US	2	03/05/02	Below reinforced concrete slab at center
	'T' TC	SC900_DAS	3	03/02/02	Air adjacent to DAS
	'T' TC	SC904	25	03/02/02	Air, above monolith
	'T' TC	SC905	4	03/02/02	Below reinforced concrete slab at center
	'T' TC	SC913	26	03/02/02	Air, south exposure
	'T' TC	SC916	27	03/02/02	Air, north exposure

a TC = thermocouple; TM = thermistor

CALIBRATION

The DAS and all sensors used in the SMC tests were calibrated against standards traceable to NIST at Sandia's Primary Standards Laboratory. The DAS was calibrated over three voltage ranges (10 V, 1 V, and 0.1 V) and one resistance range (10,000 Ω). Each temperature sensor was calibrated over a range of 0 to 80 °C even though the operating range for the sensors was considerably greater as shown in Table 1. The calibration range was selected to correspond with the range of temperatures anticipated during the actual tests. Calibration records are maintained on file in Sandia's NWMP Records Center, Carlsbad, NM (Records Package No. 523485 and No. 520499).

The DAS was calibrated against Sandia's Multimeter/Multifunction Station (MMS #9300). The 10-V-range of the DAS was certified to an accuracy of ± (0.005% of reading + 0.008% of range), while the 1-V and 0.1-V ranges were certified to accuracies of ± (0.005% of reading + 0.01% of range). Resistance measurement accuracy was certified at ± 5 Ω. Thermocouple and thermistor calibrations were performed with the sensors configured in their normal operating position, i.e., sensors were connected to the DAS using the identical cables and electrical connectors installed during the SMC tests.

The sensor calibration consisted of comparison of the sensor output with the internal Pt resistance thermometer in a Hart Scientific 9107 dry well. The sensor output was measured using a Datron 1081 Autocal Standards Multimeter. The Type E and Type T thermocouple accuracies were certified as ± 1.0 °C and ± 0.5 °C, respectively. The accuracy of the thermistors was certified as ± 0.3 °C.

Test Method and Chronology

Three field-scale tests were identified in the SMC test program. Two tests were considered to be small-scale because of the small volume of concrete to be batched (i.e., 5-yd^3 and 1-yd^3 requiring only a single mix truck). The third test was termed a large-scale test because its volume was 30-yd^3 requiring the batching of SMC using five separate mix trucks and placement in a steel-reinforced plywood box (10-ft-length by 10-ft-width by 8-ft-height). The three field tests used identical mix designs referred to by the M&OC as the SMC3.5 design. Although the mix design was identical for each test, some differences in batching procedure occurred during actual mixing. The sequence in which the various mix ingredients were added to the batch was different, in some cases, as well as the target value for the initial mixing temperature. In addition, water was added to some batches after initial mixing to achieve the desired slump (~7 to 8 in) for the mixture. Table 3 presents the SMC3.5 design specifications used in the three field tests.

Sandia instrumented each of the three SMC field tests with temperature sensors. In the 5-yd^3 and 1-yd^3 tests, sensors were inserted in portions of fresh SMC placed in steel drums. Temperatures of the curing concrete and surrounding air were then monitored for up to 3 weeks, primarily to evaluate the capabilities of the sensors and DAS. In the 30-yd^3 test, the temperature sensors were installed at various locations inside and adjacent to a steel-reinforced plywood box constructed on a concrete slab. SMC was then placed in the plywood box in five lifts and heat of hydration temperature increase measurements, as well as other boundary condition temperatures, were measured over a 65-day period. The objectives in the 30-yd^3 field test were to measure the maximum temperature and temperature gradients in the SMC monolith as it cured. Details of each test, including a test chronology, are summarized below under separate headings.

FIVE-YARD^3 TEST

On July 30, 2002 under the direction of the M&OC, Constructors Inc. batched a 5-yd^3 mixture at their production facility located in Carlsbad, NM. Following initial sampling and testing of the fresh mixture, approximately 30 gals of water were added to the mix because of the low slump (~1.5 in) observed for the batch. After some additional mixing and a limited amount of production of the SMC through a pump truck, a portion of the 5-yd^3 SMC mixture was placed in a 96-gal drum mounted on a portable utility trailer. When the drum was filled to within 1 in of its top, the drum lid was installed and five temperature sensors (two Type E and two Type T thermocouples and one thermistor) were inserted through the center of the lid to a depth coincident with the drum mid- height. The portion of the SMC remaining in the pump truck was subsequently pumped into a ditch to evaluate pumpability and flow characteristics.

Table 3. SMC3.5 Batch Design Specification

Ingredient	Weight Proportion (lbs/yd^3)
Class H Cement	193
Chem Comp III	112
Fly Ash	267
Coarse Aggregate	1,686
Fine Aggregate	1,316
Water	250
Sodium Chloride	85
Defoaming Agent	5.9
Sodium Citrate	1.75

Monitoring of SMC and air temperatures was initiated using 10-min logging intervals by activating the data acquisition protocol programmed into the DAS immediately after the sensors were installed in the 96-gal drum. The DAS was located inside a protective, Hoffman fiberglass enclosure mounted on the utility trailer along with the solar panel kit used to recharge the on-board DAS battery. During the first week of monitoring, the utility trailer containing the drum, DAS, and solar panel remained in the Constructors Inc. yard. Then, the trailer was towed about 1.5 miles to the Sandia fenced storage yard where temperature monitoring continued for two additional weeks. During the 3-week monitoring period, the DAS and drum were covered with a tarp and data from the DAS were periodically uploaded to a portable laptop computer. These data were then imported into Microsoft Excel for plotting and trend evaluation. Table 4 provides a chronological summary of relevant activities associated with the 5-yd^3 test.

ONE-YARD TEST

Because of the low slump observed in 5-yd^3 test batch, the M&OC instructed Constructors Inc. to mix a 1-yd^3 batch according to the same SMC3.5 mix specifications used for the 5-yd^3 test, but changing the order in which the ingredients were added and lowering the initial mixing temperature from approximately 22 to 17 °C. On August 20, 2002, Constructors

Inc. mixed a 1-yd^3 SMC3.5 batch at their Carlsbad facility. Following initial sampling and testing of the fresh SMC, a portion of the 1-yd^3 mix was placed in a 55-gallon drum mounted on the portable utility trailer used for the 5-yd^3 test. When the drum was filled, the drum lid was installed and two Type E thermocouples were inserted through the center of the lid to a depth coincident with the drum midheight.

Following the installation of the thermocouples, the drum was transported to the Sandia facility where it was moved from the trailer into an environmentally-controlled shop area located in Sandia Building NPHB. The thermocouples were connected to the DAS mounted to a wall in the shop and the data acquisition protocol was initiated. SMC and air temperatures were monitored for approximately 3 weeks with the portable laptop computer continuously connected to the DAS. Table 5 provides a chronological summary of relevant activities associated with the 1-yd^3 test.

THIRTY-YARD^3 TEST

To field the 30-yd^3 test, a large concrete form was designed by the M&OC and constructed by Constructors Inc. at its yard in Carlsbad, NM. As shown previously in Figure 1, the form comprised a 9-in-thick by 14-ft-square steel reinforced freshwater concrete pad and a box constructed of 1-in-thick plywood sheets. The plywood box was 10 ft in length and width by 8 ft in height and was supported around its perimeter at four locations using square steel hoops constructed of I-beams having various cross-sectional dimensions (e.g., W8x15, W6x12, and W4x13). The steel beams were welded at the corners and positioned vertically using 4-in by 4-in wooden posts. The base of the box was fastened to a 4-in by 4-in wooden sill secured to the concrete slab using Hilti™ bolts. A canopy attached to an adjustable-height wooden support was placed above the box by Sandia to provide protection from direct sunlight and precipitation.

Following construction of the steel-reinforced plywood form, Sandia installed a stainless-steel wire rope framework to position and support the temperature sensors used in the 30-yd^3 field test. The 3/32-in-diameter wire rope was positioned within the box to form a three-dimensional orthogonal array with the origin of the array located at the center of the box as shown in Figure 2. The array consisted of two horizontal axes, aligned approximately north-south and east-west and a single vertical axis. The horizontal wire ropes extended through the plywood and were secured to the steel I-beams supporting the plywood form. The single vertical rope was installed by anchoring its lower end in a cut-out in the center of the reinforced freshwater slab and its upper end to a composite beam (6-in by 6-in wooden beam reinforced using 4-in-square steel tubing) spanning the top of the plywood box. The cutout in the slab was filled in a two-step process using Wel-Cote™ anchoring cement (product 587) and masonry (product 505). All three ropes were tensioned using a one-ton chain come-along.

Table 4. Chronological Summary of Temperature Monitoring Activities Associated with the 5-yd^3 SMC Test

Activity	Date Completed	Time Completed (hr:min)
Temperature sensors calibrated	3/2/02	–
DAS certified	5/28/02	–
DAS hardware and software configured, including connection and check-out of temperature sensors	5/29/02	–
DAS and solar panel mounted on utility trailer	5/29/02	–
Utility trailer towed to Constructors Inc. facility	7/30/02	5:50
5-yd^3 SMC batch initially mixed	7/30/02	~ 7:30
Water added to 5-yd^3 SMC batch to increase slump followed by additional mixing.	7/30/02	~8:00
96-gal drum filled with portion of 5-yd^3 SMC mixture. Manually checked temperature of mixture.	7/30/02	9:35
Temperature sensors installed at midheight of 96-gal drum and began temperature monitoring.	7/30/02	9:37
Utility trailer with SMC drum and DAS towed to SNL CPG storage yard.	8/6/02	10:00
Temperature monitoring terminated.	8/18/02	18:10

Table 5. Chronological Summary of Temperature Monitoring Activities Associated with the 1-yd^3 SMC Test

Activity	Date Completed	Time of Day Completed (hr:min)
Temperature sensors calibrated	2/8/02	–
DAS certified	5/28/02	–
DAS hardware and software configured for 1-yd^3 test. DAS mounted on wall in shop area of Sandia Building NPHB	8/15/02	–
Utility trailer towed to Constructors Inc. facility	8/20/02	5:50
1-yd^3 SMC batch mixed	8/20/02	~ 7:10
Temperature of fresh mix determined manually	8/20/02	7:22
55-gal drum filled with portion of 1-yd^3 SMC mixture. Temperature of mixture determined manually	8/20/02	8:16
Temperature sensors installed at midheight of 55-gal drum	8/20/02	8:17
Utility trailer with 55-gal drum towed to SNL facility	8/20/02	8:35
Drum moved from trailer to shop area in Building NPHB. Temperature of mixture determined manually	8/20/02	8:50
Temperature sensors connected to DAS and monitoring initiated	8/20/02	9:00
Building NPHB air conditioner malfunctioned	8/22/02 8/23/02	– –
Temperature monitoring terminated	9/9/02	10:40

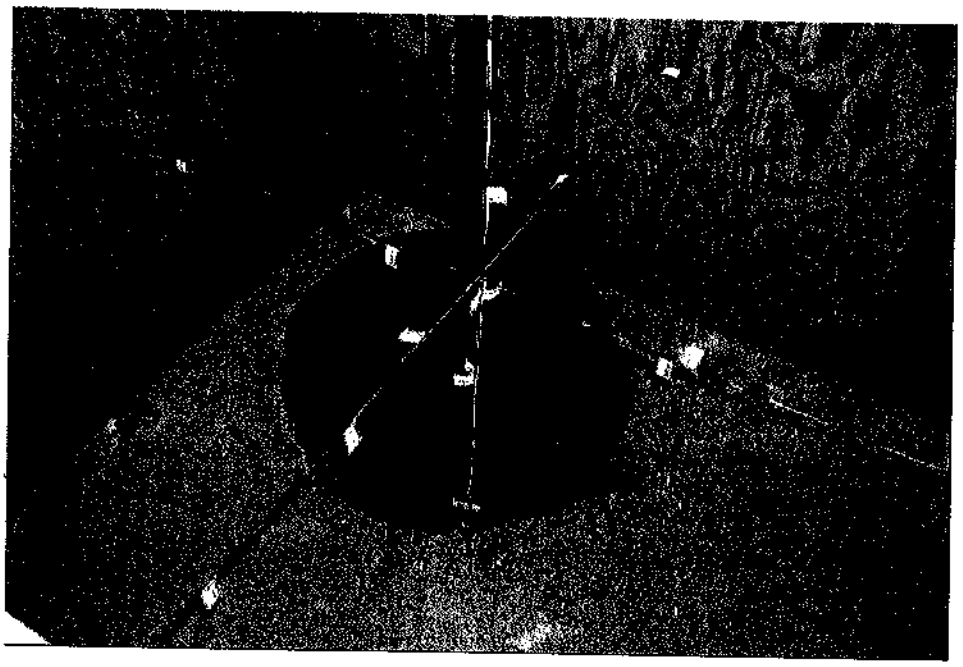

Figure 2. Wire rope support framework and temperature sensor array for the 30-yd^3 field test.

The temperature sensors were secured to the steel rope framework using color-coded electrical tape. Sensors placed in the horizontal arrays received a 90-degree bend 1 in from the sensor tip so each tip was positioned 1 in below the wire rope (the location of the horizontal axes was positioned 1 in above the mid-height of the box to ensure that the sensor tips were located at the box mid-height). The position of each sensor was determined using standard ruled tapes. Sensors were located as shown previously in Figure 1. A total of 30 sensors were installed including: 4 placed below the slab, 4 placed in air (1 each on the north and south sides of the box and 2 above the box); and 22 placed at various locations within the box. Of the 22 sensors installed in the box, 17 were active and 5 were inactive spares. Instrumentation cables were connected both to the sensors and the DAS (mounted on the outside north face of the plywood box) and were also taped to the wire rope for support. Each sensor was temporarily cooled and heated with its output monitored by the DAS to check polarity and operation. Following the installation of the instrumentation system, the data acquisition protocol loaded on the DAS was initiated and all active sensors were monitored for 4 days at a 10-min logging interval to simulate actual operating conditions and to evaluate system performance.

Under the direction of the M&OC, Constructors Inc. batched the 30-yd^3 SMC mixture on September 24, 2002. The batching of the SMC and its subsequent placement in the plywood form required the use of five mix trucks and a pump truck. Sampling and testing of the SMC from each truck was performed because of the variability observed in the 5-yd^3 and 1-yd^3 tests. Based on the sampling/testing, water was added (approximately 30 to 35 gals) to each of the five truck batches except Batch 2. With the exception of Batch 3, each of the five batches was pumped into the plywood form sequentially. In contrast, the truck used to mix Batch 3 was

placed on standby for about 1.5 h to simulate a delay in delivery time to the site. Therefore, this batch was the last to be pumped into the form.

During placement of the SMC, the flow of the mixture forced the vertical axis of the sensor array to be displaced horizontally. The displacement was estimated to be about 1.5 in to the north near the midpoint of the array. After the final truck load of SMC was placed in the plywood form, the top surface of the concrete was quite irregular and was located below the top of the form in most locations as seen in Figure 3. As a result, the uppermost temperature sensor located on the vertical axis of the array was exposed to the air rather than embedded in the SMC as planned. This sensor was moved down approximately 6 in while the SMC was still fresh to ensure that it was located in the top portion of the SMC monolith.

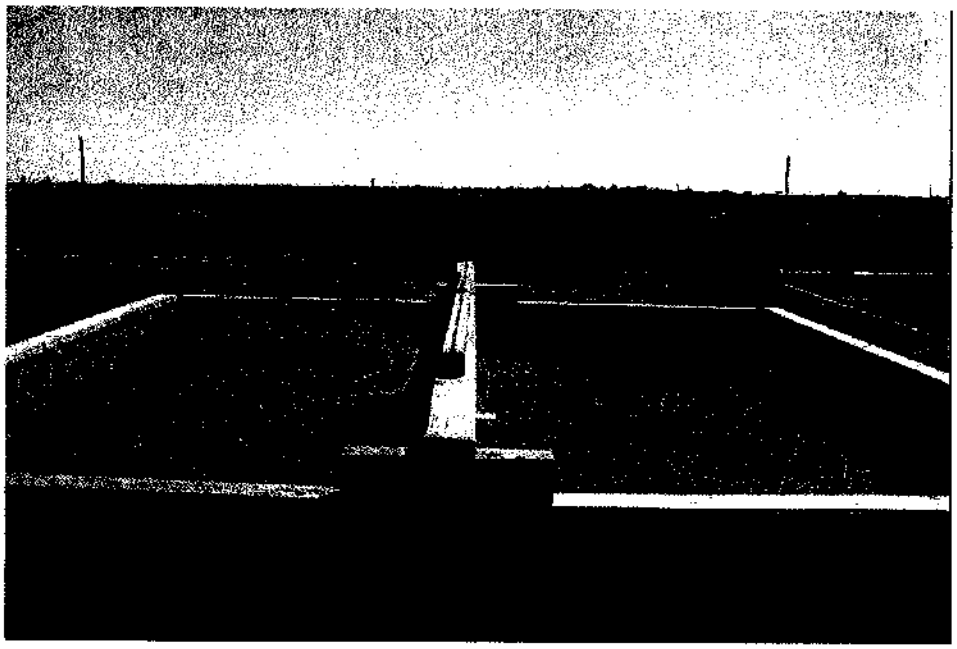

Figure 3. Top surface of 30-yd^3 monolith following emplacement of the last truck-load of SMC.

Temperature data were acquired during placement of the SMC in the form and during the 65-day curing period following placement. Output from all active sensors and a thermocouple placed in the air near the DAS was logged at 10-min intervals. This logging interval was maintained throughout the test. Power for the DAS was provided by an on-board battery continuously recharged during daylight hours using a solar panel kit mounted on the south side of the plywood form. The acquired data were periodically uploaded to a portable computer and then transferred to Microsoft Excel for plotting and trend evaluation. Table 6 provides a chronological summary of relevant activities associated with the 30-yd^3 test.

Table 6. Chronological Summary of Temperature Monitoring Activities Associated with the 30-yd^3 SMC Test

Activity	Date Completed	Time of Day Completed (hr:min)
Two Type E thermocouples calibrated	2/8/02	–
Two Type E thermocouples calibrated on 2/8/02 placed below reinforced concrete slab during slab construction	2/18/02	–
Steel-reinforced concrete slab poured	2/18/02	–
Temperature sensors calibrated	3/5/02	–
DAS certified	5/28/02	–
10 ft x 10 ft x 8 ft steel-reinforced plywood form erected by Constructors Inc.	9/13/02	–
Stainless steel wire rope framework for instrumentation support installed	9/17/02	–
Temperature sensors installed	9/19/02	–
Instrumentation system tested to evaluate performance	9/24/02	–
SMC from 1st mix truck placed in form	9/24/02	7:27
SMC from 2nd mix truck placed in form	9/24/02	8:15
SMC from 4th mix truck placed in form	9/24/02	9:38
SMC from 5th mix truck placed in form	9/24/02	10:09
SMC from 3rd mix truck placed in form	9/24/02	10:47
Topography of top surface of monolith mapped	10/2/02	–
Temperature monitoring terminated	11/25/02	15:02
Instrumentation system disassembled. DAS removed from field site	11/26/02	15:45
Instrumentation cables removed from plywood form	12/3/02	14:45

Test Results

FIVE-YARD^3 TEST

Figure 4 provides temperature data from two thermocouples monitored during the 5-yd^3 field test: (1) one Type-T thermocouple (Instrument no. SS700-AT) embedded in the SMC mix at the mid-height of the 96-gal drum, and (2) a second Type-T thermocouple (Instrument SS900-AT) located near the DAS to monitor ambient air temperature. As shown, the ambient and SMC mix temperatures vary between 20 and 43.5 °C and 24 and 40 °C, respectively, and are cyclical. Changes in mix temperature are influenced predominantly by changes in the ambient temperature; however, the mix temperatures lag the ambient temperatures by several hours. In addition, the amplitude of the mix temperature cycles is smaller than the amplitude of the ambient temperature cycles. The increase in mix temperature produced by the heat of hydration of cement is largely masked by the ambient temperature and, thus, is considered to be small indicating that the mix is behaving as a low heat-of-hydration concrete. The 5-yd^3 test verified that the sensors and DAS selected for use in the large-scale 30-yd^3 test would perform well.

ONE-YARD^3 TEST

The temperature data acquired from two temperature sensors monitored during the 1-yd^3 field test are shown in Figure 5. One sensor, a Type E thermocouple (Instrument no. SS700-BE), was embedded in SMC at the midpoint of a 55-gal drum. The other sensor, a Type T thermocouple (Instrument No. SS900-AT), was located near the DAS mounted on the wall of the Sandia shop, and thus monitored the room temperature where the 55-gal drum was located.

As shown in Figure 5, the room temperature during the test was cyclical with a mean of about 22.5 °C and an amplitude of about 5 °C. On two occasions however, the room temperature exceeded 30 °C when the building air conditioner failed. Following repair of the air conditioning unit on August 23, 2002, the cyclic behavior of the room temperature was observed once again; but the frequency of the temperature cycle was significantly higher than before the repair was made. Although the SMC temperature at the midpoint of the 55-gal drum exhibited some low-frequency cyclic behavior in response to the room temperature, it initially increased to a peak of 28 °C approximately 15 h after the initial mixing of the 1-yd^3 batch and then decreased steadily until it equilibrated with the mean room temperature. A manual field check of the SMC temperature immediately following the mixing of the 1-yd^3 batch indicated a starting value of about 16.5 °C, so the temperature increase during curing was about 11.5 °C suggesting that the concrete is again responding as a low heat-of-hydration concrete. However, the magnitude of the observed temperature increase is probably not indicative of a large SMC monolith because the room temperature likely affected the small SMC volume in the drum.

A total of 27 active temperature sensors were monitored during the 30-yd^3 field test including the thermocouple located near the DAS. Of this total, 5 sensors monitored air temperatures, 4 monitored the temperatures below the steel-reinforced concrete slab, and 18 monitored temperatures in the SMC monolith. Two sensors, both thermistors (Instrument nos. SC805-TS and SC805-US), malfunctioned during the test.

These thermistors were located directly under and directly above the reinforced concrete slab. In addition to the continuous temperature measurements made during the test, the M&OC directed its subcontractors to record the initial temperatures of each of the five SMC batches as they arrived at the test site. These temperatures ranged from 12.8 to 15.5 °C with a mean value of 13.8 °C.

Figure 6 plots the ambient temperatures measured at the top of and along the north and south faces of the monolith and at the DAS. As expected, these temperatures are cyclical and vary from about 10 to 55 °C along the south face and from 10 to 35 °C in shaded areas (i.e., top, north face, and at the DAS). The much higher air temperatures on the south face are attributed to thermal loading from the sun, particularly in the vicinity of steel I-beams used to support the plywood form. The temperature history below the concrete slab is shown in Figure 7. The temperature below the slab decreased initially after the SMC mix was placed in the formwork. Then, the temperature increased for 10 days reaching a peak of approximately 34 °C, followed by a gradual decrease to a stabilized value of approximately 15 °C. The temperatures below the slab do not appear to be affected by the cyclical ambient temperatures recorded during the test.

Figure 8 presents the temperature history of the sensors located along the vertical axis of the instrumentation array. Initially, temperatures at the various locations decreased when the SMC mix contacted the sensors. Then, the temperatures increased at all locations subsequently peaking between 7 and 10 days following the pour. Peak temperatures were followed by gradual decreases in temperatures at all locations with temperature stabilization (~15 °C) occurring at about 50 days. The maximum observed temperature was approximately 38.5 °C occurring at the block midpoint and/or slightly below midpoint. Sensors near the boundaries (top and bottom) were influenced by the boundary temperature history. For example, the two sensors (SC704 and SC702-1) located near the top of the test block were clearly influenced by the cyclical nature of the ambient temperature.

Figures 9 and 10 present the temperature histories for the north-south axis and the east-west axis, respectively. The temperature trends are consistent with those seen for the vertical axis. That is, the temperatures initially decreased, but then increased over the next 7 to 10 days to reach a peak value of about 38.5 °C. After the peak temperatures were reached, the temperatures gradually decreased and attained stable values (~15 °C) after approximately 50 days. Sensors located near the formwork were strongly influenced by the cyclical behavior of the ambient temperature as demonstrated by the histories of Sensors SC716, SC 713, and SC725.

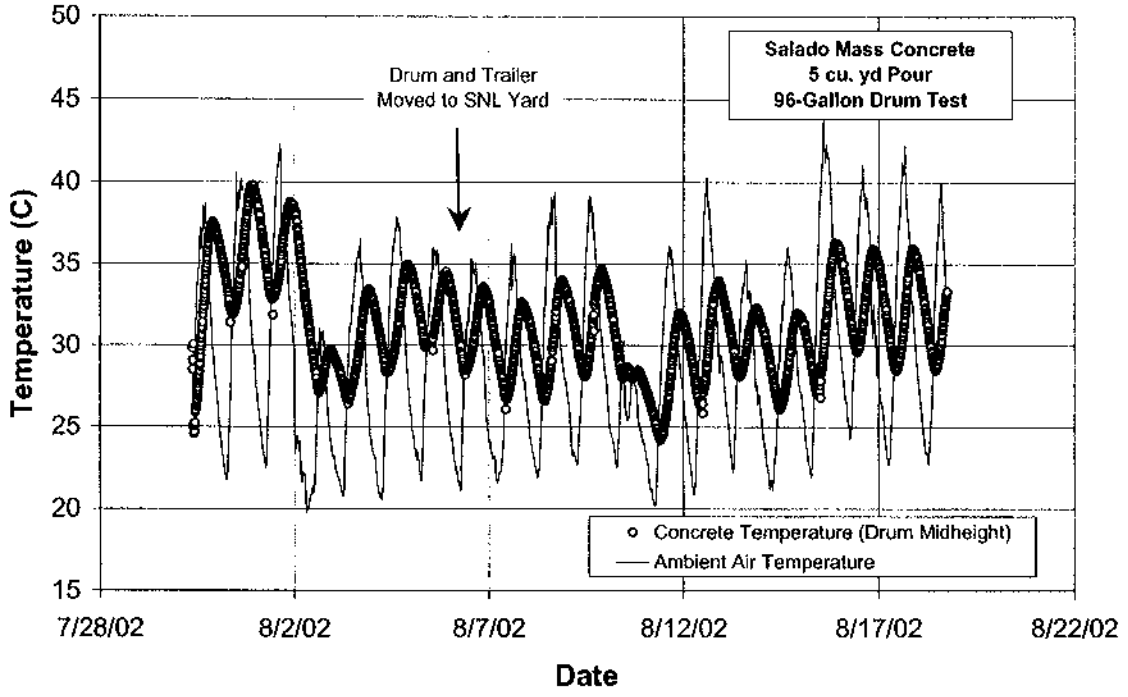

Figure 4. SMC mixture and ambient temperatures acquired during the 5-yd^3 test.

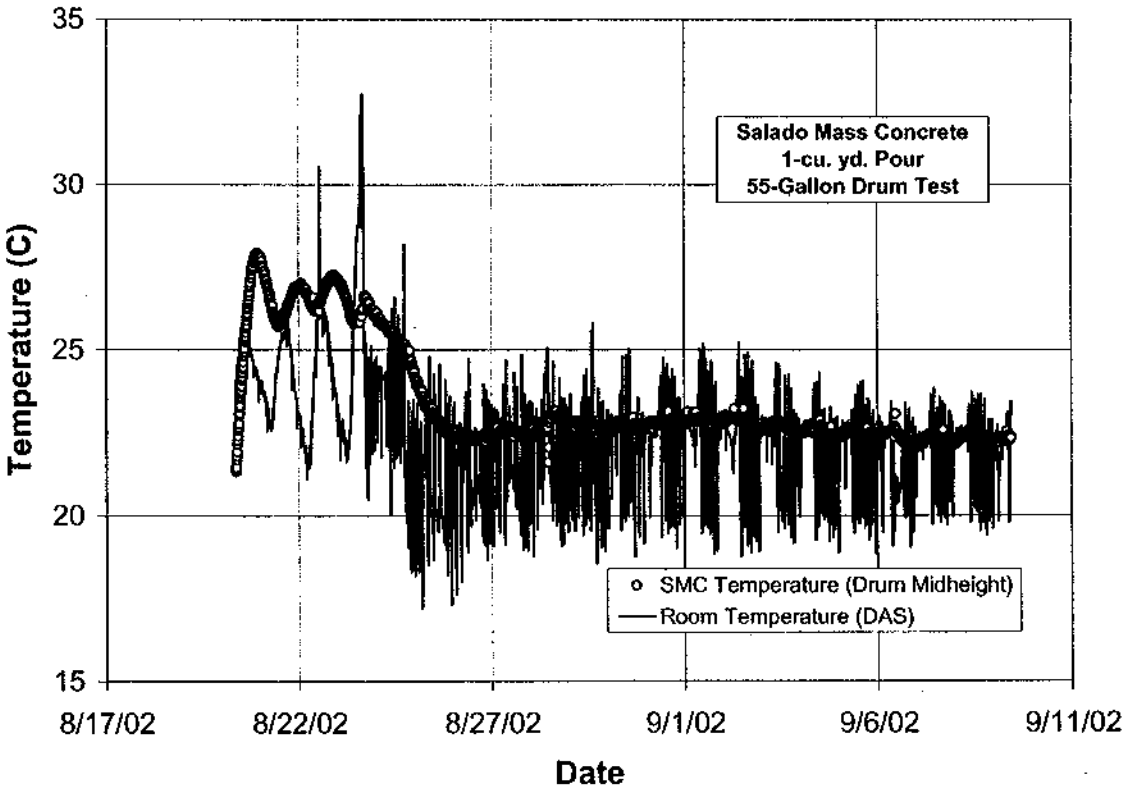

Figure 5. SMC mixture and room temperatures acquired during the 1-yd^3 test.

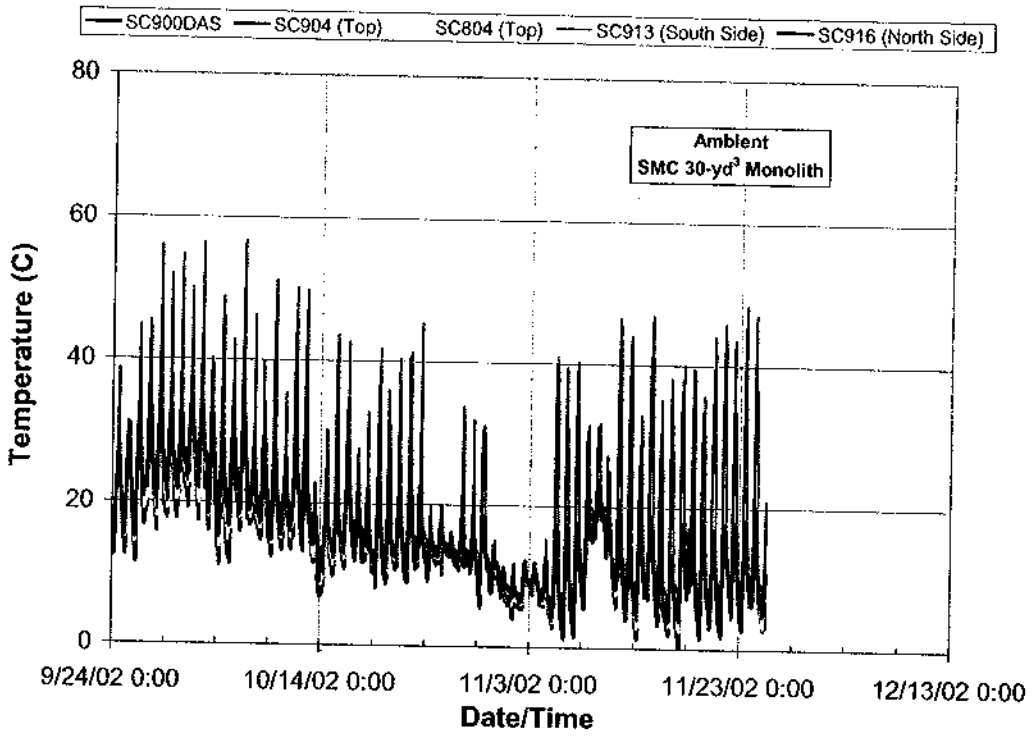

Figure 6. Ambient temperature history during the 30-yd^3 field test.

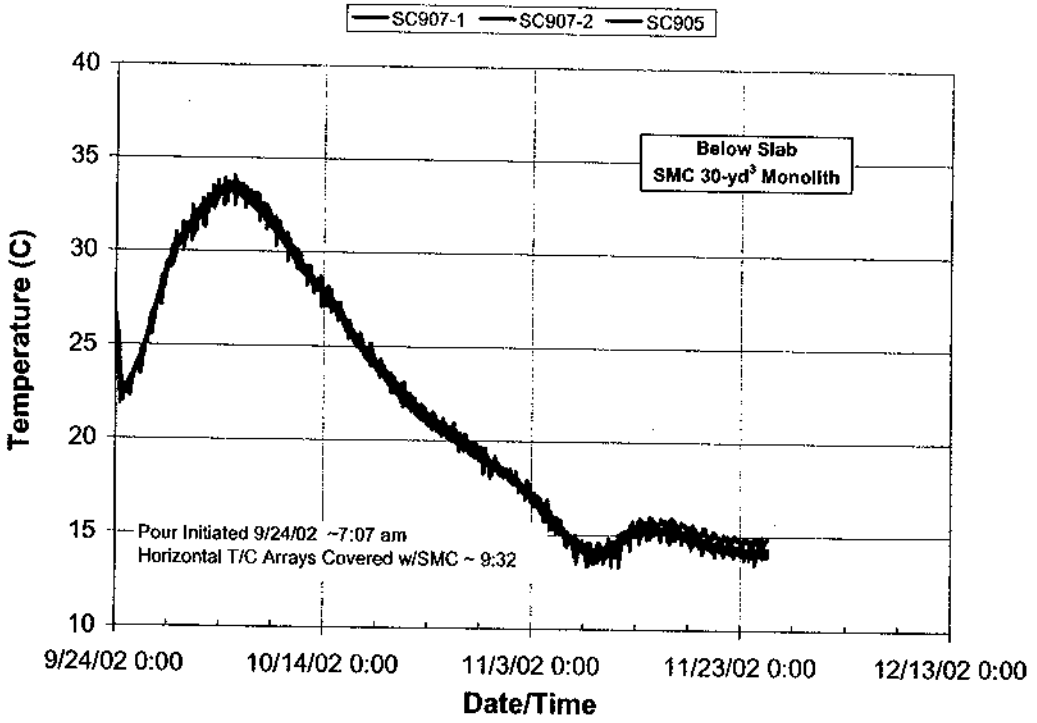

Figure 7. Temperature history below the steel reinforced concrete slab during the 30-yd^3 field test

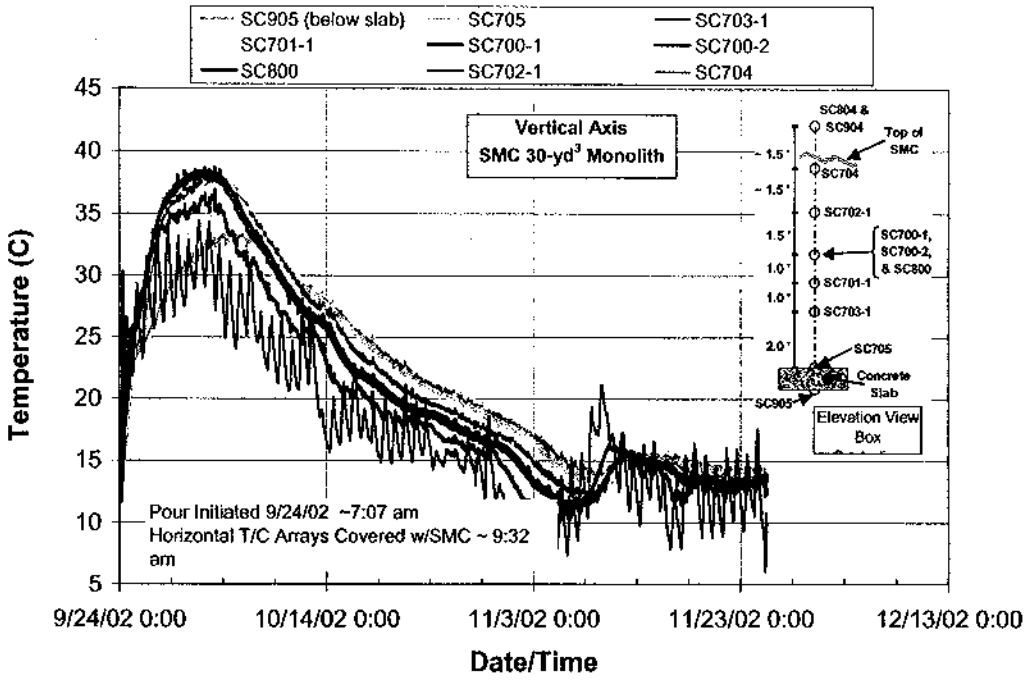

Figure 8. Temperature history along the central vertical axis of the 30-yd^3 field test.

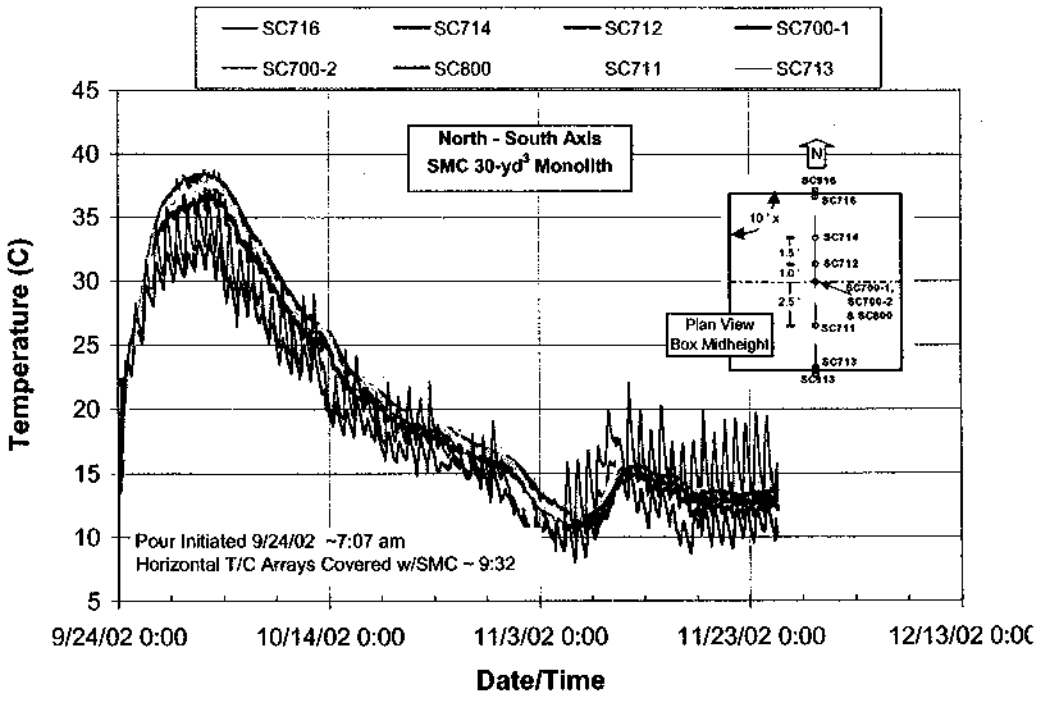

Figure 9. Temperature history along the north-south axis of the 30-yd^3 field test.

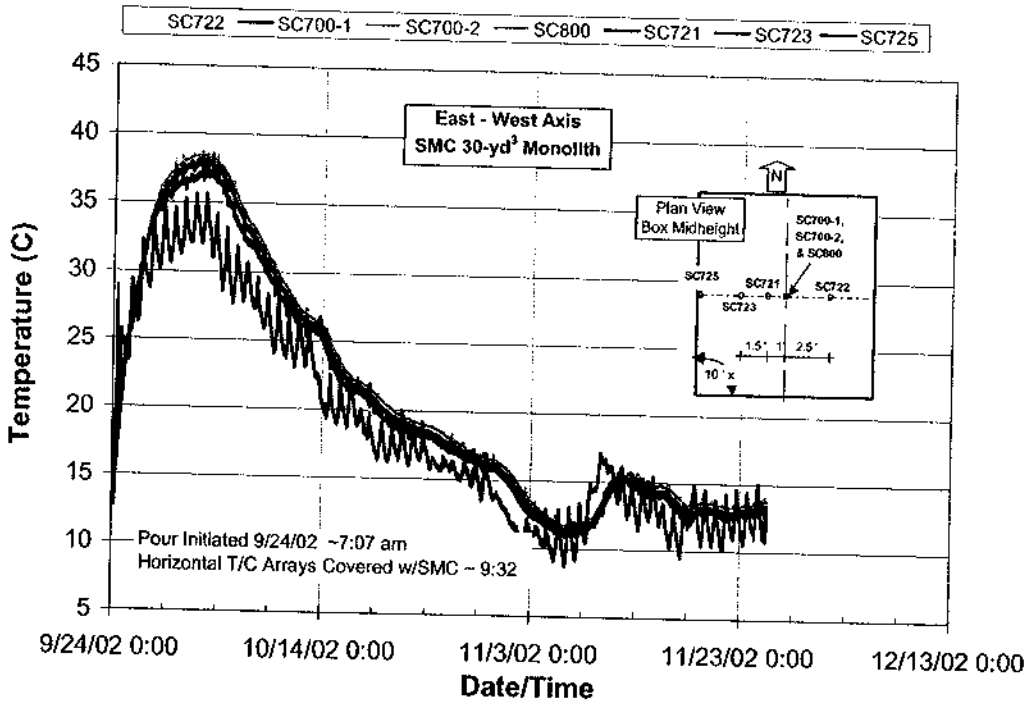

Figure 10. Temperature history along the east-west axis of the 30-yd^3 field test.

The SMC cast in the 30-yd^3 field test generated heat of hydration similar to previous laboratory tests (Wakeley et al., 1994). In particular, Mixture 6R of Wakeley et al. was cast at 12.8 °C and attained a temperature increase approaching 33 °C. The 30-yd test was batched at approximately 13.8 °C and achieved a maximum temperature of 38.5 °C, an increase of 24.7 °C.

The WIPP underground setting maintains a nominal constant temperature of 27.8 °C, such that if a PCS were constructed with an SMC concrete equivalent to the 30-yd^3 material, the maximal differential temperature gradient from hydration would be approximately 10 °C above ambient underground conditions. As noted previously in the shaft seal design report (SNL, 1996), temperatures attained in the 30-yd^3 test are significantly below temperatures modeled for SMC shaft seal components (i.e., 52.5 °C). Thus, by comparison to the thorough analysis in the shaft seal design report, temperatures of the 30-yd^3 test are well within any possible thermally-induced tensile strain concerns.

Summary

In support of the SMC test program, Sandia designed, tested, and validated a robust DAS and used the DAS to acquire heat-of-hydration temperature increase data during emplacement and curing of a large-scale test. The maximum temperature increase of approximately 25 °C observed in test indicated the SMC monolith was responding as a low heat-of-hydration concrete as expected. Based on the results, the tested SMC mix design is expected to perform well should it be used in the PCS planned for the WIPP.

Acknowledgment

The work presented in this document represents the combined efforts of the cited authors and W. F. DeYonge, R. T. Parsons, and A. T. Schaub, RESPEC Inc., Carlsbad, NM. Scheduling and overall management of the SMC test program was performed by WTS. The professionalism shown and support offered during the test by the WTS staff, including S. J. Patchet, G. R. Maples, and B. F. Zimmerly, are greatly appreciated. The authors also appreciate the logistical support provided at the test site by the Constructors Inc. staff, in particular, M. Brooks.

References

MacDonald, T.L. 2002. "Salado Mass Concrete Test Plan." Unpublished test plan. TP 02-03, Rev. 0. Carlsbad, NM: Sandia National Laboratories.

Chavez, M. 2002. "Software Requirements." Unpublished quality assurance procedure, NP 19-1, Rev. 9. Carlsbad, NM: Sandia National Laboratories.

NMED. 1999. *Hazardous Waste Facility Permit Issued to Waste Isolation Pilot Plant EPA No. NM4890139088.* Santa Fe, NM: New Mexico Environment Department.

SNL, 1996. *Waste Isolation Pilot Plant Shaft Sealing System Compliance Submittal Design Report.* SAND96-1326. Albuquerque, NM: Sandia National Laboratories.

U.S. Code. 1976. *Resource Conservation and Recovery Act.* 42 U.S.C. §3251 et seq., Washington, DC: U.S. Government Printing Office.

U.S. EPA. 1993. "40 CFR Part 191 Environmental Radiation Protection Standards for the Management and Disposal of Spent Nuclear Fuel, High-Level and Transuranic Radioactive Wastes; Final Rule," *Federal Register*, Vol. 58, No. 242, 66398-66416. Washington, DC: U.S. Environmental Protection Agency Office of Radiation and Indoor Air.

U.S. EPA. 1996. "40 CFR Part 194, Criteria for the Certification and Recertification of the Waste Isolation Pilot Plant's Compliance with the Disposal Regulations: Final Rule," *Federal Register.* Washington, DC: U.S. Environmental Protection Agency Office of Radiation and Indoor Air. Vol. 61, No. 28, 5224-5245.

U.S. EPA. 1998. "40 CFR Part 194, Criteria for the Certification and Recertification of the Waste Isolation Pilot Plant's Compliance with the Disposal Regulations: Certification Decision; Final Rule," *Federal Register.* Washington, DC: U.S. Environmental Protection Agency Office of Radiation and Indoor Air. Vol. 63, No. 95, 27354-27406.

Wakeley, L.D., J.J. Ernzen, B.D. Neeley, and F.D. Hansen. 1993. *Salado Mass Concrete: Mixture Development and Preliminary Characterization.* SAND93-7066. Albuquerque, NM: Sandia National Laboratories.